TECHNOLOGIES ASI PATENTS PORTFOLIO

UNITATED STATES PATENTE PUBBLICATION OFFICE

Document No.

US2011/0091438A1

Publication Date

20091020

Applicant

AGENZIA SPAZIALE ITALIANA

Title

RADIOPROTECTIVE SOD SOLUBLE ISOFORM AND USES THEREOF

US 20110091438A1

(19) **United States**

(12) **Patent Application Publication**

Mancini

(10) **Pub. No.: US 2011/0091438 A1**

(43) **Pub. Date: Apr. 21, 2011**

(54) **RADIOPROTECTIVE SOD SOLUBLE ISOFORM AND USES THEREOF**

(75) Inventor: **Aldo Mancini**, Naples (IT)

(73) Assignee: **ASI AGENZIA SPAZIALE ITALIANA**, Rome (IT)

(21) Appl. No.: **12/581,980**

(22) Filed: **Oct. 20, 2009**

Publication Classification

(51) **Int. Cl.**
A61K 38/44 (2006.01)

(52) **U.S. Cl.** **424/94.4**

(57) **ABSTRACT**

The invention refers to a specific isoform of MnSOD (Mn-superoxide dismutase) and its uses for protecting and curing subjects exposed to radiations, specifically space radiations.

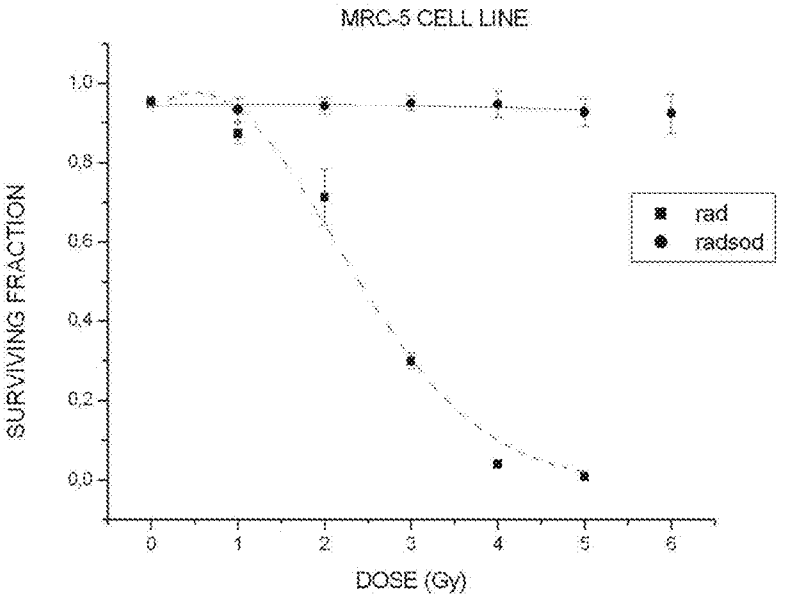
MRC-5 CELL LINE
SURVIVING FRACTION
1.0
0.8
0.6
0.4
0.2
0.0
0
1
2
3
4
5
6
DOSE (Gy)
rad
radsod

FIG. 1

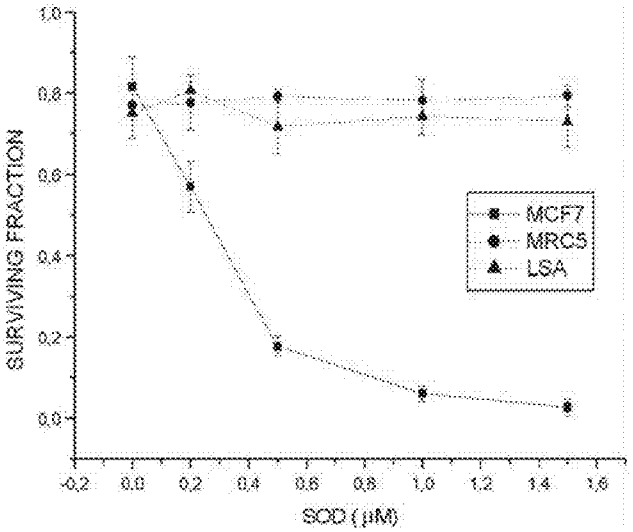
SURVIVING FRACTION
1.0
0.8
0.6
0.4
0.2
0.0
-0.2
0.0
0.2
0.4
0.6
0.8
1.0
1.2
1.4
1.6
SOD (µM)
MCF7
MRC5
LSA

FIG. 2

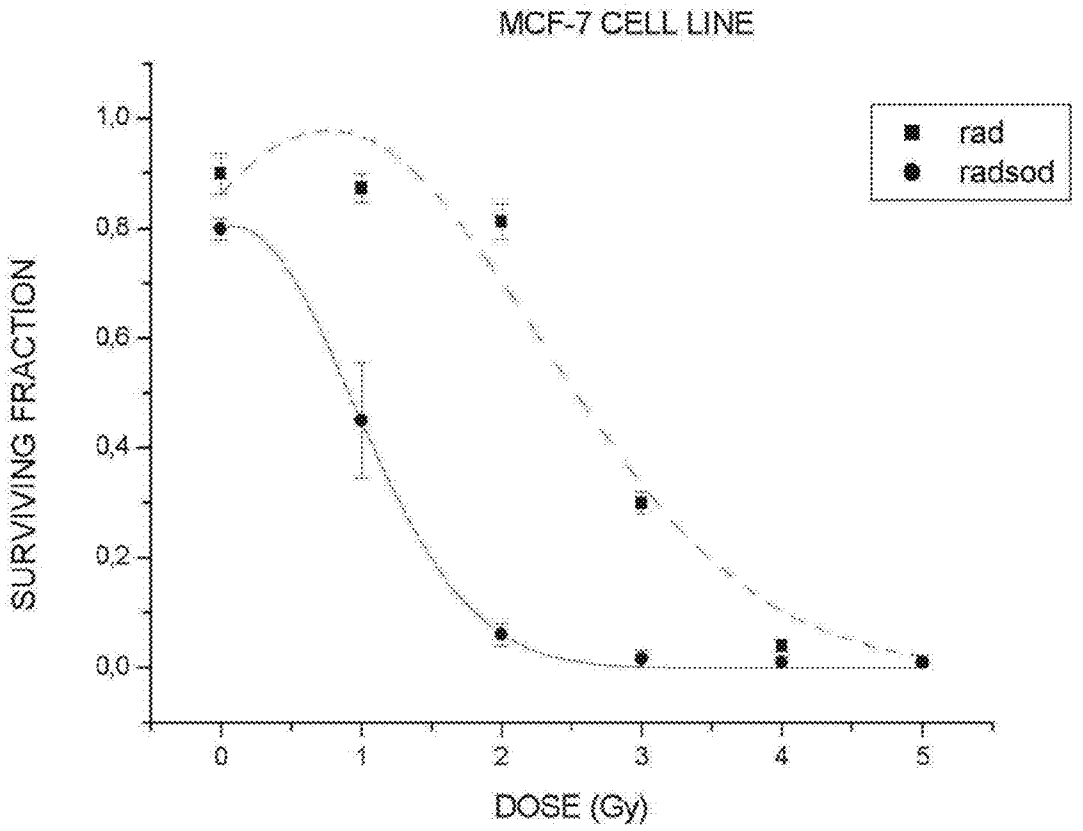
MCF-7 CELL LINE
rad
radsod
SURVIVING FRACTION
1,0
0,8
0,6
0,4
0,2
0,0
0
1
2
3
4
5
DOSE (Gy)

FIG. 3

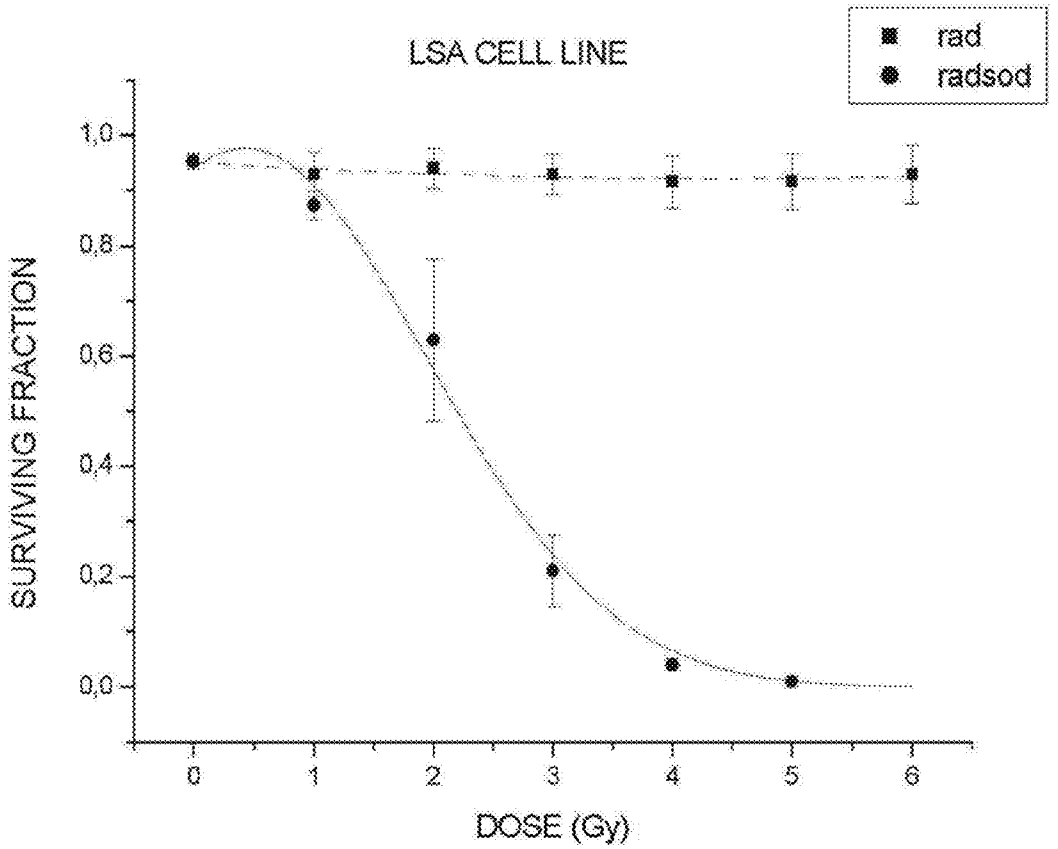
LSA CELL LINE
rad
radsod
SURVIVING FRACTION
1,0
0,8
0,6
0,4
0,2
0,0
0
1
2
3
4
5
6
DOSE (Gy)

FIG. 4

FIG. 5

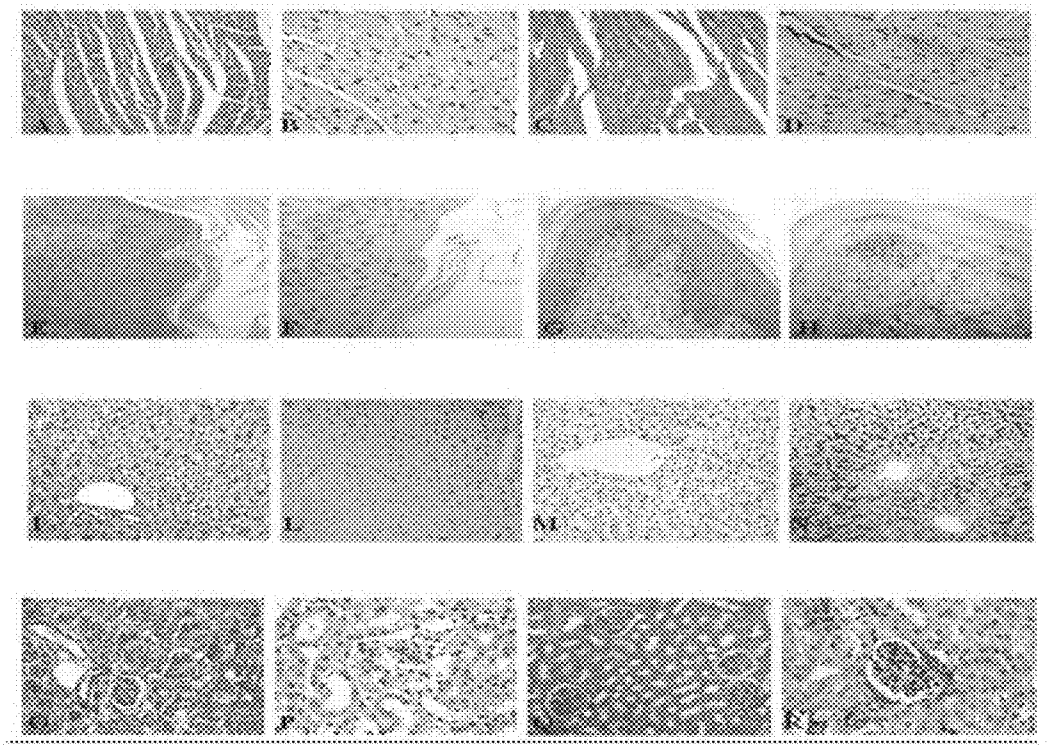

FIG. 6

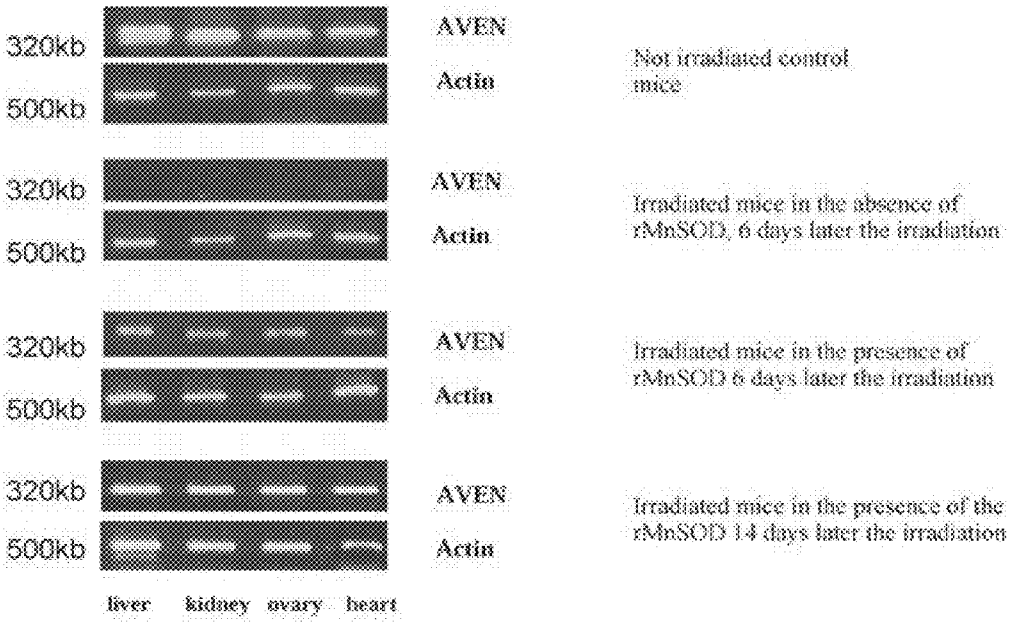
320kb
500kb
AVEN
Actin
Not irradiated control mice
320kb
500kb
AVEN
Actin
Irradiated mice in the absence of rMnSOD, 6 days later the irradiation
320kb
500kb
AVEN
Actin
Irradiated mice in the presence of rMnSOD 6 days later the irradiation
320kb
500kb
AVEN
Actin
Irradiated mice in the presence of the rMnSOD 14 days later the irradiation
liver
kidney
ovary
heart

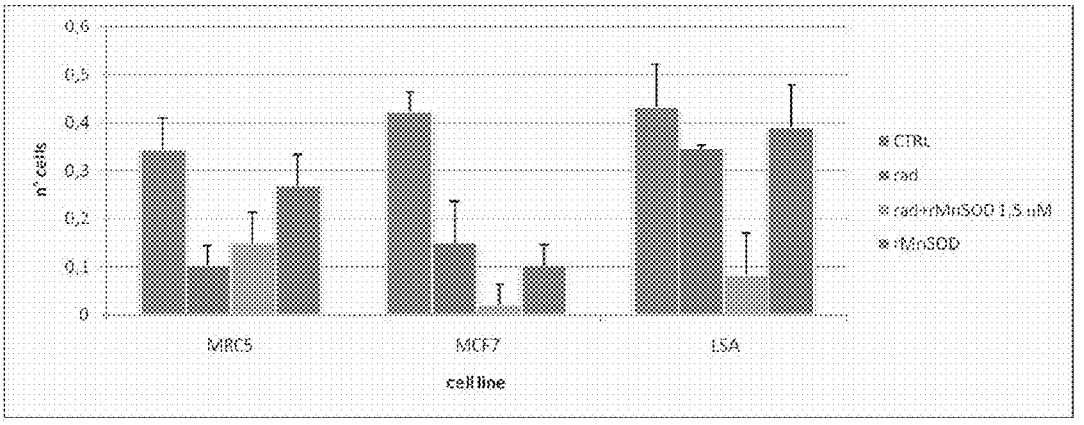
0,6
0,5
0,4
0,3
0,2
0,1
0
n° cells
MRC5
MCF7
LSA
cell line
CTRL
rad
rad+rMnSOD 1,5 uM
rMnSOD

FIG. 7

RADIOPROTECTIVE SOD SOLUBLE ISOFORM AND USES THEREOF

FIELD OF THE INVENTION

[0001] The invention refers to a specific isoform of MnSOD (Mn-superoxide dismutase) and its uses for protecting and curing subjects exposed to radiations, specifically space radiations.

BACKGROUND

[0002] Organisms exposed to ionizing radiations are mainly damaged by free radicals, which are generated by the radiolysis of water contained in the cells.

[0003] The superoxide dismutase (SOD) family of proteins is necessary to protect oxygen-utilizing cells from the toxicity of the reactive oxygen species (ROS) produced during normal metabolism. Besides being protective proteins, these enzymes are also key components of signalling pathways that regulate cell physiology. SODs catalyze the reaction: with hydrogen peroxide being then removed by catalases (CATs) and peroxidases, of which glutathione peroxidase (GPx) has been the most widely studied. There are three known forms of SOD in mammalian cells: a copper- and zinc-containing superoxide dismutase (CuZnSOD) found mainly in the cytoplasm and in the nucleus, a manganese-containing superoxide dismutase (MnSOD) found in the mitochondria, and an extracellular superoxide dismutase (ecSOD) found primarily in the extracellular compartments. The superoxide dismutase are enzymes of remarkable pharmacological interest for their potential role in the prevention of all pathologies involving oxidative damage. It has been recently proposed that these enzymes can be useful in the prevention and in the treatment of damages caused by physical agents and, particularly by ionizing radiations (1) which generate high levels of free radicals (2-6).

[0004] The large scientific and practical interest toward MnSOD has resulted in intensive developments of new technologies for its production but, despite great efforts, efficient production of recombinant human SOD in prokaryotic systems or simple eukaryotes failed. This failure has so far hindered its large-scale production and protein genetic engineering (7). Recently a new technology for radio-protective gene therapy using the transgene for the antioxidant manganese superoxide dismutase, delivered to specific target organs (lung, esophagus, oral cavity, oropharynx, and bladder) using gene transfer vectors including plasmid/liposomes (PL) and adenovirus was developed. Significant reduction of organ specific tissue injury has been demonstrated in several organ systems in rodent models.

[0005] Moreover, the application of MnSOD-PL gene therapy in the setting of fractionated chemo-radiotherapy is being tested in clinical trials for the prevention of esophagitis during the treatment of lung non-small-cells carcinoma, and in the prevention of mucositis during combination therapy of carcinomas of the head and neck. Encouraging results in pre-clinical models have suggested that radioprotective gene therapy may facilitate dose escalation protocols to allow increases in the therapeutic ratio of cancer radiotherapy (8).

[0006] Recently a significant reduction of tissue injury from irradiation damages was demonstrated by using the MnSOD-plasmid/liposome treatments in the protection of murine lung.

DESCRIPTION OF THE INVENTION

[0007] The author of the instant invention have shown that a new active recombinant human MnSOD (rMnSOD; disclosed in Mancini et al. Int J. Cancer 119; 932-943, 2006 and in WO03/072768), easily administrable in vivo, exerts the same radioprotective effect on the normal cells and organisms as any MnSOD, and it is also radio-sensitizing for tumour cells (Borrelli A., et al. Free Radic Biol Med. 2009 46:110-6). rMnSOD has the following aa. sequence (Swiss Prot. Acc. No P04179; SEQ ID No. 1):

```
MLSRAVCGTSRQLAPALGYLGSRQKHSLPDLPYDYGALEPHINAQIMQ
LHHSKHHAAYVNNLNVTEEKYQEALAKGDVTAQIALQPALKFNGGGHI
NHSIFWTNLSPNGGGEPKGELLEAIKRDFGSFDKFKEKLTAASVGVQG
SGWGWLGFNKERGHLQIAACPNQDPLQGTTGLIPLLGIDVWEHAYYLQ
YKNVRPDYLKAIWNVINWENVTERYMACKK.
```

[0008] No data are available on the protective effect on radiations present in the atmosphere and more general in the space, as ionizing and protonizing radiations. Authors here show how healthy animals, exposed to lethal dose of ionizing and protonizing radiations and daily injected with rMnSOD, resulted protected by radio-damages and were still alive 30 days after the irradiation. Animals treated with only PBS solution, while in the absence of rMnSOD, died after 7-8 days from the radio-treatments. The molecular analysis of all irradiated tissues revealed that the anti-apoptotic AVEN gene (UniProtKB/Swiss-Prot: AVEN_HUMAN, Q9NQS1) is activated only in the animals treated in the presence of rMnSOD. The data suggest that rMnSOD deserves to be considered as a pharmaceutical tool to make radiotherapy more selective on cancer cells and to prevent and/or cure the accidental damages derived by the exposure to ionizing and protonizing radiations.

[0009] Authors show the radio-protective role of a specific isoform of a human recombinant protein (rMnSOD) which possesses the specific SOD antioxidative and antiradical activity and which can be easily administrated in vivo through the systemic pathway, reaching and penetrating into the cells, without require any additional manipulation (9,10).

[0010] rMnSOD effects were studied in vitro, on irradiated normal and cancer cells, and in vivo, on normal C57BL/6J mice exposed to lethal doses of ionizing radiations.

[0011] The results demonstrated that rMnSOD exerts a radio-protective effect on normal cells (in vitro) and on normal tissues (in vivo) while it is radiosensitizing for cancer cells (in vitro). Moreover, while the animals treated in the absence of rMnSOD would survive no longer than 6-7 days after radiations, those treated with rMnSOD survived for a much longer period up to 30 days considered as the experimental time point.

[0012] Therefore it is an object of the instant invention a method for protecting a subject from exposure to radiations comprising the administration of an effective protective amount of rMnSOD of SEQ ID No. 1, or functional fragments thereof. Preferably the rMnSOD is administered in an amount from 0.08 g/Kg body weight to 0.1 g/Kg body weight for at least 30 days before the exposure to radiations.

[0013] In a preferred embodiment said radiations are space radiations.

[0014] In another preferred embodiment said radiations are sun radiations.

[0015] In another preferred embodiment said radiations are from depleted uranium.

[0016] In another preferred embodiment said radiations are from anti-tumoral metabolic therapies administration of radioactive isotopes or radiating therapies. Such application is particularly useful for protecting the kidney parenchyma of subjects treated with radio-isotopes and for protecting from skin burns and ulcers.

[0017] In another preferred embodiment said radiations from radioactive isotopes for radio-diagnostics.

[0018] In another preferred embodiment said radiations are ionizing and/or protonizing radiations.

[0019] It is another object of the invention a method for treating a subject exposed to radiations comprising the administration of an effective therapeutically active amount of rMnSOD of SEQ ID No. 1. or functional fragments thereof. Preferably the rMnSOD is administered in an amount from 0.08 g/Kg body weight to 0.1 g/Kg body weight for at least 30 days after the exposure to radiations.

[0020] In a preferred embodiment said radiations are space radiations.

[0021] In another preferred embodiment said radiations are ionizing and/or protonizing radiations.

FIGURE LEGENDS

[0022] FIG. **1** The cell strains were treated in the presence of rMnSOD (0-1.5 μM). 1 days after irradiation, the cells were detached with Trypsin-EDTA, and plated at a concentration of 200 cells/dishes in drug-free medium. Fourteen days later the colonies were fixed and counted by using a crystal violet staining to evaluate the number of colonies present in the dishes.

[0023] FIG. **2** On the MRC-5 normal cells the sole irradiation induces a dose-dependent radiodamage that with 3 Gy of X-rays leads to the death of cells (rad). The same radiotreatment, in the presence of 0.5 μM rMnSOD, results in a significant radioprotection and survival of cells(rad+sod).

[0024] FIG. **3** On the MCF-7, the sole radiation with 3 Gy of X-rays (rad) led to the death of the cells after 14 days, whereas the same cells are killed when they are irradiated with 2 Gy and in the presence of 0.5 μM rMnSOD(rad+sod).

[0025] FIG. **4** On the LSA cells, the sole irradiation with 6 Gy of X-rays (rad) do not effect the cell survival of LSA cells (rad). On the contrary, when the LSA cells are irradiated with only 3 Gy, in the presence of 0.5 μM rMnSOD, the cells are killed (rad+sod).

[0026] FIG. **5** (A-R) Histologic sections of organs of normal mice underwent to a lethal dose of ionizing radiations, treated in the presence or in the absence of rMnSOD Heart: the histological examination revealed that in the heart of mice which didn't receive the rMnSOD, were present intensive areas of miofibrillolisis and a hydropic degeneration (A), ×250, and the absence of endogenous expression of rMnSOD at the immunochemical evaluation (B)×250. On the contrary, in the hearts of animals treated in presence of rMnSOD, the tissue integrity was clear (C)×250, and rMnSOD was strongly represented in the interstitial space, at immunochemical detection (D)×250 Cervix uteri: the histological examination revealed that in the cervix uteri of mice which didn't receive the rMnSOD, were present intensive areas of structural discontinuity (E)×250, and the absence of endogenous expression of rMnSOD at the immunochemical evaluation (F)×250. On the contrary, in the cervix uteri of mice treated in presence of rMnSOD, the tissue integrity was clear (G)×250, and was also evident the presence of rMnSOD in the cytoplasm and in the interstitial space, at immunochemical detection (H)×250 Liver: The lobulo-laminar structure resulted preserved both in the control (I) and in the treated section (L). The positive immunochemical reaction has been evident either in the sinusoid that in the hepatocytes cells, particularly it is evident the positivity of the membrane, (M) with high increasing in the treated animals (N)×250. Kidney: the histological examination revealed that in the kidney of mice which didn't receive the rMnSOD, showed a glomerular coarctation and tubular degeneration (O)×250, and the absence of endogenous expression of rMnSOD at the immunochemical evaluation (P)×250., while the animal's kidneys treated in presence of rMnSOD, a total integrity of the structures (Q)×250, with an ubiquitous presence of rMnSOD in the interstitial space, at immunochemical detection (R)×250. The quantitative evaluations of immunochemical reaction were obtained by using an imaging analyzer Leica50.

[0027] FIG. **6** AVEN expression in irradiated mice in the presence or in the absence of rMnSOD. The figure showed the amplified fragments of AVEN gene (352 bp) in the different experimental groups. Three groups of inbreed C57BI 6 mice were used in PCR experiments. The first group was of untreated control animals; the second group received high lethal dose of ionizing radiations and at the third group was treated before irradiation 0.08 mg/Kg/die, for 15 days of in the presence of recombinant rMnSOD. The actin transcripts (500 bp) was shown as control of cDNA quantity (inferior line).

[0028] FIG. **7** Target cells, in three independent experiments, were exposed to radiations by a proton beams having an energy of 62 MeV with a dose of 6 Gy. On the normal cells (MRC-5) the killing effect of the sole radiations resulted of 67% of the cell death, but when the same cells were irradiated in the presence of rMnSOD, 86.9% of them survived to radiotreatment. On tumor cells, the sole proton beams produced a killing effect of 34% for MCF-7 cells and 29% for LSA cells. On the contrary, when these tumor cells were irradiated in the presence of rMnSOD the killing effect was of 96% for MCF-7 cells and 56% for LSA cells.

MATERIALS AND METHODS

Enzymes

[0029] rMnSOD was obtained as previously described (9), while its enzymatic activity evaluated according to McCord and Fridovich (11). Commercial Cu/Zn-SOD was from SIGMA.

Cell Cultures

[0030] The cell lines investigated here (MCF-7, MRC-5) are described and available from ATTC (MCF-7: cat. n° HTB-22™; MRC-5: ca. n° CCL-171™). Cells were grown in Dulbecco's modified Eagle's medium supplemented with 5% of fetal bovine serum (FCS) at 37° C. in a humidified atmosphere containing 5% of CO_2. The culture medium was replaced every 3-4 days. The liposarcoma-derived cell line (LSA) was obtained and cultured as previously described (12; WO03/072768; DSMZ n. 2029).

[0031] Clonogenic tests on cells following X-rays treatment in the presence or in the absence of rMnSOD Confluent 75 cm2 flasks of cells were trypsinized, counted with a haemocytometer and diluted in complete media to obtain 100 cells mL. Two mL of cell suspension was plated in each well of a 6 well tissue culture plate to obtain 200 cells per well. For

each cell line used in the present experiments were performed, in triplicate, clonogenic tests on four different cells groups:

A: CTRL as cells cultured in their specific medium and considered as negative control

B: SOD as cells treated in the presence of the sole rMnSOD to determine the effect of rMnSOD on clonogenic survival. The cells were treated with different concentration of rMnSOD (0-1.5 μM), trypsinized after 24 h and plated in drug-free medium.

C: RAD as cells irradiated in the absence of rMnSOD to determine the effect of radiation on clonogenic survival. The cells were irradiated (0-6 Gy) with X photons generated by a linear accelerator Philips SL 75 having nominal acceleration potential of 6 MV, and with 42, 127 U/Monitor and a dose-rate of 300 cGy/min.

D: RAD+SOD as cells irradiated in the presence of rMnSOD to determine the effect of combination treatment on clonogenic survival.

[0032] In the clonogenic tests to evaluate the effect of the sole rMnSOD on the normal or tumoural cells, it was noted that the concentration of 0.5 μM of rMnSOD is the concentration of which were not observed any harmful effects on the cell lines used. So to test the radiosensitizing or radioprotective effect of rMnSOD was chosen precisely the concentration of 0.5 μM.

[0033] The cells were treated with 0.5 μM rMnSOD for 24 h, irradiated and plated after 1 h. Colonies were stained with crystal violet after 14 days and those containing at last 30 cells were counted as surviving colonies. The plating efficiency and the survival fraction, for each cell line after each treatment, were calculated according to the method proposed by Franken (13) averaged approximately 80% for all cell lines. Survival was calculated in comparison to non-irradiated samples using an average of three determinations for the same dose-rate to cells (±SE). The surviving fraction of cells following the above mentioned dose of X-rays exposure, was used as a measure of cell sensitivity to X-rays and radioprotection of rMnSOD. In particular, the surviving fraction at a fixed X-rays exposure was used as a measure of cell sensitivity as several reports indicate that the clonogenic survival of cells at a fixed dose (usually 2 Gy of ionizing radiation) is a single parameter of the survival curve that correlates well with cell sensitivity (14-18).

[0034] The surviving fraction of cells following 0 to 6 Gy/min was able to discriminate between the radio-sensitivity of normal and cancer cells (19,20). Average values with standard deviation were determined from 3 independent experiments using different rMnSOD preparations.

Animals Treatment

[0035] Thirty-five female C57BL/6J mice, from Charles River, were used for all experimental procedures. Fifteen of them were divided into three groups of five animals each.

[0036] The first (1st) group was exposed to a lethal dose of ionizing radiations, achieved by using X-ray generated by a Linac (Philips SL 75) with a nominal potential of 6 MV and a dose-rate of 300 U.M./min. The mice were put in a dedicated phantom (21×30×35 cm3) and were irradiated with an isocentric technique. The prescription dose to mice (6 Gy) was delivered with two opposing fields (30×25 cm2), at source-phantom distance of 89.5 cm and depth of 10.5 cm. It was estimated, for each mouse, a minimum dose (at skin) of 5 Gy and a maximum dose (at mouse mid-line) of 6.3 Gy. Immediately after the radio-treatments, mice of 1st group were treated in the presence of 0.08 mg/kg rMnSOD in 100 μl PBS while the 2nd group received a daily injection of PBS. The 3rd group of animals did not receive the irradiation but was injected in the presence of 100 μl PBS. All animals were maintained in the standard feeding condition and with a cycle of dark and light. Seven days later the mice were sacrificed through cervical dislocation and their organs were examined in search of structural modifications and for the detection of the rMnSOD by immunochemical analysis. The other twenty animals were divided into four groups of five each. The first group received irradiation only, the second group received irradiation plus rMnSOD, the third group received rMnSOD only and the fourth group received only PBS. The animals were used to evaluate their survival after being exposed to ionizing radiation, in the presence or in the absence of rMnSOD. The observation of animals continued until 30 days that was considered as the experimental time point.

RNA Extraction

[0037] 50 mg of tissue derived from liver, kidney, ovary and heart of experimental C57Bl/6 mice exposed to ionizing radiations was used for total RNA extraction (RNAzol, Invitrogen) (21) according to the manufacturer's instructions and the integrity of all tested total RNA was verified by agarose gel electrophoresis.

[0038] Reverse transcription: 2 μg of total RNA in a final volume of 20 μl was reverse-transcribed by Avian myeloblastosis virus (AMV) reverse transcriptase (Gibco BRL-Invitrogen) according to manufacturer's instruction in presence of random examer primers at 37° C. per 60 min.

PCR Amplification

[0039] PCR analysis of AVEN gene expression was performed by using a Gene Amp PCR system 9700 (Applied Biosystem) with Taq Gold (Applera) and mouse sequence-specific primers. Actin was used as housekeeping control gene. The primer used were:

(SEQ ID No. 2)
Aven Fw GAA TCT CAG CGG GGC ACA G;

(SEQ ID No. 3)
Aven Rw GGG CAA GCA CCA GCA GCA G.

(SEQ ID No. 4)
Actin Fw GAC TAC CTC ATG AAG ATC CT;

(SEQ ID No. 5)
Actin Rw GCT TGC TGA TCC ACA TCT GC.

[0040] The PCR condition was: initial denaturation at 95° per 10 min followed by 36 cycles: 95°, 45"; 58°, 45" and 72° 45" with a final extension at 72° per 10 min.

[0041] The amplification products were run on 1% agarose gel in 0.5×TBE (Tris Borate EDTA) buffer for the control of the amplicons length.

Histology and Immunocytochemistry

[0042] Light Microscopy and immunochemical determinations were performed according to the methods previously described (9). The quantitative evaluation of the immunochemical determinations was obtained by using an Imaging Analyzer Leica Q50.

Statistical Analysis

[0043] Data obtained from the clonogenic tests on all cell lines (MCF-7, MRC-5, LSA) in two different condition: irradiated in absence (rad) and in the presence of rMnSOD (rad+

sod), were statistically analysed by using the linear-quadratic (LQ) formulation e-(αD+βD2) as model of biological response to radiation.

Results

[0044] Clonogenic Assay of Cells Irradiated in the Presence or in the Absence of rMnSOD

[0045] The biological effect of the sole rMnSOD on MRC-5 cells produces only a low inhibition of their growth rate, suggesting that rMnSOD at 0.5 or 1.5 μM is poorly toxic for normal cells. (FIG. **1**), while the exposure to ionizing radiations of MRC-5 cells, in the absence of rMnSOD resulted in the 90% of cell death. On the contrary, 80% of these cells, irradiated in the presence of rMnSOD, survived to radio-treatment and 14 days later, many colonies were counted (FIG. **2**).

[0046] In the test performed on MCF-7 cells, to kill all cancer cells with the sole rMnSOD, was enough a dose of 1.5 μM (FIG. **1**), and with the sole radiations, the killing effect was obtained with 5 Gy. (FIG. **3**). The same result was reached by irradiating the cells in the presence of 0.5 μM and 3 Gy of X-rays (FIG. **3**).

[0047] On the LSA cells was not found any damage when the cells were treated with the sole protein (FIG. **1**) or with the sole radiations (FIG. **4**), but a rapid mortality of LSA cells was observed when the cells were irradiated with a dose of 3 Gy and in the presence of 0.5 μM rMnSOD (FIG. **4**).

Statistical Analysis

[0048] The statistical analysis of the clonogenic tests on the cell lines underwent to irradiation in the presence or in the absence of rMnSOD by using the linearquadratic (LQ) formulation $e^{-(\alpha D+\beta D}2)$ as model of biological response to radiation, was significant and allowed the determination of the α/β ratio for all treated cells lines. By these data it is possible to observe that rMnSOD exerts a radiosensitizing effect on the MCF-7 and LSA cells, while for the MRC-5 cell line the rMnSOD provides a radio-resistance ($\alpha/\beta_{radsod}<\alpha/\beta_{rad}$) (Table II).

TABLE II

	R^2	α	β	α/β
		MCF-7 cells		
Rad	0.969	−0.33 ± 0.18	0.21 ± 0.07	−1.5 ± 0.9
Rad + rMnSOD	0.999	−0.13 ± 0.11	071 ± 0.10	0.2 ± 0.2
		MRC-5 cells		
Rad	0.985	−0.19 ± 0.11	0.19 ± 0.04	−1.0 ± 0.6
Rad + rMnSOD	0.536	−0.03 ± 0.007	0.0011 ± 0.0011	−3 ± 7
		LSA cells		
Rad	0.709	−0.014 ± 0.006	0.0016 ± 0.0010	−9 ± −7
Rad + rMnSOD	0.993	−0.18 ± 0.08	−0.21 ± 0.03	−0.8 ± 0.4

Radio-Treatments of Healthy Animals in the Presence or in the Absence of rMnSOD

[0049] After radio-treatment each animal of the test group (3rd), received an intraperitoneal injection (i.p) of rMnSOD (0.08 mg/kg), and the injections continued for 6 additional days. The control group (2nd) received only an equal volume of PBS i.p. At the histological analysis, the selected organs (Heart, Cervix uterus, Liver and Kidneys) of animals treated in the presence of rMnSOD, did not show signs of radio-damages. The presence of rMnSOD in the animal's tissues exposed to radio-treatments was detected and quantified, by immunochemical analysis, using an imaging analyzer Leica Q50. The presence of rMnSOD was only observed in the interstitial spaces of the animal's tissues who underwent radiotreatment in the presence of rMnSOD. On the contrary, the control mice, which did not receive rMnSOD injections, showed clear signs of radio-necrosis, and their tissues were found free of rMnSOD in the interstitial space (FIG. **5** A-R). Moreover, in parallel experiments, 80% of animals irradiated and daily treated in the presence of rMnSOD, (0.08 mg/kg) were still alive after 30 days from the radio-treatment, considered as the time point of experiment, while the control group irradiated in the absence of rMnSOD died after 6-7 days from the radiotreatment (Table I).

[0050] The quantitative analysis of the immunochemical localization of rMnSOD in the animal's tissue irradiated in the presence or in the absence of rMnSOD was correlated to its radioprotective effect. The differences in radioprotection on animals between rMnSOD and mock-treated groups of mice were assessed using the Fisher's exact test ($p<0.02$).

TABLE I

		% Positive Stromal cells	% Positive Parenchimal cells	Statistic evaluation on 50 areas
Heart	Control	2%	3%	P > 0.001
	Treated	25%	30%	
Kidney	Control	6%	10%	P > 0.005
	Treated	6%	40%	
Liver	Control	6%	10%	P > 0.001
	Treated	60%	80%	
Cervix	Control	1%	2%	P > 0.001
Utery	Treated	60%	40%	

AVEN Expression in Irradiated Mice in Presence o in the Absence of rMnSOD

[0051] The Aven anti-apoptotic gene was found constitutively activated in the healthy animals who did not receive any kind of treatments. In the group of animals who underwent to lethal doses of X-rays, in the absence of rMnSOD, the Aven gene was found completely switched off and their organs structurally degenerated. On the contrary, at the 7th day of treatment the Aven gene expression was decreased in the animal's organs who were treated with rMnSOD, following the lethal dose of X-rays. However after 14 days from irradiation, the gene resulted fully active, indicating that the radio-damage was recovered (FIG. **6**).

[0052] The data presented show that rMnSOD, a specific human recombinant isoform of Manganese Superoxide Dismutase liposarcoma derived, produces a radio-protective effect on normal cells while it is radio-sensitizing for cancer cells, both in vitro and in vivo. In particular, we have observed that the exposure to ionizing irradiation of human normal fibroblasts(MRC-5 cell line) with different doses of X-rays, have point out that the radio-damages were dose dependent (as expected) and that the 3 Gy of X-rays could be sufficient to kill cells after 14 days from irradiation. The same cells, grown in the presence of the sole rMnSOD, at a growing concentrations, until the maximal dose of 1.5 μM/100 μl PBS, did not influence negatively on the cell growth in the clonogenic test. On the contrary, when the same cells were exposed to lethal dose (6 Gy) of X-rays and in the presence of 0.5 μM/100 μl PBS rMnSOD, the cells were clearly protected from radio-damage.

[0053] On the tumor cells the effect of rMnSOD was radiosensitizing. Indeed, while for the MCF-7 cells, the killing effect with the sole radiation was reached with 4 Gy, or with the sole rMnSOD with 0.5 μM/100 μl PBS. The same signifi-

cant killing effect was obtained by the exposure of these cells with only 2 Gy of ionizing radiations, and in the presence of only 0.5 μM/100 μl PBS.

[0054] Also in the case of liposarcoma, the same radio-sensitizing effect of rMnSOD was observed, although with some difference that reflects the characteristic radioresistance of liposarcoma. On these cells the sole lethal dose (6 Gy) of x-rays or the sole maximal dose of rMnSOD, i.e. 1.5 μM/100 μl PBS, not have the slightest impact on the cell growth and therefore their survival.

[0055] On the contrary, when the LSA cells were irradiated with only 3 Gy of X-rays and in the presence of 0.5 μM/100 μl PBS rMnSOD, a significant killing effect was registered, thereby indicating that the protein has a clear radio-sensitizing role on the cancer cells tested.

[0056] Although have been used only two cancer cell lines, the fact that ionizing radiations produce free radicals in all the cells, suggests that the rMnSOD could be useful to amplify the radio-damage effect for all kind of cancers.

[0057] Moreover, the convinction that it is precisely the rMnSOD to provide radioprotection or radio-sensitizing, derives by the observations that when it was used a commercial SOD or a thermal inactivated rMnSOD both the effects were not highlighted.

[0058] Both the observed effect, respectively, on the normal and tumoural cells could have a common molecular base which was previously discussed (9,10). Briefly, it is being linked to the fact that in cancer cells, unlike normal cells, are produced limited amounts of catalase (22,23) which converts hydrogen peroxide into molecular oxygen. Since ionizing radiations, as indeed any other anticancer molecule, induce the production of high levels of free radicals both in normal cells and in cancer cells, the threshold of toxicity will be achieved more easily in cancer cells than in normal ones and thus leading tumor cells to apoptosis (10).

[0059] The presence of rMnSOD in the irradiated cells might create an oxidative difference that leads to preferential inhibition of cell proliferation and increases cell death in cancer cells. Such mechanism seems to be very promising since it could foresee a therapeutic use of rMnSOD to amplify the effect of anticancer radiotherapies, especially in the case of radio-resistant tumours like liposarcoma and, at the same time, to reduce their dose-rate.

[0060] Further the study was extended to investigate if the radioprotective effect of rMnSOD is obtained also when the cells are exposed to proton beams, in the presence or in the absence of the rMnSOD. Thus normal (MRC-5) and tumoral (MCF-7 and LSA) cells were exposed to 62 Mev equivalent from proton beams. The results clearly indicated that the rMnSOD provide the same selective effect also in the case of proton beams (FIG. **7**). Such protection is of relevance as protective and therapeutic means of subjects exposed to space radiations.

[0061] Radio-protective and radio-sensitizing effects of MnSOD have already been reported by using molecular medicine and gene-therapy methods (24-28). However prior art cases require methods necessitating the manipulation of the MnSOD, to get the molecule into the cells. In the case of the rMnSOD used in the instant invention, the protein is easily administrable in vivo, and does not require any prior manipulation. This is an undoubted advantage for therapeutic applications.

[0062] The radio-protective effect of rMnSOD was also studied in vivo. Animals exposed to lethal doses of X-rays and daily injected with 0.08 mg/kg rMnSOD resulted protected by the damages generated by ionizing radiations. The animal's organs irradiated in the presence of rMnSOD showed an high and statistically significant concentration of rMnSOD at the interstitial spaces level that was absolutely absent in the animals who did not receive the rMnSOD treatment following the ionizing radiation. Moreover, in all of animals which did not receive the rMnSOD, the organs resulted completely degenerated, leading to animals death after only 7-8 days from the radio-treatments. On the contrary, animals who received the rMnSOD treatment were still alive 30 days after the radiation. Also in these cases, the thermally inactivated rMnSOD or the commercially available SOD (Sigma) used as control, did not show the same radio-protection effect or survival rate. These data suggest that rMnSOD might protect the mitochondria thus contributing to maintain their integrity. This hypotheses, is indeed strongly supported by the results obtained by molecular analysis of the expression of the anti-apoptotic Aven gene in all the examined animal's tissues. The Aven gene was actively expressed in control animals that had not undergone radiating treatment, while it appeared completely switched off in those animals irradiated in the absence of rMnSOD. In the animals irradiated in the presence of rMnSOD, the Aven gene was partially inactivated up to the 7th day after the irradiation. However, after 14 days, the Aven gene turned to be fully active, suggesting that the damaged tissues were completely restored, and that rMnSOD provided protection of the normal cells by inhibiting the apoptotic pathway, and it is appropriate to point out that these data also agree with that one observed in vitro, on normal fibroblasts. The product of the Aven gene binds the cytochrome-c released by the injuried mitochondria during apoptosis. A high amount of cytochrome-c inactivates the Aven gene facilitating the caspases activation, which in turn will lead damaged cells to death (29-32). Then rMnSOD provides a protective effect by inhibiting the inactivation of the Aven gene, and more probably by shielding the mitochondria from radio-damages, inhibiting cytochrome-c release.

[0063] By considering the enzymatic nature of rMnSOD, usually confined into the mitochondrial matrix, we believe that this latter hypotheses could be more reasonable, although it has not yet been well investigated and not yet clarified. The use of a single and lethal dose radiation in experiments on animals is certainly restraining and does not allow us to understand exactly the limits within which rMnSOD exerts its radio-protective effect or its radio-sensitizing one in cancer cells. Notwithstanding, we believe that the enhanced survival of the animals treated was due to the sole rMnSOD. Therefore, among the several observed radioprotection structural, ultra-structural or molecular indicators, both in vitro and in vivo, the one related to the survival of animals exposed to lethal dose of x-Rays is the most convincing. A further study on a large population of animals is, however, necessary. New experiments will have to test, for instance, the effects of larger doses of ionizing radiations and rMnSOD, as we have done with the in vitro experiments. At the same time, it will also be necessary to extent the investigation rMnSOD's radioprotection effect on all the wide range of ionizing radiations, included those produced by protons and heavy ions, which are particularly present in the cosmic space and in our lab we are currently working on such topics.

[0064] In conclusion, the data presented clearly indicate that the rMnSOD provides a radio-protection for normal cells and confirm also the previous observations of a radio-protective effect of MnSOD proposed by others researches. At the same time, the rMnSOD was radio-sensitizing for tumour cells, and both the effects resulted statistically significant. Such data could lead to direct applications in clinical practice, especially because the molecule does not require any manipulation to be safely injected into organisms, its therapeutic

potentiality, as well as the possibility to prevent the damages generated by exposure of normal cells to ionizing radiations, indicate that the rMnSOD deserves to be considered as a tool to amplify the effects of cancer radio-therapy, increasing their specific and selective effect on cancer cells and, at the same time to provide a protection to the organism daily or accidentally exposed to ionizing radiations.

BIBLIOGRAPHY

[0065] 1) Epperly, M. W.; Gretton, J. E.; Sikora, C. A.; Jefferson, M.; Bernarding, M.; Nie, S.; and Greenberger, J. S. Mitochondrial localization of superoxide dismutase is required for decreasing radiation cellular damage. Radiat Res; 160: 568-578; 2003

[0066] 2) Valko, M.; Rhodes, C. J.; Moncol, J.; Izakovic, M.; Mazur, M.; Free radicals, metals and antioxidants in oxidative stress-induced cancer. Chem Biol Interact.; 160: 1-40; 2006

[0067] 3) Robbins, M. E.; Zhao, W.; Chronic oxidative stress and radiation-induced late normal tissue injury: a review. Int J Radiat Biol.; 80:251-259; 2004

[0068] 4) Zhao, W.; Diz, D. I.; Robbins, M. E.; Oxidative damage pathways in relation to normal tissue injury. Br J Radiol. 80:23-31; 2007

[0069] 5) Kalen, A. L.; Sarsour, E. H., Venkataraman, S.; Goswami, P. C.; Mn-superoxide dismutase overexpression enhances G2 accumulation and radioresistance in human oral squamous carcinoma cells. Antioxid Redox Signal. 8:1273-1281; 2006

[0070] 6) Martin, R. C.; Ahn, J.; Nowell, S. A.; Hein, D. W.; Doll, M. A.; Martini, B. D. et al. Association between manganese superoxide dismutase promoter gene polymorphism and breast cancer survival. Breast Cancer Res; 8:R45; 2006

[0071] 7) Stenlund, P. and Tibell, L. A. Chimeras of human extracellular and intracellular superoxide dismutases. Analysis of structure and function of the individual domains. Protein Eng; 12:319-325; 1999

[0072] 8) Greenberger, J. S.; Epperly, M. W.; Gretton, J.; Jefferson, M.; Nie, S., Bernarding, M.; Kagan, V.; and Guo, H. L. Radioprotective Gene Therapy. Curr Gene Ther.; 3:183-95; 2003

[0073] 9) Mancini, A.; Borrelli, A.; Schiattarella, A.; Fasano, S.; Occhiello, A.; Pica, A.; Tommasino, M.; Nüesch, J. P. F.; and Rommelaere, J. Tumor Suppressive Activity of a Variant Isoform of Mn Superoxide Dismutase Released by a Human Liposarcoma Cell Line. Int. J. Cancer: 119, 932-943; 2006

[0074] 10) Mancini, A.; Borrelli, A.; Schiattarella, A.; Aloj, L; Aurilio, M.; Morelli, F., Pica, A;. Occhiello, A; Lorizio, R.; Mancini, R; Sica, A; Mazzarella, L; Sica, F.; Grieco, P.; Novellino, E.; Pagnozzi, D; Pucci, P; and Rommelaere J. Biophysical and Biochemical Characterization of a Liposarcoma Derived Recombinant MnSOD Protein Acting as Anticancer Agent. Int. J. Cancer: 123, 2684-2695 (2008); 2008

[0075] 11) McCord, J. M.; Fridovich, I.; Superoxide dismutase. An enzymic function for erythrocuprein (hemocuprein). J Biol. Chem.; 244:6049-55; 1969

[0076] 12) Mancini A.; Garbi C.; D'Armiento, F.; Borrelli A.; and Ambesi-Impiombato F. S. Culture and cloning of an adipocytes cell line from a human liposarcoma. Bollettino dell'Istituto dei Tumori di Napoli.; 38:43-49; 1991

[0077] 13) Franken, N. A.; Rodermond, H. M.; Stap, J.; Haveman, J.; van Bree, C. Clonogenic assay of cells in vitro. Nat. Protoc. 1; 2315-19; 2006

[0078] 14) Biade, S.; Stobbe, C.; and Chapman J. D. The intrinsic radiosensitivity of some human tumor cells throughout their cell cycles. Radiat Res; 147: 416-421; 1997

[0079] 15) Tucker, S. L.; Is the mean inactivation dose a good measure of cell radiosensitivity? Radiat Res; 105:18-26; 1986

[0080] 16) Tucker, S. L. Parameters of radiosensitivity. Radiat Res.; 108:226-9; 1986

[0081] 17) Fertil, B.; and Malaise, E. P. Intrinsic radiosensitivity of human cell lines is correlated with radioresponsiveness of human tumors: Analysis of 101 published survival curves. Int J Radiat Oncol Biol Phys; 11:1699-1707; 1985

[0082] 18) Malaise, E. P. Fertil, B.; Chavaudra, N.; Guichard, M; Distribution of radiation sensitivities for human tumor cells of specific histological types: Comparison of in vitro to in vivo data. Int J Radiat Oncol Biol Phys; 12:617-624; 1986

[0083] 19) Deschavanne, P. J.; Debieu, D.; Fertil, B.; Malaise, E. P.; Re-evaluation of in vitro radiosensitivity of human fibroblasts of different genetic origins. Int J Radiat Biol; 50 279-293; 1986.

[0084] 20) Malaise, E. P.; Fertil B.; Deschavanne, P. J.; Chavaudra, N.; Brooks W. A. Initial slope of radiation survival curves is characteristic of the origin of primary anestablished cultures of human tumor cells and fibroblasts. Radiat. Res. 111, 319-333; 1987

[0085] 21) Chomczynski, P.; Sacchi, N. The single-step method of RNA isolation by acid guanidinium thiocyanate-phenol-chloroform extraction: twenty-something years on. Nat. Protoc.; 1:581-5; 2006

[0086] 22) Chung-man Ho, J.; Zheng, S.; Comhair, S. A.; Farver, C.; Erzurum, S. C. Differential expression of manganese superoxide dismutase and catalase in lung cancer. Cancer Res; 61:8578-85; 2001

[0087] 23) Pljesa-Ercegovac, M.; Mimic-Oka, J.; Dragicevic, D.; Savic-Radojevic, A.; Opacic, M.; Pljesa, S.; Radosavljevic, R.; Simic, T. Altered antioxidant capacity in human renal cell carcinoma: role of glutathione associated enzymes. Urol Oncol.; 26:175-81; 2008

[0088] 24) Greenberger, J. S.; Epperly, M. W. Antioxidant gene therapeutic approaches to normal tissue radioprotection and tumor radiosensitization. In Vivo.; 21:141-6; 2007

[0089] 25) Epperly M. W.; Epstein, C. J.; Travis, E. L. and Greenberger J. S. Decreased Pulmonary Radiation Resistance of Manganese Superoxide Dismutase (MnSOD)-Deficient Mice Is Corrected by Human Manganese Superoxide Dismutase-Plasmid/Liposome (SOD2-PL) Intratracheal Gene Therapy. Radiation Research, 154:365-374; 2000

[0090] 26) Dolgachev, V.; Oberley, L. W.; Huang, T. T.; Kraniak, J. M.; Tainsky, M. A.; Hanada, K.; Separovic, D. A role for manganese superoxide dismutase in apoptosis after photosensitization Biochem Biophys Res Commun.; 332:411-7; 2005.

[0091] 27) Murley, J. S.; Kataoka, Y.; Cao, D.; Li, J. J.; Oberley, L. W.; Grdina D. J Delayed radioprotection by NF kappa B-mediated induction of Sod2 (MnSOD) in SA-NH tumor cells after exposure to clinically used thiolcontaining drugs. Radiat Res. 162:536-46; 2004

[0092] 28) Yan, S.; Brown; S. L.; Kolozsvary, A.; Freytag, S. O.; Lu, M.; Kim, J. H. Mitigation of radiation-induced skin injury by AAV2-mediated MnSOD gene therapy. J Gene Med.; 10:1012-8; 2008

[0093] 29) Chau, B. N.; Cheng, E. H.; Kerr, D. A.; Hardwick, J. M.; Aven, a novel inhibitor of caspase activation, binds Bcl-xL and Apaf-1. Mol Cell 6:31-40; 2000

[0094] 30) Liu, X.; Kim, C. N.; Yang, J.; Jemmerson, R.; Wang, X. Induction of apoptotic program in cell-free extracts: requirement for dATP and cytochrome c, Cell 86:147-157; 1996

[0095] 31) Bertini, I.; Cavallaro, G.; Rosato, A.; Cytochrome c: occurrence and functions. Chem. Rev. 106:90-115; 2006.

[0096] 32) Bernard, D.; Gosselin, K.; Monte, D.; Vercamer, C.; Bouali, F.; Pourtier, A.; Vandenbunder, B.; Abbadie, C. Involvement of Rel/nuclear factor-transcriptor factors in keratinocytes senescence. Cancer res. 64:472-481; 2004.

SEQUENCE LISTING

<160> NUMBER OF SEQ ID NOS: 5

<210> SEQ ID NO 1
<211> LENGTH: 222
<212> TYPE: PRT
<213> ORGANISM: Homo sapiens
<300> PUBLICATION INFORMATION:
<308> DATABASE ACCESSION NUMBER: P04179
<309> DATABASE ENTRY DATE: 1990-04-01
<313> RELEVANT RESIDUES IN SEQ ID NO: (1)..(222)

<400> SEQUENCE: 1

```
Met Leu Ser Arg Ala Val Cys Gly Thr Ser Arg Gln Leu Ala Pro Ala
1               5                   10                  15

Leu Gly Tyr Leu Gly Ser Arg Gln Lys His Ser Leu Pro Asp Leu Pro
            20                  25                  30

Tyr Asp Tyr Gly Ala Leu Glu Pro His Ile Asn Ala Gln Ile Met Gln
        35                  40                  45

Leu His His Ser Lys His His Ala Ala Tyr Val Asn Asn Leu Asn Val
    50                  55                  60

Thr Glu Glu Lys Tyr Gln Glu Ala Leu Ala Lys Gly Asp Val Thr Ala
65                  70                  75                  80

Gln Ile Ala Leu Gln Pro Ala Leu Lys Phe Asn Gly Gly Gly His Ile
                85                  90                  95

Asn His Ser Ile Phe Trp Thr Asn Leu Ser Pro Asn Gly Gly Gly Glu
            100                 105                 110

Pro Lys Gly Glu Leu Leu Glu Ala Ile Lys Arg Asp Phe Gly Ser Phe
        115                 120                 125

Asp Lys Phe Lys Glu Lys Leu Thr Ala Ala Ser Val Gly Val Gln Gly
    130                 135                 140

Ser Gly Trp Gly Trp Leu Gly Phe Asn Lys Glu Arg Gly His Leu Gln
145                 150                 155                 160

Ile Ala Ala Cys Pro Asn Gln Asp Pro Leu Gln Gly Thr Thr Gly Leu
                165                 170                 175

Ile Pro Leu Leu Gly Ile Asp Val Trp Glu His Ala Tyr Tyr Leu Gln
            180                 185                 190

Tyr Lys Asn Val Arg Pro Asp Tyr Leu Lys Ala Ile Trp Asn Val Ile
        195                 200                 205

Asn Trp Glu Asn Val Thr Glu Arg Tyr Met Ala Cys Lys Lys
    210                 215                 220
```

<210> SEQ ID NO 2
<211> LENGTH: 19
<212> TYPE: DNA

-continued

<213> ORGANISM: Artificial Sequence
<220> FEATURE:
<223> OTHER INFORMATION: primer

<400> SEQUENCE: 2

gaatctcagc ggggcacag 19

<210> SEQ ID NO 3
<211> LENGTH: 19
<212> TYPE: DNA
<213> ORGANISM: Artificial Sequence
<220> FEATURE:
<223> OTHER INFORMATION: primer

<400> SEQUENCE: 3

gggcaagcac cagcagcag 19

<210> SEQ ID NO 4
<211> LENGTH: 20
<212> TYPE: DNA
<213> ORGANISM: Artificial Sequence
<220> FEATURE:
<223> OTHER INFORMATION: primer

<400> SEQUENCE: 4

gactacctca tgaagatcct 20

<210> SEQ ID NO 5
<211> LENGTH: 20
<212> TYPE: DNA
<213> ORGANISM: Artificial Sequence
<220> FEATURE:
<223> OTHER INFORMATION: primer

<400> SEQUENCE: 5

gcttgctgat ccacatctgc 20

1. A method for protecting a subject from exposure to radiations comprising the administration of an effective protective amount of rMnSOD of SEQ ID No. 1. or functional fragments thereof.

2. The method according to claim **1** wherein the rMnSOD is administered in an amount from 0.08 g/Kg body weight to 0.1 g/Kg body weight for at least 30 days before the exposure to radiations.

3. The method according to claim **1** wherein said radiations are space radiations.

4. The method according to claim **1** wherein said radiations are sun radiations.

5. The method according to claim **1** wherein said radiations are from depleted uranium.

6. The method according to claim **1** wherein said radiations are from anti-tumoral metabolic therapies administration of radioactive isotopes.

7. The method according to claim **1** wherein said radiations from radioactive isotopes for radio-diagnostics.

8. The method according to claim **1** wherein said radiations are ionizing and/or protonizing radiations.

9. A method for treating a subject exposed to radiations comprising the administration of an effective therapeutically active amount of rMnSOD of SEQ ID No. 1, or functional fragments thereof.

10. The method according to claim **9** wherein the rMnSOD is administered in an amount from 0.08 g/Kg body weight to 0.1 g/Kg body weight for at least 30 days after the exposure to radiations.

11. The method according to claim **9** wherein said radiations are space radiations.

12. The method according to claim **9** wherein said radiations are ionizing and/or protonizing radiations.

* * * * *

ITALIAN PATENT OFFICE

Document No.

102014902299335A1

Publication Date

20160408

Applicant

AGENZIA SPAZIALE ITALIANA

Title

PANNELLO SANDWICH DI PROTEZIONE TERMICA

PANNELLO SANDWICH DI PROTEZIONE TERMICA

* * *

La presente invenzione riguarda un pannello sandwich di protezione termica che consente in modo efficiente, affidabile, semplice, ed economico di integrare in un unico componente la resistenza termica necessaria per la protezione di strutture ad altissime temperature e la funzione strutturale per la realizzazione di dispositivi di protezione termica comprendenti uno o più pannelli sandwich ed operanti da struttura primaria, a titolo esemplificativo, ma non limitativo, di un veicolo aerospaziale. In particolare, il pannello sandwich secondo l'invenzione può essere impiegato per applicazioni in cui si verificano elevate temperature di esercizio e importanti sollecitazioni meccaniche, ad esempio per applicazioni aerospaziali ed aeronautiche (e.g. consentendo una protezione termica durante la fase di rientro atmosferico, in particolare di aeromobili ipersonici), automobilistiche, ferroviarie e navali nonché per applicazioni nel settore energetico e nucleare. La presente invenzione riguarda altresì un procedimento di fabbricazione del pannello sandwich.

Sebbene nel seguito venga principalmente fatto riferimento ad applicazioni del pannello sandwich secondo l'invenzione ai settori aerospaziale ed aeronautico, si deve comprendere che il pannello sandwich secondo l'invenzione può essere utilizzato per qualsiasi applicazione in cui si verificano elevate temperature di esercizio ed importanti sollecitazioni meccaniche, ad esempio per applicazioni automobilistiche, ferroviarie e navali nonché per applicazioni nel settore energetico e nucleare, rimanendo nell'ambito di protezione come definito dalle rivendicazioni allegate.

E' noto che in alcune applicazioni aerospaziali ed aeronautiche, allo scopo di minimizzare il più possibile la quantità di calore trasmessa alla struttura di un aeromobile, e.g. un aeromobile ipersonico durante la fase di rientro atmosferico, vengono utilizzati dispositivi di protezione termica.

Attualmente esistono diverse soluzioni per la protezione termica di aeromobili che possono essere raggruppate in due categorie: protezioni termiche

ablative e protezioni termiche riutilizzabili. La scelta del tipo di protezione termica da impiegare dipende essenzialmente dal tipo di missione cui è destinato il velivolo da proteggere e dalle caratteristiche termo-meccaniche cui è sottoposto, come descritto ad esempio da J. Howe in "*Hypervelocity Atmospheric Flight: Real Gas Flow Fields*", NASA TM 101055, 1989.

Le protezioni termiche ablative garantiscono la protezione dissipando energia attraverso il meccanismo di ablazione. Per tale motivo non sono dei dispositivi riutilizzabili e vanno necessariamente sostituiti dopo ogni utilizzo. Questo tipo di protezioni si rendono indispensabili per profili di missione caratterizzati da alte velocità e da particolari condizioni termodinamiche del flusso incidente altamente energetico.

Le protezioni termiche riutilizzabili sono caratterizzate da una elevata emissività che consente di re-irradiare verso l'esterno circa l'80% dell'energia incidente riducendo notevolmente il calore che raggiunge la struttura, e.g. come descritto da B. Laub et al nell'articolo "*Thermal Protection System Technology and Facility Needs for Demanding Future Planetary Missions*" presentato all'International Workshop on Planetary Probe Atmospheric Entry and Descent Trajectory Analysis and Science, Lisbon, Portugal, 6-9 October 2003. I materiali utilizzati sono materiali a bassa densità e quindi molto più leggere dei materiali ablativi, che sono invece ad alta densità (e conseguentemente più pesanti). Inoltre, al fine di garantire una maggiore resistenza all'ossidazione ed una maggiore emissività, vengono di solito applicati dei rivestimenti superficiali. La morfologia, la tecnica di deposizione ed il materiale utilizzato per la deposizione di tali rivestimenti varia a seconda delle caratteristiche dei flussi termici incidenti (i.e. della radiazione incidente).

Come detto, la scelta della tipologia di protezione da utilizzare è legata principalmente al tipo di missione a cui è destinato il velivolo e alle caratteristiche aero-termodinamiche dello stesso. Inoltre, differenti zone dell'aeromobile possono essere soggette a differenti sollecitazioni termo-meccaniche dovute a differenti condizioni di flusso termico incidente determinate dal profilo aerodi-

namico a cui è sottoposta la struttura.

Nella tecnica anteriore, sono state sviluppate varie soluzioni di protezione termica riutilizzabile, come quelle, ad esempio, messe a punto dalla NASA nell'ambito del progetto Shuttle. Tali soluzioni, basate sul concetto di struttura passiva, prevedono l'utilizzo sia di schiume (*foam*) o materassini (*mat*), sia di elementi rigidi in fibra di carbonio, che vengono ancorati alla struttura primaria attraverso l'impiego di rivetti, bulloni o collanti e che vanno a costituire un supporto alla struttura primaria stessa.

Il documento US 2009/0149100 A1 descrive un'altra soluzione di protezione termica in materiale composito rinforzato con fibre realizzato a partire da una preforma avente una pluralità di strati verticali ed una pluralità di strati orizzontali di tessuto che si intersecano definendo una pluralità di celle cave all'interno della preforma.

Altre analoghe soluzioni di protezione termica riutilizzabile sono state descritte da D. E. Glass in *Ceramic Matrix Composite (CMC) Thermal Protection Systems (TPS) and Hot Structures for Hypersonic Vehicles*, 15th AIAA International Space Planes and Hypersonic Systems and Technologies Conference, 2008, e da B. Behrens et al. in *Technologies for thermal protection systems applied on reusable launcher*, Acta Astronautica, Vol. 55, No. 3-9, November 2004, pp. 529-536.

Tuttavia, le soluzioni della tecnica anteriore soffrono di alcuni inconvenienti.

Innanzitutto, per renderle completamente affidabili, è necessario accoppiare le protezioni termiche alla struttura portante dell'aeromobile tramite arrangiamenti piuttosto complessi e, di conseguenza, costosi. Ciò comporta altresì che il disegno delle protezioni termiche non consente un facile accesso alla struttura portante dall'esterno, rendendo necessaria la rimozione delle protezioni termiche per eseguire eventuali operazioni di ispezione e/o manutenzione.

Inoltre, i procedimenti di fabbricazione di tali protezioni termiche risultano piuttosto complessi, lunghi e costosi.

Lo scopo della presente invenzione è, pertanto, quello di consentire, in modo efficiente, affidabile, semplice, ed economico di realizzare una protezione termica riutilizzabile per applicazioni in cui si verificano elevate temperature di esercizio e importanti sollecitazioni meccaniche.

Forma oggetto specifico della presente invenzione un pannello sandwich di protezione termica comprendente:

- una pelle inferiore disposta su una faccia interna del pannello sandwich non esposta all'ambiente,
- un nucleo centrale,
- una pelle superiore disposta su una faccia esterna del pannello sandwich esposta all'ambiente, ed
- un rivestimento superficiale applicato sulla pelle superiore configurato per proteggere la pelle superiore dall'ossidazione,

la pelle inferiore essendo solidalmente accoppiata ad una prima faccia del nucleo centrale tramite un primo strato di adesivo, la pelle superiore essendo solidalmente accoppiata ad una seconda faccia del nucleo centrale, contrapposta alla prima faccia del nucleo centrale, tramite un secondo strato di adesivo, per cui la pelle inferiore e la pelle superiore sono incollate al nucleo centrale, la pelle inferiore essendo realizzata in materiale composito selezionato dal gruppo comprendente carbonio rinforzato da fibre di carbonio e carbonio rinforzato da fibre in carburo di silicio, la pelle superiore essendo realizzata in materiale composito selezionato dal gruppo comprendente carbonio rinforzato da fibre di carbonio e carbonio rinforzato da fibre in carburo di silicio, il nucleo centrale essendo realizzato con una schiuma a base di carburo di silicio.

Secondo un altro aspetto dell'invenzione, detta schiuma a base di carburo di silicio può avere una densità di pori variabile da 60 a 140 PPI (Pores per inch – pori per pollice - in cui 1 pollice è pari a 2,54 cm), opzionalmente da 70 a 130 PPI, più opzionalmente da 80 a 120 PPI, ancora più opzionalmente da 90 a 110 PPI.

Secondo un ulteriore aspetto dell'invenzione, il nucleo centrale 12 può

avere spessore variabile da 8 mm a 40 mm, opzionalmente da 12 mm a 36 mm, più opzionalmente da 16 mm a 32 mm, ancora più opzionalmente da 20 mm a 28 mm, persino più opzionalmente da 23 mm a 25 mm.

Secondo un aspetto aggiuntivo dell'invenzione, la pelle superiore può avere spessore variabile da 1 mm a 10 mm, opzionalmente da 1,5 mm a 8 mm, più opzionalmente da 2 mm a 6 mm, ancora più opzionalmente da 2 mm a 4 mm.

Secondo un altro aspetto dell'invenzione, la pelle inferiore può avere spessore variabile da 1 mm a 10 mm, opzionalmente variabile da 1,5 mm a 8 mm, più opzionalmente variabile da 2 mm a 6 mm, ancora più opzionalmente variabile da 2 mm a 4 mm, persino più opzionalmente pari a 3mm.

Secondo un ulteriore aspetto dell'invenzione, la pelle inferiore e la pelle superiore possono essere realizzate nello stesso materiale.

Secondo un aspetto aggiuntivo dell'invenzione, la pelle inferiore e la pelle superiore possono essere entrambe realizzate in carbonio rinforzato da fibre in carburo di silicio.

Secondo un altro aspetto dell'invenzione, l'adesivo del primo strato può essere selezionato dal gruppo comprendente resina fenolica carbonizzata, adesivi a base di grafite, adesivi a base di ossido di alluminio, adesivi a base di allumina-silice, adesivi a base di carbonio, adesivi a base di carburo di silicio, adesivi a base di nitruro di boro, adesivi a base di ossido di ittrio, adesivi a base di ossido di zirconia, e l'adesivo del secondo strato può essere selezionato dal gruppo comprendente resina fenolica carbonizzata, adesivi a base di grafite, adesivi a base di ossido di alluminio, adesivi a base di allumina-silice, adesivi a base di car- bonio, adesivi a base di carburo di silicio, adesivi a base di nitruro di boro, adesivi a base di ossido di ittrio, adesivi a base di ossido di zirconia.

Secondo un ulteriore aspetto dell'invenzione, l'adesivo del primo strato e l'adesivo del secondo strato possono avere ognuno un materiale riempitivo di tipo grafitico, opzionalmente l'adesivo del primo strato e l'adesivo del secondo strato essendo ognuno un adesivo liquido di tipo ceramico a base grafitica.

Secondo un aspetto aggiuntivo dell'invenzione, il primo strato di adesivo

può avere spessore variabile da 0,1 mm a 1 mm, opzionalmente variabile da 0,2 mm a 0,8 mm, più opzionalmente variabile da 0,2 mm a 0,8 mm, ancora più opzionalmente pari a 0,4 mm, ed il secondo strato di adesivo può avere spessore variabile da 0,1 mm a 1 mm, opzionalmente variabile da 0,2 mm a 0,8 mm, più opzionalmente variabile da 0,2 mm a 0,8 mm, ancora più opzionalmente pari a 0,4 mm.

Secondo un altro aspetto dell'invenzione, il rivestimento superficiale può comprendere uno o più materiali selezionati dal gruppo comprendente zirconia, zirconia stabilizzata con ittrio, e carburo di silicio (SiC).

Secondo un ulteriore aspetto dell'invenzione, il rivestimento superficiale può avere spessore variabile da 0,1mm a 0,5mm.

Forma altresì oggetto specifico della presente invenzione un procedimento di fabbricazione di un pannello sandwich di protezione termica come descritto, il procedimento comprendendo le seguenti fasi:

A. avere a disposizione una pelle inferiore realizzata in materiale composito selezionato dal gruppo comprendente carbonio rinforzato da fibre di carbonio e carbonio rinforzato da fibre in carburo di silicio, un nucleo centrale realizzato con una schiuma a base di carburo di silicio, ed una pelle superiore realizzata in materiale composito selezionato dal gruppo comprendente carbonio rinforzato da fibre di carbonio e carbonio rinforzato da fi- bre in carburo di silicio;
B. disporre un primo substrato, selezionato tra la pelle inferiore ed il nucleo centrale, in una prima cornice in modo da avere una faccia del primo substrato accessibile;
C. accoppiare alla prima cornice due o più fili calibrati ad una distanza da una superficie della faccia accessibile del primo substrato;
D. deporre un primo adesivo sulla faccia accessibile del primo substrato;
E. scorrere una spatola sui fili calibrati accoppiati alla prima cornice e rimuovere eventuale primo adesivo in eccesso;
F. rimuovere i fili calibrati dalla prima cornice;

G. disporre una faccia di un primo componente da incollare sul primo adesivo steso sulla faccia accessibile del primo substrato, ottenendo l'incollaggio del primo componente al primo substrato, in cui quando il primo substrato è la pelle inferiore detta faccia del primo componente è una prima faccia del nucleo centrale e quando il primo substrato è il nucleo centrale detta faccia del primo componente è una faccia della pelle inferiore, per cui si ot- tiene l'incollaggio di una faccia della pelle inferiore ad una prima faccia del nucleo centrale;

H. rimuovere la prima cornice;

I. disporre un secondo substrato, selezionato tra la pelle superiore ed il nucleo centrale, in una seconda cornice in modo da avere una faccia del secondo substrato accessibile;

J. accoppiare alla seconda cornice due o più fili calibrati ad una distanza da una superficie della faccia accessibile del secondo substrato;

K. deporre un secondo adesivo sulla faccia accessibile del secondo substrato;

L. scorrere una spatola sui fili calibrati accoppiati alla seconda cornice e rimuovere eventuale secondo adesivo in eccesso;

M. rimuovere i fili calibrati dalla seconda cornice;

N. disporre una faccia di un secondo componente da incollare sul secondo adesivo steso sulla faccia accessibile del secondo substrato, ottenendo l'incollaggio del secondo componente al secondo substrato, in cui quando il secondo substrato è la pelle superiore detta faccia del secondo componente è una seconda faccia del nucleo centrale, contrapposta alla prima faccia del nucleo centrale, e quando il secondo substrato è il nucleo centrale detta faccia del secondo componente è una faccia della pelle superiore, per cui si ottiene l'incollaggio di una faccia della pelle superiore alla seconda faccia del nucleo centrale;

O. rimuovere la seconda cornice;

P. depositare un rivestimento superficiale sulla faccia esposta della pelle superiore che è non incollata al nucleo centrale.

Secondo un altro aspetto dell'invenzione, nella fase B il primo substrato può essere la pelle inferiore, nella fase G il primo componente può essere il nucleo centrale, nella fase I il secondo substrato può essere la pelle superiore, e nella fase N il secondo componente può essere il nucleo centrale.

Secondo un ulteriore aspetto dell'invenzione, nella fase D, prima di deporre il primo adesivo, una o più prime pellicole protettive possono essere posizionate su parti del primo substrato e/o del primo componente che non sono da incollare, e dopo la fase G dette una o più prime pellicole protettive possono essere rimosse, e nella fase K, prima di deporre il secondo adesivo, una o più seconde pellicole protettive possono essere posizionate su parti del secondo substrato e/o del secondo componente che non sono da incollare, e che dopo la fase N dette una o più seconde pellicole protettive possono essere rimosse.

I vantaggi offerti dal pannello sandwich secondo l'invenzione rispetto alle soluzioni della tecnica anteriore sono numerosi e significativi.

Innanzitutto, il pannello sandwich secondo l'invenzione integra in un unico componente la resistenza termica necessaria per la protezione di strutture ad altissime temperature e la funzione strutturale per la realizzazione di dispositivi di protezione termica comprendenti uno o più pannelli sandwich ed operanti da struttura primaria. In particolare, nel caso di una applicazione in un veicolo aerospaziale, il pannello sandwich secondo l'invenzione integra la leggerezza e la resistenza dei materiali compositi con l'isolamento termico delle schiume in una struttura a "sandwich" che è in grado di adempiere ad una funzione strutturale, poiché i pannelli stessi costituiscono gli elementi della struttura primaria del veicolo aerospaziale, ad una funzione protettiva come scudo termico per la fase di rientro, ed una funzione protettiva dall'ambiente spaziale.

Inoltre, il pannello sandwich secondo l'invenzione ha una migliore compatibilità del coefficiente di espansione termica, detto anche CTE (*Coefficient of Thermal Expansion*) dei materiali dei vari strati che compongono il pannello stesso.

Ulteriormente, il pannello sandwich secondo l'invenzione ha una migliore

resistenza a temperature di esercizio molto più alte, in particolare consentendo di operare fino a temperature di almeno 1450°C.

Infine, il pannello sandwich secondo l'invenzione ha una migliore resistenza all'ossidazione, dato che la specifica schiuma (*foam*) utilizzata per il nu- cleo (*core*) centrale è stabile anche dimensionalmente rispetto alle altre schiume, come ad esempio quelle carboniose, che sono invece soggette a forti degrada- zioni intorno ai 1000°C se non sono stabilizzate termicamente e che, in ogni caso, anche se stabilizzate, mostrano dei valori di dilatazione termica così elevati da non essere compatibili con i materiali degli altri strati del pannello provocando elevati stress termici. La selezione della specifica schiuma utilizzata per il nucleo centrale è uno degli aspetti più innovativi della presente invenzione, garantendo un funzionamento affidabile del pannello sandwich anche in ambienti estremi.

La presente invenzione verrà ora descritta, a titolo illustrativo, ma non limitativo, secondo sue preferite forme di realizzazione, con particolare riferimento alle Figure dei disegni allegati, in cui:

la Figura 1 mostra una rappresentazione schematica esplosa di una preferita forma di realizzazione del pannello sandwich secondo l'invenzione;

la Figura 2 mostra una vista prospettica del pannello sandwich di Figura 1;

la Figura 3 mostra un ingrandimento di una porzione del pannello sandwich di Figura 2;

la Figura 4 mostra le curve del CTE e della dilatazione relativa al variare della temperatura di un campione del pannello sandwich di Figura 1;

la Figura 5 mostra schematicamente alcuni elementi utilizzati nel procedimento di fabbricazione del pannello sandwich di Figura 1;

la Figura 6 mostra un primo grafico relativo ai risultati di alcuni test dilatometrici effettuati su campioni del pannello sandwich di Figura 1;

la Figura 7 mostra un ingrandimento del grafico di Figura 6;

la Figura 8 mostra un secondo grafico relativo ai risultati di alcuni test dilatometrici effettuati su campioni del pannello sandwich di Figura 1;

la Figura 9 mostra la configurazione di test a flessione di utilizzata per

campioni del pannello sandwich di Figura 1;

la Figura 10 mostra un terzo grafico relativo ai risultati di alcuni test a flessione effettuati su campioni del pannello sandwich di Figura 1;

la Figura 11 mostra un particolare di un campione del pannello sandwich di Figura 1 dopo l'esecuzione del test a flessione; e

la Figura 12 mostra un ingrandimento di una porzione del campione di Figura 11.

Nelle Figure numeri di riferimento identici saranno utilizzati per elementi analoghi.

Facendo riferimento alle Figure 1-3, si può osservare che una preferita forma di realizzazione del pannello sandwich secondo l'invenzione comprende uno strato o pelle (*skin*) inferiore 10, i.e. disposta sulla faccia interna del pannello sandwich non esposta all'ambiente, uno strato o nucleo (*core*) centrale 12 ed uno strato o pelle (*skin*) superiore 14, i.e. disposta sulla faccia esterna del pannel- lo sandwich esposta all'ambiente (e conseguentemente al flusso termico 25 nel caso in cui il pannello sandwich sia utilizzato come protezione termica di un aeromobile). La pelle inferiore 10 e la pelle superiore 14 sono solidalmente accoppiate al nucleo centrale 12 tramite, rispettivamente, un primo strato 16 di adesivo ed un secondo strato 18 di adesivo. Un rivestimento (*coating*) superficiale 20 è applicato sulla pelle superiore 14.

La pelle superiore 14 è lo strato direttamente esposto all'ambiente esterno ed è realizzata in materiale composito. Se le temperature sono dell'ordine dei 1000°C, il materiale composito utilizzato è carbonio rinforzato da fibre di carbonio, i.e. C/C (*Carbon/Carbon*). Per garantire utilizzi affidabili del pannello sandwich anche a temperature superiori, precisamente almeno fino a 1500°C, è vantaggioso utilizzare il materiale composito ceramico (CMC) comprendente o consistente di carbonio rinforzato da fibre in carburo di silicio, i.e. C/SiC (*Carbon/Silicon Carbide*): la selezione di tale materiale composito ceramico consente di fornire al pannello sandwich una notevole resistenza termica alle altissime temperature ed una notevole resistenza ad importanti sollecitazioni meccaniche,

come si verifica nei principali ambiti operativi cui è destinato il pannello quali, ad esempio, le condizioni di un rientro atmosferico ad altissime velocità (ipersoniche). Lo spessore della pelle superiore 14 varia da 1 mm a 10 mm, opzionalmente da 1,5 mm a 8 mm, più opzionalmente da 2 mm a 6 mm, ancora più opzionalmente da 2 mm a 4 mm.

Il nucleo centrale 12 ha come principale funzione quella di operare da isolante termico, per cui viene realizzato in un materiale fortemente isolante in grado di operare affidabilmente in sicurezza ad altissime temperature, precisamente almeno ad una temperatura variabile da 1500°C a 1600°C. Sebbene sia possibile impiegare sia materiali di tipo massivo che materiali che presentino dei "vuoti", per meglio soddisfare il requisito di isolamento termico, per il nucleo centrale 12 del pannello sandwich secondo la presente invenzione gli inventori hanno selezionato una schiuma (*foam*) a base di carburo di silicio (SiC). Lo spessore del nucleo centrale 12 varia da 8 mm a 40 mm, opzionalmente da 12 mm a 36 mm, più opzionalmente da 16 mm a 32 mm, ancora più opzionalmente da 20 mm a 28 mm, persino più opzionalmente da 23 mm a 25 mm. La schiuma a base di carbu- ro di silicio ha una elevata resistenza a temperature di esercizio molto alte, precisamente almeno fino a 1450°C, ed ha una elevata resistenza all'ossidazione; in proposito, gli inventori hanno eseguito vari test che hanno accertato che la schiuma a base di carburo di silicio è più stabile anche dimensionalmente rispetto alle schiume di altri materiali. Infine, la schiuma a base di carburo di silicio ha una migliore compatibilità di CTE con quelli dei materiali delle pelli inferiore 10 e superiore 12 e del primo e secondo strato 16 e 18 di adesivo, che verranno descritti più avanti, riducendo drasticamente gli stress termici della struttura complessiva del pannello sandwich.

Come già detto, la selezione della schiuma utilizzata per il nucleo centrale 12 è uno degli aspetti più innovativi della presente invenzione, garantendo un funzionamento affidabile del pannello sandwich anche in ambienti estremi. In particolare, le proprietà della schiuma a base di carburo di silicio utilizzata per il nucleo centrale 12 della preferita forma di realizzazione del pannello sandwich

secondo l'invenzione sono le seguenti:

- densità dei pori: 100 PPI (Pores per inch – pori per pollice - , in cui 1 pollice è pari a 2,54 cm);
- CTE variabile da 4,8 × 10^{-6} K^{-1} a 5,0 × 10^{-6} K^{-1} per temperature variabili da 1300°C a 1500°C; la Figura 4 mostra le curve del CTE 40 (in 10^{-6} K^{-1}) e della dilatazione relativa 45 (in micron) al variare della temperatura (da circa 20°C a circa 1450°C) di un campione della schiuma a base di carburo di silicio (che è un materiale isotropo) in condizioni di vuoto;
- resistenza alla compressione (*compression strength*) non inferiore a 11 MPa;
- carico di rotture (*tensile strength*) non inferiore a 5,5 MPa;
- resistenza di taglio (*shear strength*) non inferiore a 5,5 MPa;
- massa volumica (*bulk density*) pari a 0,6 ± 0.05 g/cm3.

Altre forme di realizzazione del pannello sandwich secondo l'invenzione possono avere il nucleo centrale 12 realizzato con una schiuma a base di carburo di silicio avente una densità dei pori variabile da 60 a 140 PPI, opzionalmente da 70 a 130 PPI, più opzionalmente da 80 a 120 PPI, ancora più opzionalmente da 90 a 110 PPI.

La pelle inferiore 10 è lo strato avente funzione di tipo strutturale in quanto su di esso possono essere applicati dei dispositivi di fissaggio, e quindi viene sottoposto a carichi derivanti dalle sollecitazioni di esercizio contribuendo in maniera determinante alla resistenza meccanica di tutto il pannello sandwich. Vantaggiosamente, nella pelle inferiore 10 vengono previsti degli alloggiamenti adeguati per tali dispositivi di fissaggio, che tuttavia non sono oggetto della presente invenzione. Analogamente alla pelle superiore 14, per la pelle inferiore 10 è possibile utilizzare diversi tipi di materiali compositi ceramici o metallici selezionati dal gruppo comprendente C/C e C/SiC. Lo spessore della pelle inferiore 10 è variabile da 1 mm a 10 mm, opzionalmente variabile da 1,5 mm a 8 mm, più opzionalmente variabile da 2 mm a 6 mm, ancora più opzionalmente variabile da 2 mm a 4 mm, persino più opzionalmente pari a 3mm.

In particolare, non è necessario che la pelle inferiore 10 e la pelle superiore 14 siano realizzate nello stesso materiale, per cui, ad esempio, una delle due può essere in C/C e l'altra in C/SiC. In ogni caso, il C/SiC garantisce utilizzi affidabili del pannello sandwich anche a temperature estremamente elevate, precisamente almeno fino a 1500°C, ed ha una compatibilità ottimale con i materiali degli altri strati del pannello sandwich, riducendo drasticamente gli stress termici della struttura complessiva del pannello sandwich e sopportando i carichi termici dovuti a conducibilità anche elevate del materiale utilizzato per il nucleo centrale 12.

Come detto, l'assemblaggio della pelle inferiore 10 e della pelle superiore 14 al nucleo centrale 12 viene realizzato utilizzando un primo ed un secondo strato 16 e 18 di adesivo, rispettivamente, che permettono di ottenere la confi- gurazione finale del pannello sandwich, in cui l'adesivo è vantaggiosamente di ti- po ceramico. L'adesivo è stato selezionato dagli inventori in modo tale da avere una elevata resistenza termica e meccanica, in particolare a temperature anche elevate, precisamente almeno ad una temperatura variabile da 1500°C a 1600°C, ed in modo tale che garantisca l'adesione necessaria alla stabilità strutturale del pannello sandwich e la compatibilità, principalmente in termini di CTE, con i materiali da incollare (i.e. la pelle inferiore e superiore 10 e 14 ed il nucleo centrale 12) allo scopo di minimizzare gli stress termici indotti nella struttura complessiva del pannello sandwich dalle alte temperature di utilizzo; in particolare, l'adesivo è stato selezionato dagli inventori per garantire il trasferimento degli sforzi di taglio, evitando il sopraggiungere di scollamenti con conseguente danneggiamento irreversibile della struttura del pannello sandwich, e la durata dell'incollaggio della pelle inferiore e superiore 10 e 14 al nucleo centrale 12 durante tutta la vita operativa del pannello sandwich. A titolo esemplificativo, ma non a titolo limitativo, l'adesivo può essere selezionato dal gruppo comprendente resina fenolica carbonizzata, adesivi a base di grafite, adesivi a base di ossido di alluminio, adesivi a base di allumina-silice, adesivi a base di carbonio, adesivi a base di carburo di silicio, adesivi a base di nitruro di boro, adesivi a base di ossido di ittrio, adesivi a

base di ossido di zirconia. Allo scopo di garantire una buona adesione agli strati con i quali entra il contatto l'adesivo, il materiale riempitivo (*filler*) dell'adesivo può vantaggiosamente essere di tipo grafitico. In particolare, l'adesivo può essere un adesivo liquido di tipo ceramico a base grafitica; a titolo esemplificativo e non limitativo, l'adesivo può comprendere o consistere di una miscela di fenolo, esametilentetrammina, fibre di carbonio, grafite, isopropanolo e formaldeide.

La preferita forma di realizzazione del pannello sandwich secondo l'invenzione utilizza sia per il primo che per il secondo strato 16 e 18 l'adesivo Graphi-Bond^{TM} 669 disponibile dall'azienda Statunitense Aremco Products, Inc.

Lo spessore del primo strato 16 di adesivo e quello del secondo strato 18 di adesivo possono essere variabili da 0,1 mm a 1 mm, opzionalmente variabili da 0,2 mm a 0,8 mm, più opzionalmente variabili da 0,2 mm a 0,8 mm, ancora più opzionalmente pari a 0,4 mm. In particolare, non è necessario che il primo strato 16 ed il secondo strato 18 siano realizzati con lo stesso adesivo, né che abbiano lo stesso spessore.

Il rivestimento superficiale 20 è applicato sulla pelle superiore 14 per fornire il pannello sandwich di una protezione dall'effetto ossidante dell'ambiente esterno nel caso di utilizzo alle alte temperature. Il materiale depositato con il rivestimento superficiale 20 può comprendere uno o più materiali selezionati dal gruppo comprendente zirconia, zirconia stabilizzata con ittrio, e carburo di silicio (SiC); in particolare, nel caso in cui il materiale del rivestimento superficiale 20 sia SiC, quest'ultimo avrebbe una elevatissima compatibilità di CTE con il materiale della pelle superiore 18, garantendo una adesione ottimale. Lo spessore del rivestimento superficiale 20 può variare da 0,1mm a 0,5mm.

Gli inventori hanno sviluppato anche un procedimento di fabbricazione del pannello sandwich secondo l'invenzione, in cui le procedure di incollaggio ed assemblaggio dei vari strati sono particolarmente accurate. La procedura di incollaggio preserva la qualità dell'adesivo garantendo le giusta efficacia dell'incollaggio, mantenendo un controllo dello spessore di deposizione al fine di ottenere una stesura omogenea, una efficace adesione ed una adeguata resi-

stenza strutturale. La procedura di assemblaggio garantisce l'integrità ed il corretto posizionamento dei singoli strati componenti del pannello sandwich al fine di rispettare i vincoli geometrici.

Durante la procedura di incollaggio, per controllare lo spessore dell'adesivo che viene steso su un substrato 55, come mostrato in Figura 5 ven- gono utilizzati dei fili calibrati 58 ben tesi a formare dei binari per la spatola 50 che viene utilizzata per stendere omogeneamente l'adesivo (non mostrato) sul substrato 55; in particolare, il substrato 55 viene posizionato in una cornice (non mostrata) alla quale vengono accoppiati i fili calibrati 58 ad una distanza precisa dalla superficie del substrato 55. In tal modo, l'adesivo viene deposto sul substra- to 55 e l'eccesso viene rimosso facendo scorrere la spatola 50 sui fili 58. Il sub- strato 55 di Figura 5 coincide con la faccia della pelle inferiore 10 che deve essere incollata al nucleo centrale 12, oppure con la faccia del nucleo centrale 12 che deve essere incollata alla pelle inferiore 10, oppure con la faccia della pelle supe- riore 14 che deve essere incollata al nucleo centrale 12, oppure con la faccia del nucleo centrale 12 che deve essere incollata alla pelle superiore 14. L'allineamento dei vari strati componenti (e.g. il nucleo centrale 12 sul quale vie- ne steso l'adesivo e la pelle superiore 14 che viene incollata al nucleo centrale
12) viene garantito dall'utilizzo di una cornice (non mostrata in Figura 5). Per evitare la contaminazione di parti che non devono essere incollate, si utilizza una pellicola protettiva che non danneggi il substrato 55 stesso.

La preferita forma di realizzazione del procedimento di fabbricazione del pannello sandwich secondo l'invenzione comprende le seguenti fasi:

A. avere a disposizione la pelle inferiore 10, il nucleo centrale 12 e la pelle superiore 14 come descritte in precedenza;
B. disporre la pelle inferiore 10 in una prima cornice in modo da avere una faccia accessibile;
C. accoppiare alla prima cornice due o più fili calibrati 58 ad una distanza precisa dalla superficie della faccia accessibile della pelle inferiore 10;
D. deporre un adesivo, del tipo come descritto in precedenza, sulla faccia ac-

cessibile della pelle inferiore 10;

E. scorrere la spatola 50 sui fili calibrati 58 e rimuovere l'eventuale adesivo in eccesso;

F. rimuovere i fili calibrati 58 dalla prima cornice;

G. disporre il nucleo centrale 12 sull'adesivo steso sulla faccia accessibile della pelle inferiore 10, ottenendo l'incollaggio del nucleo centrale 12 alla pelle inferiore 10;

H. rimuovere la prima cornice;

I. disporre la pelle superiore 14 in una seconda cornice (eventualmente coincidente con la prima cornice) in modo da avere una faccia accessibile;

J. accoppiare alla seconda cornice due o più fili calibrati 58 ad una distanza precisa dalla superficie della faccia accessibile della pelle superiore 14;

K. deporre un adesivo, del tipo come descritto in precedenza, sulla faccia accessibile della pelle superiore 14;

L. scorrere la spatola 50 sui fili calibrati 58 e rimuovere l'eventuale adesivo in eccesso (nel caso in cui l'adesivo non sia lo stesso utilizzato nelle fasi D-G, la spatola deve essere preliminarmente pulita oppure deve essere utilizzata una spatola differente);

M. rimuovere i fili calibrati 58 dalla seconda cornice;

N. disporre il nucleo centrale 12 sull'adesivo steso sulla faccia accessibile della pelle superiore 14, ottenendo l'incollaggio del nucleo centrale 12 alla pelle superiore 14;

O. rimuovere la seconda cornice;

P. depositare un rivestimento superficiale 20 sulla faccia esposta della pelle superiore 14 (i.e. sulla faccia non incollata al nucleo centrale 12).

In particolare, la fase A è la fase iniziale, la sequenza di fasi B-H può essere sia precedente che successiva alla sequenza di fasi I-O, e la fase P può essere eseguita sia prima che dopo la sequenza di fasi I-O.

Come già detto, il pannello sandwich secondo l'invenzione ha una notevole resistenza meccanica e termica, essendo in grado di operare affidabilmente ad

altissime temperature. La schiuma a base di SiC utilizzata per il nucleo centrale 12 è uno degli aspetti più innovativi della presente invenzione, garantendo un funzionamento affidabile del pannello sandwich anche in ambienti estremi, che in particolare possono essere più ossidanti e che possono essere caratterizzati da temperature elevate, anche non inferiori a circa 1500°C.

Il pannello sandwich secondo l'invenzione ha una configurazione estremamente semplice che garantisce nello stesso tempo affidabilità e riusabilità con conseguenti bassi costi, anche in virtù della scalabilità dei costi di produzione dovuti alla relativa semplicità delle operazioni di assemblaggio.

La selezione effettuata per tutti i materiali, incluso l'adesivo, permette al pannello sandwich secondo l'invenzione di avere un comportamento di dilatazione termica molto stabile.

In proposito, gli inventori hanno eseguito alcuni test dilatometrici sia lungo lo spessore (i.e. fuori del piano) che nel piano su campioni della preferita forma di realizzazione del pannello sandwich secondo l'invenzione. La Figura 6 mostra le curve del CTE 60 (in 10^{-6} K^{-1}) e della dilatazione relativa 65 (in micron) fuori del piano al variare della temperatura da circa 20°C a circa 1320°C, mentre la Figura 7 mostra un ingrandimento delle curve di Figura 6 nell'intervallo di temperatura da 500°C a circa 1320°C; nelle Figure 6 e 7 si può osservare che la dilatazione relativa 65 fuori dal piano si stabilizza per temperature superiori a 500°C e l'incremento medio dello spessore per temperature variabili nell'intervallo da 600°C a 1300°C è di circa 90 micron. La Figura 8 mostra le curve del CTE 80 (in 10^{-6} K^{-1}) e della dilatazione relativa 85 (in micron) nel piano al variare della temperatura (da 500°C a circa 1450°C), in cui si può osservare che i pannello sandwich sotto test subisce una contrazione fino a circa 1000°C e poi comincia ad espandersi. Ciò dimostra che il pannello sandwich secondo l'invenzione ha dilatazioni estremamente ridotte ed un comportamento particolarmente stabile: ciò riduce drasticamente gli stress termici sia all'interno del pannello sandwich secondo l'invenzione che all'interno di un dispositivo di protezione termica formato da una pluralità di pannelli sandwich secondo l'invenzione utilizzati come pia-

strelle (*tile*) interfacciate tra loro, precisamente all'interfaccia tra piastrelle contigue, come ad esempio nel caso di un dispositivo di protezione termica montato su un aeromobile. Per esempio, alla temperatura di 1232°C, il pannello sandwich sottoposto ai test ha un CTE pari 4,99 10^{-6} K^{-1}.

Gli inventori hanno inoltre eseguito alcuni test a flessione, secondo la norma C393 (*Standard Test Method for Core Shear Properties of Sandwich Constructions by Beam Flexure*) stabilita dall'ente ASTM International, di cui la Figura 9 mostra la configurazione di test, su campioni della preferita forma di realizzazione del pannello sandwich secondo l'invenzione aventi spessore di 30 mm e dimensioni nel piano pari a 60 mm × 85 mm (in cui, rispetto alla Figura 9, L_1 è una distanza lungo la dimensione lineare maggiore, con L_1 pari a 40 mm, ed un puntone esercita una forza P_1 sul rivestimento superficiale 20 del pannello sandwich).

La Figura 10 mostra i risultati dei test, in cui "Load" è la forza in kN esercitata dal puntone sul pannello sandwich e "Displacement" è lo spostamento della traversa della macchina di test che rappresenta la deflessione (ovvero lo scostamento dalla planarità) del punto del rivestimento superficiale 20 del pannello sandwich su cui il puntone esercita la forza. Come mostrato in Figura 11, la rottura del campione 110 ha una penetrazione del puntone 120 nel rivestimento superficiale 20 e nella pelle superiore 14, interessando una piccolissima zona della nucleo centrale 12, rimasta circoscritta in prossimità della pelle superiore 14 e del puntone 120. Come mostrato nell'ingrandimento di Figura 12, il foro ha un diametro di circa 5 mm.

I risultati dei test dimostrano che la resistenza meccanica del pannello sandwich secondo l'invenzione è estremamente elevata.

In quel che precede sono state descritte le preferite forme di realizzazione e sono state suggerite delle varianti della presente invenzione, ma è da intendersi che gli esperti del ramo potranno apportare modificazioni e cambiamenti senza con ciò uscire dal relativo ambito di protezione, come definito dalle rivendicazioni allegate.

RIVENDICAZIONI

1. Pannello sandwich di protezione termica comprendente:

- una pelle inferiore (10) disposta su una faccia interna del pannello sandwich non esposta all'ambiente,
- un nucleo centrale (12),
- una pelle superiore (14) disposta su una faccia esterna del pannello sandwich esposta all'ambiente, ed
- un rivestimento superficiale (20) applicato sulla pelle superiore (14) configurato per proteggere la pelle superiore dall'ossidazione,

la pelle inferiore (10) essendo solidalmente accoppiata ad una prima faccia del nucleo centrale (12) tramite un primo strato (16) di adesivo, la pelle superiore (14) essendo solidalmente accoppiata ad una seconda faccia del nucleo centrale (12), contrapposta alla prima faccia del nucleo centrale (12), tramite un secondo strato (18) di adesivo, per cui la pelle inferiore (10) e la pelle superiore (14) sono incollate al nucleo centrale (12), la pelle inferiore (10) essendo realizzata in materiale composito selezionato dal gruppo comprendente carbonio rinforzato da fibre di carbonio e carbonio rinforzato da fibre in carburo di silicio, la pelle superiore (14) essendo realizzata in materiale composito selezionato dal gruppo comprendente carbonio rinforzato da fibre di carbonio e carbonio rinforzato da fibre in carburo di silicio, il nucleo centrale (12) essendo realizzato con una schiuma a base di carburo di silicio.

2. Pannello sandwich secondo la rivendicazione 1, caratterizzato dal fatto che detta schiuma a base di carburo di silicio ha una densità di pori variabile da 60 a 140 PPI (Pores per inch – pori per pollice - in cui 1 pollice è pari a 2,54 cm), opzionalmente da 70 a 130 PPI, più opzionalmente da 80 a 120 PPI, ancora più opzionalmente da 90 a 110 PPI.

3. Pannello sandwich secondo la rivendicazione 1 o 2, caratterizzato dal fatto che il nucleo centrale 12 ha spessore variabile da 8 mm a 40 mm, opzionalmente da 12 mm a 36 mm, più opzionalmente da 16 mm a 32 mm, ancora più opzionalmente da 20 mm a 28 mm, persino più opzionalmente da 23 mm a 25

mm.

4. Pannello sandwich secondo una qualsiasi delle precedenti rivendicazioni, caratterizzato dal fatto che la pelle superiore (14) ha spessore variabile da 1 mm a 10 mm, opzionalmente da 1,5 mm a 8 mm, più opzionalmente da 2 mm a 6 mm, ancora più opzionalmente da 2 mm a 4 mm.

5. Pannello sandwich secondo una qualsiasi delle precedenti rivendicazioni, caratterizzato dal fatto che la pelle inferiore (10) ha spessore variabile da 1 mm a 10 mm, opzionalmente variabile da 1,5 mm a 8 mm, più opzionalmente va- riabile da 2 mm a 6 mm, ancora più opzionalmente variabile da 2 mm a 4 mm, persino più opzionalmente pari a 3mm.

6. Pannello sandwich secondo una qualsiasi delle precedenti rivendicazioni, caratterizzato dal fatto che la pelle inferiore (10) e la pelle superiore (14) sono realizzate nello stesso materiale.

7. Pannello sandwich secondo la rivendicazione 6, caratterizzato dal fatto che la pelle inferiore (10) e la pelle superiore (14) sono entrambe realizzate in carbonio rinforzato da fibre in carburo di silicio.

8. Pannello sandwich secondo una qualsiasi delle precedenti rivendicazioni, caratterizzato dal fatto che l'adesivo del primo strato (16) è selezionato dal gruppo comprendente resina fenolica carbonizzata, adesivi a base di grafite, adesivi a base di ossido di alluminio, adesivi a base di allumina-silice, adesivi a base di carbonio, adesivi a base di carburo di silicio, adesivi a base di nitruro di boro, adesivi a base di ossido di ittrio, adesivi a base di ossido di zirconia, e dal fatto che l'adesivo del secondo strato (18) è selezionato dal gruppo comprendente re- sina fenolica carbonizzata, adesivi a base di grafite, adesivi a base di ossido di alluminio, adesivi a base di allumina-silice, adesivi a base di carbonio, adesivi a base di carburo di silicio, adesivi a base di nitruro di boro, adesivi a base di ossido di ittrio, adesivi a base di ossido di zirconia.

9. Pannello sandwich secondo la rivendicazione 8, caratterizzato dal fatto che l'adesivo del primo strato (16) e l'adesivo del secondo strato (18) hanno ognuno un materiale riempitivo di tipo grafitico, opzionalmente l'adesivo del

primo strato (16) e l'adesivo del secondo strato (18) essendo ognuno un adesivo liquido di tipo ceramico a base grafitica.

10. Pannello sandwich secondo una qualsiasi delle precedenti rivendicazioni, caratterizzato dal fatto che il primo strato (16) di adesivo ha spessore variabile da 0,1 mm a 1 mm, opzionalmente variabile da 0,2 mm a 0,8 mm, più opzionalmente variabile da 0,2 mm a 0,8 mm, ancora più opzionalmente pari a 0,4 mm, e dal fatto che il secondo strato (18) di adesivo ha spessore variabile da 0,1 mm a 1 mm, opzionalmente variabile da 0,2 mm a 0,8 mm, più opzionalmente variabile da 0,2 mm a 0,8 mm, ancora più opzionalmente pari a 0,4 mm.

11. Pannello sandwich secondo una qualsiasi delle precedenti rivendicazioni, caratterizzato dal fatto che il rivestimento superficiale (20) comprende uno o più materiali selezionati dal gruppo comprendente zirconia, zirconia stabilizzata con ittrio, e carburo di silicio (SiC).

12. Pannello sandwich secondo una qualsiasi delle precedenti rivendicazioni, caratterizzato dal fatto che il rivestimento superficiale (20) ha spessore variabile da 0,1mm a 0,5mm.

13. Procedimento di fabbricazione di un pannello sandwich di protezione termica secondo una qualsiasi delle rivendicazioni da 1 a 12, il procedimento comprendendo le seguenti fasi:

A. avere a disposizione una pelle inferiore (10) realizzata in materiale composito selezionato dal gruppo comprendente carbonio rinforzato da fibre di carbonio e carbonio rinforzato da fibre in carburo di silicio, un nucleo centrale (12) realizzato con una schiuma a base di carburo di silicio, ed una pelle superiore (14) realizzata in materiale composito selezionato dal gruppo comprendente carbonio rinforzato da fibre di carbonio e carbonio rinforzato da fibre in carburo di silicio;
B. disporre un primo substrato (55), selezionato tra la pelle inferiore (10) ed il nucleo centrale (12), in una prima cornice in modo da avere una faccia del primo substrato (55) accessibile;
C. accoppiare alla prima cornice due o più fili calibrati (58) ad una distanza da

una superficie della faccia accessibile del primo substrato (55);

D. deporre un primo adesivo sulla faccia accessibile del primo substrato (55);

E. scorrere una spatola (50) sui fili calibrati (58) accoppiati alla prima cornice e rimuovere eventuale primo adesivo in eccesso;

F. rimuovere i fili calibrati (58) dalla prima cornice;

G. disporre una faccia di un primo componente da incollare sul primo adesivo steso sulla faccia accessibile del primo substrato (55), ottenendo l'incollaggio del primo componente al primo substrato (55), in cui quando il primo substrato (55) è la pelle inferiore (10) detta faccia del primo compo- nente è una prima faccia del nucleo centrale (12) e quando il primo sub- strato (55) è il nucleo centrale (12) detta faccia del primo componente è una faccia della pelle inferiore (10), per cui si ottiene l'incollaggio di una faccia della pelle inferiore (10) ad una prima faccia del nucleo centrale (12);

H. rimuovere la prima cornice;

I. disporre un secondo substrato (55), selezionato tra la pelle superiore (14) ed il nucleo centrale (12), in una seconda cornice in modo da avere una faccia del secondo substrato (55) accessibile;

J. accoppiare alla seconda cornice due o più fili calibrati (58) ad una distanza da una superficie della faccia accessibile del secondo substrato (55);

K. deporre un secondo adesivo sulla faccia accessibile del secondo substrato (55);

L. scorrere una spatola (50) sui fili calibrati (58) accoppiati alla seconda corni- ce e rimuovere eventuale secondo adesivo in eccesso;

M. rimuovere i fili calibrati (58) dalla seconda cornice;

N. disporre una faccia di un secondo componente da incollare sul secondo adesivo steso sulla faccia accessibile del secondo substrato (55), ottenendo l'incollaggio del secondo componente al secondo substrato (55), in cui quando il secondo substrato (55) è la pelle superiore (14) detta faccia del secondo componente è una seconda faccia del nucleo centrale (12), con- trapposta alla prima faccia del nucleo centrale (12), e quando il secondo

substrato (55) è il nucleo centrale (12) detta faccia del secondo componente è una faccia della pelle superiore (14), per cui si ottiene l'incollaggio di una faccia della pelle superiore (14) alla seconda faccia del nucleo centrale (12);

O. rimuovere la seconda cornice;

P. depositare un rivestimento superficiale (20) sulla faccia esposta della pelle superiore (14) che è non incollata al nucleo centrale (12).

14. Procedimento secondo la rivendicazione 13, caratterizzato dal fatto che nella fase B il primo substrato è la pelle inferiore (10), nella fase G il primo componente è il nucleo centrale (12), nella fase I il secondo substrato è la pelle superiore (14), e nella fase N il secondo componente è il nucleo centrale (12).

15. Procedimento secondo la rivendicazione 13 o 14, caratterizzato dal fatto che nella fase D, prima di deporre il primo adesivo, una o più prime pellicole protettive vengono posizionate su parti del primo substrato (55) e/o del primo componente che non sono da incollare, e che dopo la fase G dette una o più prime pellicole protettive vengono rimosse, e dal fatto che nella fase K, prima di deporre il secondo adesivo, una o più seconde pellicole protettive vengono posizionate su parti del secondo substrato (55) e/o del secondo componente che non sono da incollare, e che dopo la fase N dette una o più seconde pellicole protettive vengono rimosse.

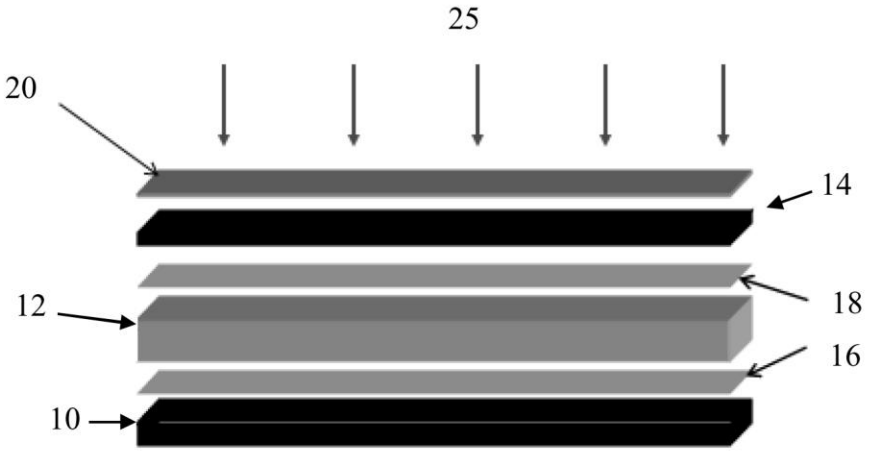

Fig. 1

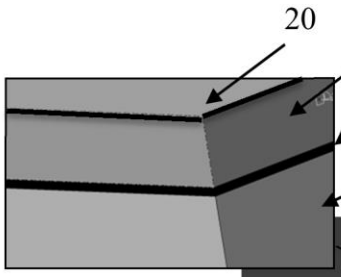

Fig. 3

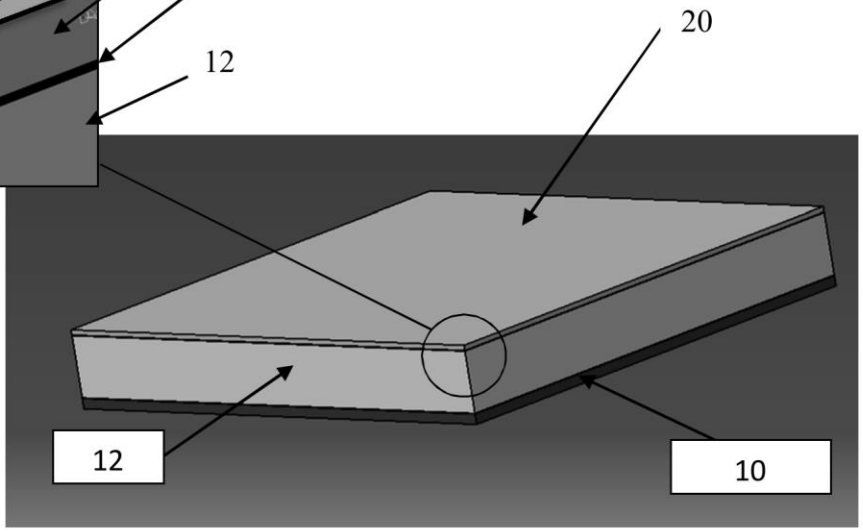

Fig. 2

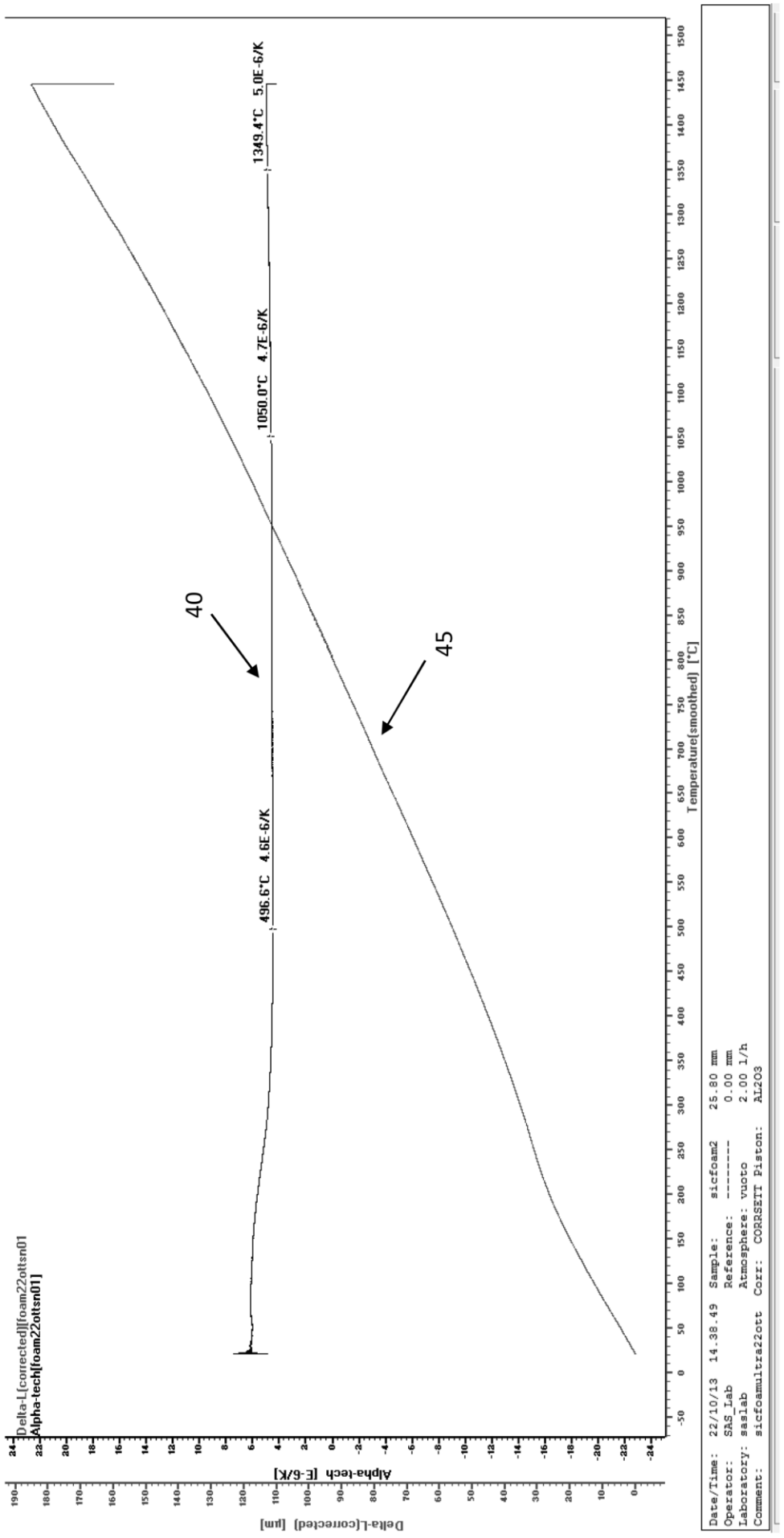
Delta-L[corrected][foam22ottsn01]
Alpha-tech[foam22ottsn01]
496.6°C 4.6E-6/K
1050.0°C 4.7E-6/K
1349.4°C 5.0E-6/K
40
45
Delta-L[corrected] [µm]
Alpha-tech [E-6/K]
Temperature[smoothed] [°C]
Date/Time: 22/10/13 14.38.49
Operator: SAS_lab
Laboratory: sasiab
Comment: sicfoamultra22ott
Sample: sicfoam2
Reference: --------
Atmosphere: vuoto
Corr: CORRSIT Piston:
25.80 mm
0.00 mm
2.00 l/h
Al203

Fig. 4

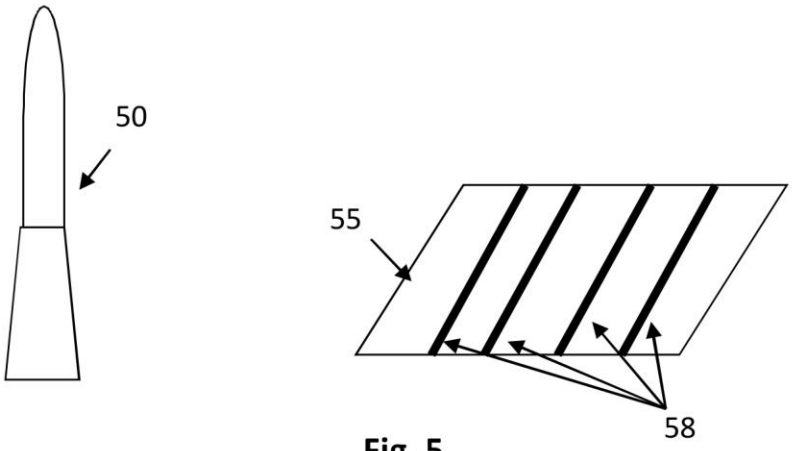

Fig. 5

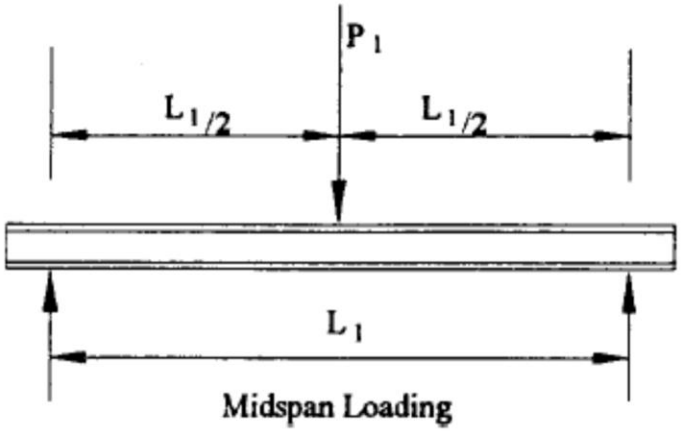

Fig. 9

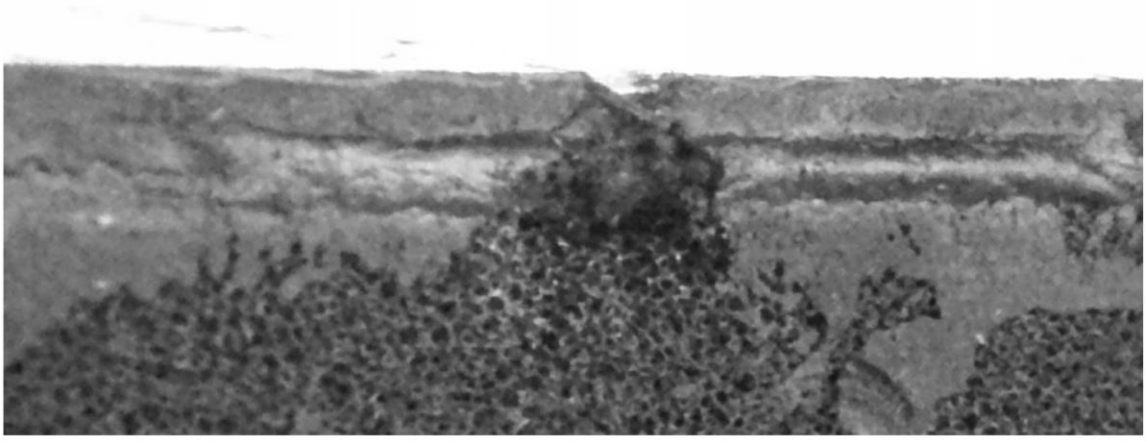

Fig. 12

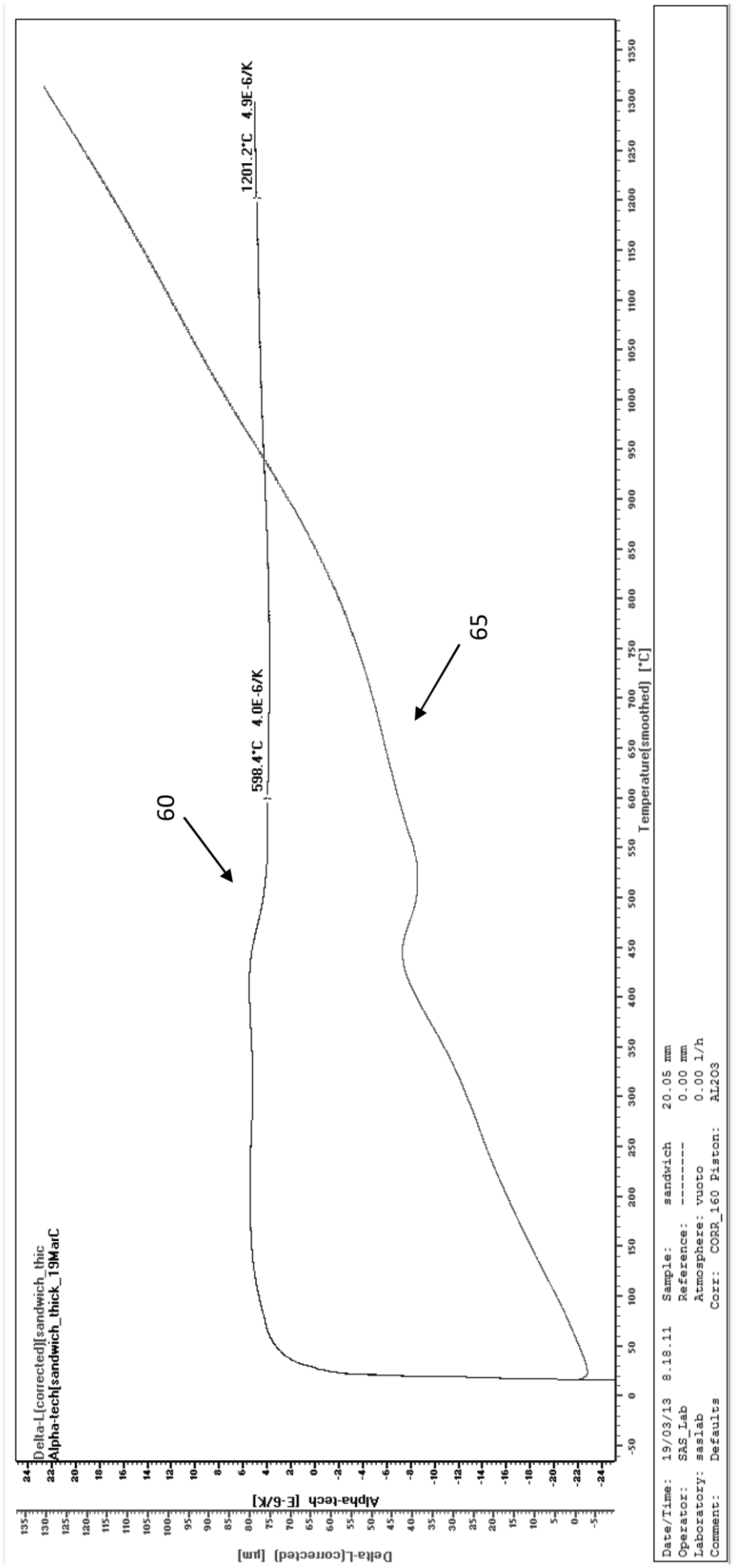
Delta-L[corrected][sandwich_thic
Alpha-tech[sandwich_thick_19MarC
598.4°C 4.0E-6/K
1201.2°C 4.9E-6/K
60
65
Delta-L[corrected] [µm]
Alpha-tech [E-6/K]
Temperature[smoothed] [°C]
Date/Time: 19/03/13 8.18.11
Operator: SAS_Lab
Laboratory: saslab
Comment: Défaults
Sample: sandwich 20.05 mm
Reference: ------- 0.00 mm
Atmosphere: vuoto 0.00 l/h
Corr: CORR_160 Piston: AL203

Fig. 6

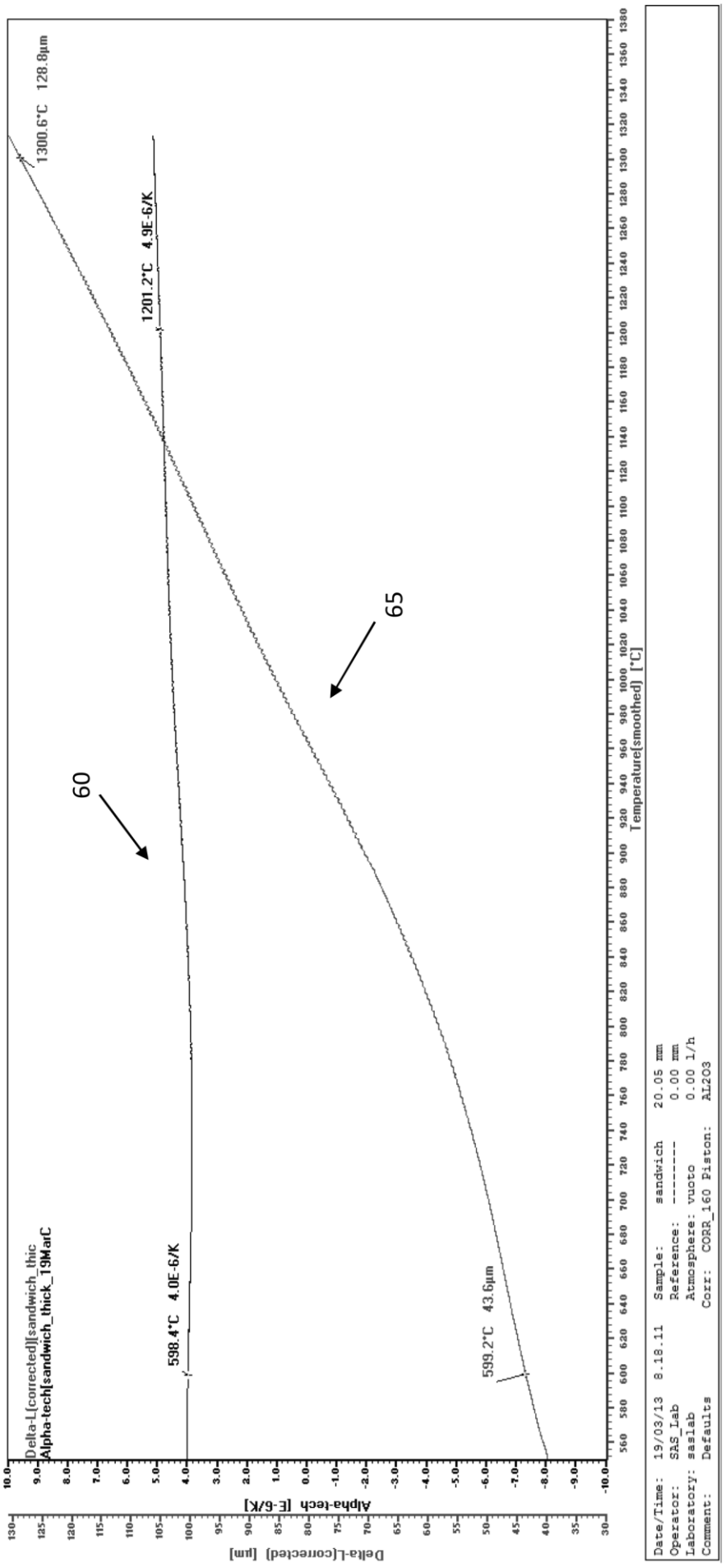
Delta-L[corrected]sandwich_thic
Alpha-tech[sandwich_thick_T9MarC
598.4°C 4.0E-6/K
599.2°C 43.6µm
1201.2°C 4.9E-6/K
1300.6°C 128.8µm
60
65
Delta-L(corrected) [µm]
Alpha-tech [E-6/K]
Temperature[smoothed] [°C]
Date/Time: 19/03/13 8.18.11
Operator: SAS_lab
Laboratory: saslab
Comment: Defaults
Sample: sandwich 20.05 mm
Reference: -------- 0.00 mm
Atmosphere: vuoto 0.00 l/h
Corr: CORR_160 Piston: AL203

Fig. 7

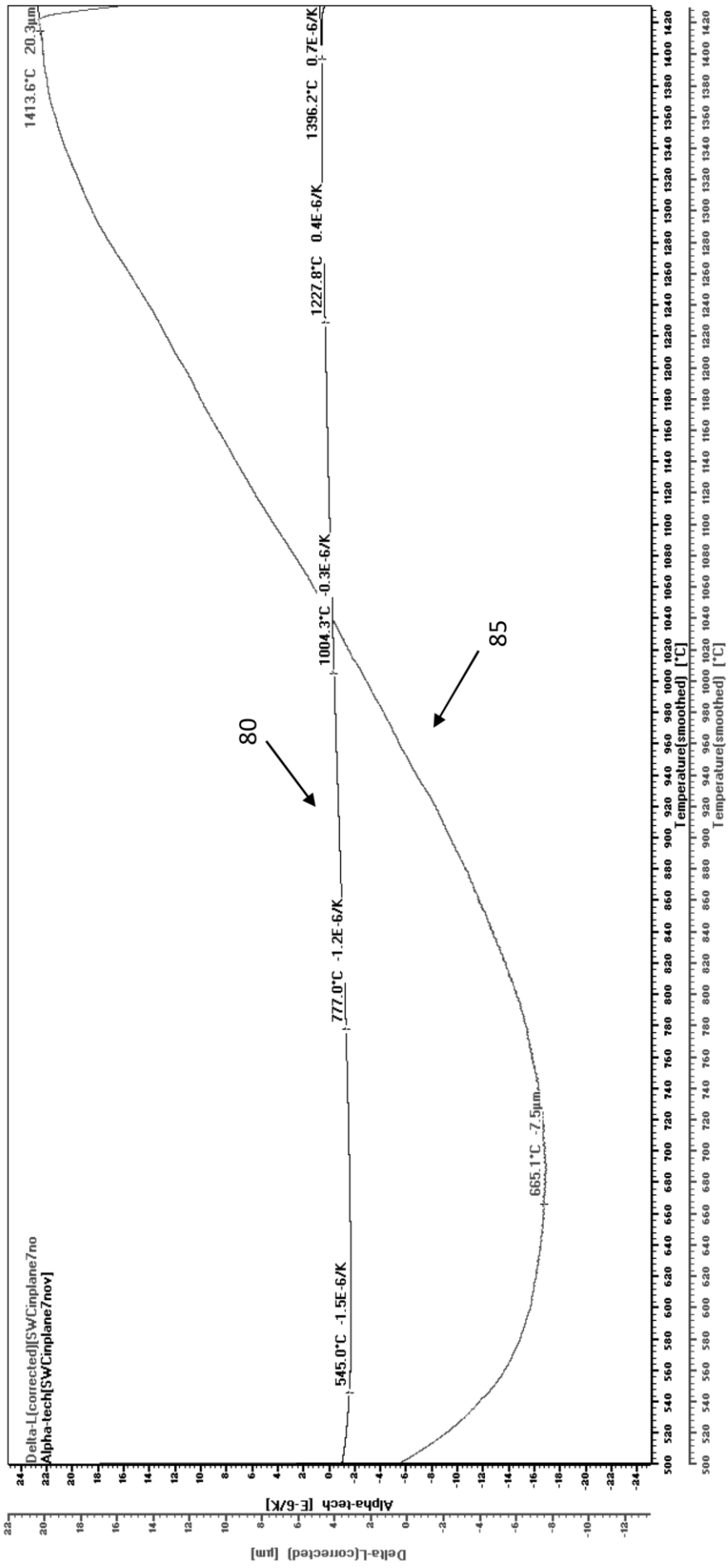
Delta-L[corrected][SWCinplane7no
Alpha-tech[SWCinplane7nov]
1413.6°C 20.3µm
1227.8°C 0.4E-6/K
1396.2°C 0.7E-6/K
1004.3°C -0.3E-6/K
777.0°C -1.2E-6/K
545.0°C -1.5E-6/K
665.1°C -7.5µm
80
85
Delta-L[corrected] [µm]
Alpha-tech [E-6/K]
Temperature[smoothed] [°C]

Fig. 8

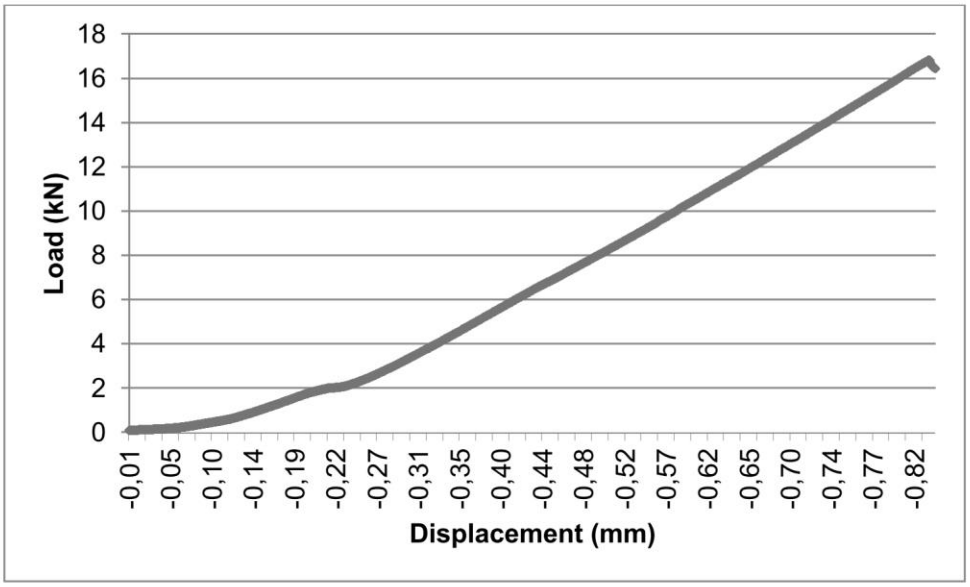
Load (kN)
18
16
14
12
10
8
6
4
2
0
-0,01
-0,05
-0,10
-0,14
-0,19
-0,22
-0,27
-0,31
-0,35
-0,40
-0,44
-0,48
-0,52
-0,57
-0,62
-0,65
-0,70
-0,74
-0,77
-0,82
Displacement (mm)

Fig. 10

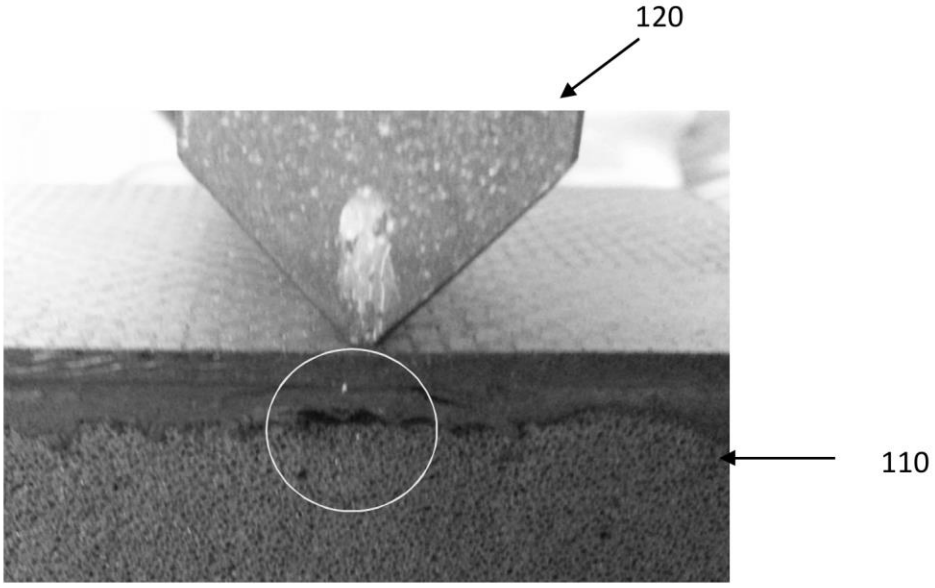
120
110

Fig. 11

ITALIAN PATENT OFFICE

Document No.

102014902259647A1

Publication Date

20151109

Applicant

AGENZIA SPAZIALE ITALIANA

Title

PROCEDIMENTO DI PRODUZIONE DI MATERIALI COMPOSITI CERAMICI RINFORZATI CON FIBRE CERAMICHE

PROCEDIMENTO DI PRODUZIONE DI MATERIALI COMPOSITI CERAMICI RINFORZATI CON FIBRE CERAMICHE

* * *

La presente invenzione riguarda un procedimento di produzione di materiali compositi ceramici rinforzati con fibre ceramiche, precisamente materiali compositi a matrice ceramica selezionati dal gruppo comprendente materiali compositi a matrice carboniosa rinforzata da fibre di carbonio (anche noti come materiali compositi “carbonio/carbonio” o “carbon/carbon” o “C/C”), materiali compositi a matrice carboniosa rinforzata da fibre in carburo di silicio (anche noti come materiali compositi “carburo di silicio/carbonio” o “SiC/C”), materiali compositi a matrice in carburo di silicio rinforzata da fibre in carburo di silicio (anche noti come materiali compositi “carburo di silicio/carburo di silicio” o “SiC/SiC”), e materiali compositi a matrice in carburo di silicio rinforzata da fibre in carbonio (anche noti come materiali compositi “carbonio/carburo di silicio” o “C/SiC”), il procedimento consentendo in modo efficiente, affidabile, semplice, ed economico di fabbricare materiali compositi aventi eccellenti proprietà meccaniche di resistenza a carichi e stress ed eccellenti proprietà termiche dovute alla bassissima conducibilità termica, inclusa una elevata resistenza a stress ed escursioni termiche, mantenendo i tempi di produzione sufficientemente brevi per consentire una produttività significativa.

I materiali compositi a matrice ceramica rinforzata da fibre ceramiche C/C e C/SiC hanno delle buone proprietà termiche e meccaniche ad alte temperature, e sono caratterizzati da una buona resistenza all’ossidazione (nel caso del C/SiC) ed agli shock termici. In virtù di tali proprietà, tali materiali compositi trovano crescente applicazione, ad esempio, nell’industria aeronautica, nell’industria aerospaziale, ed anche nei settori dell'industria nucleare ed automobilistica; a titolo di esempio tali materiali sono largamente utilizzati come protezioni termiche per velivoli da rientro atmosferico (e.g. capsule e velivoli ipersonici) ed anche per i freni nel campo ferroviario ed automobilistico di alta gamma, e nel settore nucleare come condotti nei reattori.

I procedimenti di fabbricazione di tali materiali compositi carboniosi C/C o C/SiC sono stati sviluppati nella seconda metà del XX secolo. In particolare, le specifiche tecniche di produzione di tali materiali dipendono non solo dalla tecnologia disponibile, ma anche e soprattutto dai requisiti finali che il materiale prodotto deve avere.

Le due principali tecniche attualmente disponibili sono l'infiltrazione di fase liquida (LPI: *Liquid Phase Infiltration*) e l'infiltrazione per vapore chimico (CVI: *Chemical Vapour Infiltration*).

Nella tecnica LPI, l'infiltrazione liquida avviene tramite l'utilizzo di un polimero precursore, per cui le preforme sono impregnate (a mano o con applicazione di pressione) con un precursore idoneo e poi vengono messe in una fornace per la cura ed il processo di pirolisi per la trasformazione del polimero che costituirà la matrice in carbonio od in carburo di silicio. Attualmente, il processo ancora non è ben noto a livello chimico, ed infatti in letteratura sono proposti diversi schemi cinetici, descritti ad esempio da Yamashita Y. e Ouchi K. in "*Carbon*", 1982, Vol. 20, n. 1, pp. 41-45, 47-53, e 55-58, da K.A. Trick e T.E. Saliba in "*Carbon*", 1995, Vol. 33, n. 11, pp. 1509-1515, e da B. A. Bishop et al. in "*Cer. Trans.*" 1, (B), p. 856 (1988) con descrizioni differenti l'una dall'altra. Questo comporta una non approfondita conoscenza del processo e quindi un'intrinseca difficoltà nel determinare i parametri di produzione e, soprattutto, nell'ottenere materiali compositi di elevata qualità. Alcune applicazioni degli schemi LPI sono descritte nelle domande di brevetto JP4074639 A, JP11116348 A, e KR20000046407 A. La criticità intrinseca di questa tecnica è il modello cinetico di trasformazione della resina precursore in matrice; nel caso della produzione del C/C, ad esempio, non è ancora ben individuato un modello cinetico condiviso da tutta la comunità scientifica, che ha proposto modelli differenti e talvolta contraddittori (e.g., cfr. le pubblicazioni di Ouchi, di Trick, e di Bishop e Minkowycz).

Nella tecnica CVI, le preforme sono inserite all'interno di una camera e, grazie a processi ad alta temperatura, il precursore si scinde depositando la matrice nella preforma. Questa tecnica permette delle infiltrazioni di prodotti anche

ad alto spessore. Tuttavia, la tecnica CVI ha tempi di produzione molto lunghi. A titolo esemplificativo, la tecnica CVI è descritta da G. Savage in *"Carbon-carbon composites*", Chapman & Hall, London, 1993, da John D. Buckley e Dan D. Edle in "*Carbon-carbon materials and composites*", Noyes Publications, New Jersey U.S.A., 1993, da Deborah D.L. Chung in "*Carbon fiber composite*", Butterworth-Heinemann, U.S.A., 1994, da J. E. Sheehan et al. in "*Carbon-carbon composite*", Annual Review of Material Science, Vol. 24, 1994, pp. 19-44, da Donald L. Schmidt in "*Carbon- carbon composite (CCC)- A historical perspective*", Wright Laboratory Report, September 1996, U.S.A., da L.M. Manocha in "*High perfor- mance carbon–carbon composites*", Sadhana - Academy Proceedings in Engineer-ing Sciences, Vol. 28, Issue 1-2, 2003, pp. 349-358, e da Peter Morgan in "*Carbon fibers and their composites*", Taylor & Francis Group, U.S.A., 2005. Alcune appli- cazioni della tecnica CVI sono descritte nei documenti brevettuali DE3933039 A1,WO 98/21163 A1, GB 2383053 A, e WO2008050068 A2.

Lo scopo della presente invenzione è, pertanto, quello di consentire, in modo efficiente, affidabile, semplice, ed economico di fabbricare materiali compositi di elevata qualità in tempi di produzione sufficientemente brevi per consentire una produttività significativa.

Un ulteriore scopo della presente invenzione è quella di produrre materiali compositi lavorabili meccanicamente.

Forma oggetto specifico della presente invenzione un procedimento di produzione di materiali compositi a matrice ceramica rinforzati con fibre ceramiche, in cui la matrice ceramica è selezionata dal gruppo comprendente o consistente di matrice carboniosa e matrice in carburo di silicio e le fibre ceramiche sono selezionate dal gruppo comprendente o consistente di fibre di carbonio e fibre in carburo di silicio, il procedimento comprendendo le seguenti fasi:

A. realizzare una preforma di dette fibre ceramiche,

B. effettuare una cura della preforma,

C. effettuare un primo ciclo di pirolisi sul manufatto ottenuto dalla fase B,

D. impregnare il manufatto ottenuto dalla fase C con resina liquida conte-

nente un primo precursore di detta matrice ceramica tramite infiltrazione di fase liquida (LPI),

E. effettuare un primo ciclo di infiltrazione per vapore chimico (CVI) per infiltrare almeno un primo gas, selezionato dal gruppo comprendente gas idrocarburi e gas contenenti silicio, quale secondo precursore di detta matrice ceramica nel manufatto ottenuto dalla fase D,

F. effettuare un secondo ciclo di infiltrazione per vapore chimico (CVI) per infiltrare almeno un secondo gas, selezionato dal gruppo comprendente gas idrocarburi e gas contenenti silicio, quale terzo precursore di detta matrice ceramica nel manufatto ottenuto dalla fase E, ottenendo un laminato,

G. impregnare il laminato ottenuto dalla fase F con resina liquida contenente un quarto precursore di detta matrice ceramica tramite infiltrazione di fase liquida (LPI),

H. effettuare un secondo ciclo di pirolisi sul manufatto ottenuto dalla fase G,

I. controllare se la variazione di peso del manufatto ottenuto dalla fase H rispetto al manufatto ottenuto dalla fase F è minore di una soglia percentuale del peso del laminato ottenuto dalla fase F,

J. se l'esito del controllo della fase I è negativo, ritornare ad eseguire la fase G seguita dalla fase H, altrimenti terminare il procedimento.

Secondo un altro aspetto dell'invenzione, detta soglia percentuale può essere non superiore al 5% in peso, opzionalmente non superiore al 2% in peso, più opzionalmente pari a 1% in peso.

Secondo un ulteriore aspetto dell'invenzione, almeno una tra la fase E e la fase F può essere effettuata ad una temperatura variabile da 500°C a 1400°C, opzionalmente da 800°C a 1200°C, per una durata temporale variabile da 10 ore a 2 ore, più opzionalmente variabile da 8 ore a 2 ore, ancora più opzionalmente variabile da 6 ore a 2 ore.

Secondo un aspetto aggiuntivo dell'invenzione, le fasi D e G possono utilizzare resina liquida contenente un medesimo materiale, per cui il primo precur-

sore di detta matrice ceramica è identico al quarto precursore di detta matrice ceramica, e/o detto almeno un primo gas utilizzato nella fase E può essere identico a detto almeno un secondo gas utilizzato nella fase F, per cui il secondo precursore di detta matrice ceramica è identico al terzo precursore di detta matrice ceramica.

Secondo un altro aspetto dell'invenzione, la fase D può essere effettuata utilizzando quale primo precursore almeno un materiale selezionato dal gruppo comprendente o consistente di resine epossidiche, pece, resine fenoliche, resine furaniche, polistirolo ossidato, policarbosilani, organosilani e tetraetossisilano e/o la fase G può essere effettuata utilizzando quale quarto precursore almeno un materiale selezionato dal gruppo comprendente o consistente di resine epossidiche, pece, resine fenoliche, resine furaniche, polistirolo ossidato, policarbosilani, organosilani e tetraetossisilano.

Secondo un ulteriore aspetto dell'invenzione, nella fase D micropolveri e/o nanopolveri, opzionalmente composte da nanotubi in carbonio (CNT – Carbon NanoTubes) e/o da nanofibre in carbonio (CNF – Carbon NanoFibres) e/o da nanopiastrine di grafene (GNP - Graphene NanoPlatelets), possono essere miscelate con il primo precursore, e/o nella fase G micropolveri e/o nanopolveri, opzionalmente composte da nanotubi in carbonio (CNT – Carbon NanoTubes) e/o da nanofibre in carbonio (CNF – Carbon NanoFibres) e/o da nanopiastrine di gra- fene (GNP - Graphene NanoPlatelets), possono essere miscelate con il quarto precursore.

Secondo un aspetto aggiuntivo dell'invenzione, nella fase E può essere utilizzato metano (CH_4) oppure metiltriclorosilano (CH_3SiCl_3) oppure una miscela di tetraclorosilano ($SiCl_4$) e metano (CH_4) come secondo precursore di detta matrice ceramica, idrogeno (H_2) come gas portante ed argon (Ar) come gas diluente, e/o nella fase F può essere utilizzato metano (CH_4) oppure metiltriclorosilano (CH_3SiCl_3) oppure una miscela di tetraclorosilano ($SiCl_4$) e metano (CH_4) come secondo e terzo precursore di detta matrice ceramica, idrogeno (H_2) come gas portante ed argon (Ar) come gas diluente.

Secondo un altro aspetto dell'invenzione, almeno uno tra il primo ciclo di infiltrazione per vapore chimico (CVI) della fase E ed il secondo ciclo di infiltrazione per vapore chimico (CVI) della fase F può essere realizzato mediante una tecnica isoterma e/o una tecnica a gradiente termico e/o una tecnica con gradiente di pressione.

Secondo un ulteriore aspetto dell'invenzione, almeno uno tra il primo ciclo di infiltrazione per vapore chimico (CVI) della fase E ed il secondo ciclo di infiltrazione per vapore chimico (CVI) della fase F può comprendere o consistere di due o più sotto-cicli isotermi, aventi durata temporale opzionalmente variabile da 100 ore ad 1 ora, più opzionalmente variabile da 60 ore a 1 ora, ancora più opzionalmente variabile da 30 ore a 2 ore, persino più opzionalmente pari a 4 ore.

Secondo un aspetto aggiuntivo dell'invenzione, per una o più delle fasi D, G e H possono essere individuati parametri ottimi di processo comprendenti o consistenti dei valori di temperatura e durata temporale mediante un algoritmo genetico che risolve un modello matematico rappresentato da un sistema di quattro equazioni integrali alle derivate parziali trovando le sue soluzioni ottime, detto modello matematico assumendo che

- il composito è costituito da quattro fasi chimiche: fibre, resina fenolica, char, e gas;
- le fibre non reagiscono durante la pirolisi e la loro concentrazione volumetrica è costante;
- il char è composto principalmente da pirene e fenantrene;
- il gas è costituito da idrogeno; e
- la pressione si mantiene costante,

il sistema di quattro equazioni integrali alle derivate parziali determinando la variazione di concentrazione volumetrica di ognuna delle quattro fasi.

Secondo un altro aspetto dell'invenzione, ognuna delle fasi C e H può essere effettuata utilizzando quale precursore pirolitico almeno un materiale selezionato dal gruppo comprendente o consistente di resine epossidiche, pece, re-

sine fenoliche, policarbosilani, ed organosilani.

Secondo un ulteriore aspetto dell'invenzione, almeno una tra la fase C e la fase H può essere effettuata in atmosfera inerte.

Secondo un aspetto aggiuntivo dell'invenzione, almeno una tra la fase C e la fase H può essere effettuata ad una temperatura massima variabile da 300°C a 1400°C, opzionalmente variabile da 600°C a 1300°C, più opzionalmente variabile da 800°C a 1200°C, ancora più opzionalmente pari a 1100°C, il manufatto su cui viene effettuata la pirolisi essendo mantenuto alla temperatura massima per un periodo opzionalmente variabile da 1 a 10 ore, più opzionalmente variabile da 2 a 8 ore, ancora più opzionalmente pari a 8 ore.

Secondo un altro aspetto dell'invenzione, la fase I può comprendere altresì, prima del controllo della variazione di peso del manufatto ottenuto dalla fase H, pulire il manufatto, opzionalmente tramite una spazzola metallica e/o carta abrasiva.

Secondo un ulteriore aspetto dell'invenzione, nella fase A la preforma può essere realizzata a partire da un tessuto di fibre ceramiche, la fase A comprendendo le seguenti sotto-fasi:

A.1 tagliare il tessuto di fibre ceramiche in una pluralità di strati e disporre detti strati di tessuto uno sull'altro, mantenendo un orientamento delle fibre ceramiche, in un telaio, opzionalmente comprendente o consistente in una cornice e/o dei riferimenti rigidi, ottenendo un assemblato di strati sovrapposti, detti strati di tessuto essendo impregnati, opzionalmente con resina in polvere nel caso in cui dette fibre ceramiche siano fibre di carbonio oppure con polimero liquido nel caso in cui dette fibre ceramiche siano fibre in carburo di silicio,

A.2 porre detti strati sovrapposti di tessuto in un sacco a vuoto, applicando uno strato pelabile all'assemblato di strati sovrapposti,

la fase B, opzionalmente realizzata in autoclave, comprendendo altresì, dopo la cura, la rimozione del sacco a vuoto, la cura della fase B essendo opzionalmente effettuata ad una temperatura variabile da 120°C a 180°C che viene più opzio-

nalmente mantenuta per una durata variabile da 60 minuti a 100 minuti, ancora più opzionalmente pari a 80 minuti.

Il procedimento secondo l'invenzione si basa su una inventiva combinazione delle fasi delle due tecniche LPI e CVI che ottimizza i tempi di produzione e la qualità del materiale composito fabbricato le cui proprietà meccaniche di resistenza a carichi e stress e le cui proprietà termiche dovute alla bassissima conducibilità termica, inclusa una elevata resistenza a stress ed escursioni termiche, sono ottenute in maniera immediatamente ripetibile.

Un ulteriore vantaggio offerto dal procedimento secondo l'invenzione è il fatto che i materiali compositi prodotti sono efficientemente ed affidabilmente lavorabili grazie al loro alto grado di infiltrazione che previene la formazione di cricche e delaminazioni. In particolare, tali materiali si prestano a lavorazioni meccaniche mediante taglio ad acqua, che non influisce sulle caratteristiche del materiale se questo non è sufficientemente poroso, e lavorazioni meccaniche per fresatura che permettono la creazione di geometrie anche complesse a partire dal pieno.

Un vantaggio addizionale offerto dal procedimento secondo l'invenzione deriva dalla possibilità opzionale di modellizzare il procedimento di pirolisi e di ricercare le soluzioni ottime del modello matematico tramite l'utilizzo di algoritmi genetici, che consentono di individuare la combinazione di parametri ottimi di durata e temperatura dello stesso procedimento di pirolisi. Il vantaggio di questa ottimizzazione non è solo quello di garantire la temperatura ed il tempo minimi per effettuare la pirolisi, ed in conseguenza tutto il procedimento complessivo, ma anche quello di garantire la completa conversione del precursore (o dei precursori) nella matrice.

I materiali compositi prodotti mediante il procedimento secondo l'invenzione trovano applicazione in moltissimi ambiti industriali, in particolare nell'industria aeronautica, nell'industria aerospaziale, nell'industria nucleare, e nell'industria dei trasporti automobilistici e ferroviari.

La presente invenzione verrà ora descritta, a titolo illustrativo, ma non li-

mitativo, secondo sue preferite forme di realizzazione, con particolare riferimento alle Figure dei disegni allegati, in cui:

la Figura 1 mostra una rappresentazione schematica di una preferita forma di realizzazione del procedimento secondo l'invenzione;

la Figura 2 mostra una rappresentazione schematica di una fase del procedimento di Figura 1; e

la Figura 3 mostra l'andamento di alcuni parametri di una sottofase di Figura 2.

Nelle Figure numeri di riferimento identici saranno utilizzati per elementi analoghi.

Con riferimento alla Figura 1, si può osservare che la preferita forma di realizzazione del procedimento secondo l'invenzione di produzione di un materiale composito ceramico rinforzato con fibre ceramiche comprende le seguenti fasi:

A. realizzare una preforma di fibre ceramiche (fase 10),

B. effettuare una cura della preforma (fase 20),

C. effettuare un primo ciclo di pirolisi sul manufatto ottenuto dalla fase B (fase 30),

D. impregnare il manufatto ottenuto dalla fase C con resina liquida contenente un primo precursore della matrice ceramica, tramite infiltrazione di fase liquida (LPI) (fase 40),

E. effettuare un primo ciclo di infiltrazione per vapore chimico (CVI), per infiltrare almeno un primo gas quale secondo precursore della matrice ceramica, ad una temperatura opzionalmente variabile da 500°C a 1400°C, più opzionalmente da 800°C a 1200°C, per un tempo opzionalmente variabile da 10 ore a 2 ore, più opzionalmente variabile da 8 ore a 2 ore, ancora più opzionalmente variabile da 6 ore a 2 ore (fase 50),

F. effettuare un secondo ciclo di infiltrazione per vapore chimico (CVI), per infiltrare almeno un secondo gas quale terzo precursore della matrice ceramica, ad una temperatura opzionalmente variabile da 500°C a 1400°C,

più opzionalmente pari variabile da 800°C a 1200°C, per un tempo opzionalmente variabile da 10 ore a 2 ore, più opzionalmente variabile da 8 ore a 2 ore, ancora più opzionalmente variabile da 6 ore a 2 ore (fase 60), ottenendo un laminato,

G. impregnare il laminato ottenuto dalla fase F con resina liquida contenente un quarto precursore della matrice ceramica opzionalmente tramite infiltrazione di fase liquida (LPI) (fase 70),

H. effettuare un secondo ciclo di pirolisi sul manufatto ottenuto dalla fase G (fase 80),

I. controllare se la variazione di peso del manufatto ottenuto dalla fase H rispetto al peso del laminato ottenuto dalla fase F è minore di una soglia percentuale, opzionalmente non superiore al 5% in peso, più opzionalmente non superiore al 2% in peso, ancora più opzionalmente pari a 1% in peso, (fase 90),

J. se il controllo della fase I è negativo (i.e. la variazione di peso è stata superiore alla soglia percentuale), ritornare ad eseguire la fase G (fase 70), seguita quindi dalle fasi H (fase 80) e I (fase 90), altrimenti terminare (fase 100) il procedimento.

In particolare, le fasi D e G possono utilizzare resina liquida contenente un medesimo materiale, per cui il primo precursore della matrice ceramica può essere identico al quarto precursore di detta matrice ceramica. Analogamente, detto almeno un primo gas utilizzato nella fase E può essere identico a detto almeno un secondo gas utilizzato nella fase F, per cui il secondo precursore di detta matrice ceramica può essere identico al terzo precursore di detta matrice ceramica.

Nella fase D, nel caso in cui la matrice ceramica sia una matrice carboniosa, il manufatto ottenuto dalla fase C può essere impregnato con resina liquida contenente, quale primo precursore della matrice carboniosa, ad esempio resine fenoliche e/o furaniche e/o polistirolo ossidato; nel caso in cui la matrice ceramica sia una matrice in carburo di silicio, il manufatto ottenuto dalla fase C può essere impregnato con resina liquida contenente, quale primo precursore della ma-

trice in carburo di silicio, ad esempio tetraetossisilano. L'impregnazione della fase D può essere effettuata tramite infiltrazione di fase liquida (LPI), eventualmente miscelando al primo precursore della matrice ceramica delle micropolveri e/o delle nanopolveri al fine di ottenere una matrice avente migliori prestazioni in termini di proprietà meccaniche; a titolo esemplificativo e non a titolo limitativo, può essere utilizzata una miscela semiliquida (nota come "slurry") a base di resina fenolica e pece, che consente di avere una maggiore percentuale carboniosa al termine dei cicli di pirolisi. Inoltre, possono essere utilizzate micropolveri e/o nanopolveri in grado di influenzare le caratteristiche elettromagnetiche della matrice; in particolare, in funzione della morfologia delle micropolveri e/o nanopolveri utilizzate, è possibile regolare le proprietà di assorbimento dei campi elettromagnetici in termini di potenza assorbita in funzione della frequenza del campo elettromagentico incidente. Le micropolveri e/o nanopolveri che possono essere utilizzate sono, per esempio, quelle composte da nanotubi in carbonio (CNT – Carbon NanoTubes) e/o da nanofibre in carbonio (CNF – Carbon NanoFi- bres) e/o da nanopiastrine di grafene (GNP - Graphene NanoPlatelets). La fase G può avere, in particolare con riferimento al quarto precursore ed all'infiltrazione, caratteristiche analoghe a quelle appena illustrate per la fase D.

Opzionalmente, i parametri ottimi di processo delle fasi D, G e H, precisamente i valori di temperatura e durata temporale, sono individuati mediante un algoritmo genetico, come segue.

L'algoritmo genetico risolve un modello matematico trovando le sue soluzioni ottime. Le ipotesi del modello matematico sono:

- il composito è costituito da quattro fasi chimiche: fibre, resina fenolica, char (residuo carbonioso che costituirà la matrice finale del composito stesso) e gas;
- le fibre non reagiscono (almeno fino a 1400°C) durante la pirolisi e la loro concentrazione volumetrica è costante;
- il char è composto principalmente da pirene e fenantrene;
- il gas è costituito da idrogeno (perché durante la pirolisi è il prodotto

principale); e

- la pressione si mantiene costante.

Per ogni fase chimica sono considerate:

a) la variazione di concentrazione volumetrica in funzione del tempo;
b) le reazioni chimiche tramite l'equazione di Arrhenius; e
c) la diffusione dei gas tramite la legge di Darcy.

Prima di descrivere il modello matematico, si descrivono qui di seguito l'equazione di Arrhenius ed il coefficiente di gassificazione che sono coinvolti nel modello matematico stesso.

L'equazione di Arrhenius è descritta dalla seguente equazione:

$$J = A\varphi e^{-E_a/RT}$$

dove:

- ϕ è la concentrazione volumetrica,
- A è il fattore pre-esponenziale,
- E_a è l'energia di attivazione,
- T è la temperatura, e
- R è la costante dei gas.

Il coefficiente Γ di gassificazione descrive la quota parte di gas che il materiale produce durante una reazione chimica: più è piccolo il coefficiente Γ e minore sarà la quantità di gas rilasciata durante il riscaldamento e maggiore sarà il residuo solido dopo il processo (e.g. il processo di pirolisi in questo modello). In particolare, il coefficiente Γ di gassificazione è espresso da:

$$\Gamma = 1 - \frac{\rho_m(T_{\max})}{\rho_m^0}$$

dove (come descritto da Jurij I.Dimitrienko in "*Thermomechanics of composites under high temperatures*", Kluwer Academic Publishers, Dordrecht (Holland), 1999):

- $\rho_m(T_{max})$ è la densità del materiale quando la temperatura è massima, e

- ρ_m^0 è la densità del materiale al tempo iniziale .

Per le **Errore. L'origine riferimento non è stata trovata.**fibre di carbonio si ha:

$$\frac{\partial \varphi_1}{\partial t} = -(1-\Gamma_1)J_1$$

dove

- ϕ_1 è la concentrazione volumetrica delle fibre,
- Γ_1 è il coefficiente di gassificazione per le fibre (che, ad esempio, per le fibre di carbonio grafitizzate è pari 0,05), e
- J_1 è l'equazione di Arrhenius specifica per le fibre.

Nell'ipotesi che la concentrazione delle fibre non cambi, l'equazione di Arrhenius è uguale a zero (J_1=0), per cui l'equazione diventa:

$$\varphi_1 = \varphi_1^0$$

Per la **Errore. L'origine riferimento non è stata trovata.** resina fenolica si ha:

$$\frac{\partial \varphi_2}{\partial t} = -J_2$$

Dove:

- ϕ_2 è la concentrazione volumetrica della resina fenolica, e
- J_2 è l'equazione di Arrhenius che descrive in questo caso la quantità di resina che reagisce e coinvolge il fattore pre-esponenziale A, l'energia di attivazione Ea, la temperatura T e la costante dei gas R:

$$J_2 = A\varphi_2 e^{-E_a/RT}$$

Per il char si ha:

$$\frac{\partial \varphi_3}{\partial t} = (1 - \Gamma_2) J_2 - J_3$$

dove:

- ϕ_3 è la concentrazione volumetrica del char,
- Γ_2 è il coefficiente di gassificazione per la resina fenolica,
- J_2 e J_3 sono le equazioni di Arrhenius per la resina feolica ed il char, rispettivamente.

Per il gas si ha:

$$\frac{\partial \varphi_4}{\partial t} + \nabla \rho_4 \varphi_4 v_4 = \Gamma_2 J_2$$

dove:

- il primo termine ($\partial \varphi_4 / \partial t$) rappresenta la variazione di concentrazione del gas, in cui ϕ_4 rappresenta la concentrazione volumetrica del gas,
- il secondo termine ($\nabla \rho_4 \varphi_4 v_4$) rappresenta la diffusione del gas nella matrice, in cui ν_4 è il rateo di movimento della fase gas del composito, ed
- il terzo termine ($\Gamma_2 J_2$) rappresenta la sorgente che descrive la quota parte della matrice che si trasforma in gas.

Il secondo termine può essere rappresentato, attraverso l'uso della legge diDarcy (che descrive il flusso di un fluido in un mezzo poroso), dalla seguente for- mula:

$$\rho_4 \varphi_4 v_4 = -\frac{K_4}{\mu_4} \nabla (p \varphi_4)$$

dove:

- μ_4 è la viscosità del gas,
- K_4 è il coefficiente di permeabilità che dipende da φ_4 attraverso secondo

la formula:

$$K_4 = K_0 e^{(S\varphi_4^{1/3})}$$

dove K_0 e S sono valori costanti,

- p è la pressione e può essere scritta come:

$$p = R\rho_4 T$$

L'equazione per il gas diventa quindi

$$\frac{\partial \varphi_4}{\partial t} + \nabla\left(\frac{K_4}{\mu_4} \nabla p_4 \quad T\varphi_4 \right)) = \Gamma_2 J_2$$

Da questo sistema di equazioni integrali alle derivate parziali è possibile calcolare la variazione di concentrazione volumetrica di ognuna delle quattro fasi. L'algoritmo genetico può essere eseguito per una o più delle fasi D, G e H, opzionalmente come sottofase iniziale di ognuna di tali fasi; in particolare, l'algoritmo genetico comprende opzionalmente le seguenti operazioni:

i) assegnare i valori iniziali delle concentrazioni volumetriche di fibre, resina fenolica, char (se siamo al primo ciclo di pirolisi ovviamente il char sarà pari a zero), i coefficienti di gassificazione, la permeabilità dell'idrogeno, il numero di iterazioni ed il numero di cromosomi;

ii) costruire dei cromosomi che inizializzano tutti i valori delle matrici, i quali valori vengono utilizzati per risolvere il sistema di equazioni sopradescritto;

iii) ordinare i cromosomi contenti le soluzioni (precisamente concentrazioni volumetriche, temperatura, e durata temporale) e selezionare i migliori in base alla funzione obiettivo che massimizza la

concentrazione di char;

iv) accoppiare e mutare i cromosomi in modo da ottenere l'evoluzione della famiglia di cromosomi;

v) ripetere l'algoritmo genetico a partire dalla fase ii) per il numero di iterazioni stabilito alla fase i).

L'uscita dell'algoritmo comprende una serie di soluzioni ottime che consentono di poter adattare le proprie esigenze scegliendo la durata temporale o la temperatura desiderati ed ottenendo così, rispettivamente, il tempo necessario o la temperatura per avere la completa trasformazione della resina in char (ossia una matrice completamente carboniosa). Il vantaggio quindi non è solo quello di ottenere i tempi e le temperature minime, ma anche quello di garantire la completa trasformazione del precursore, il che comporta un alto grado di purezza, una morfologia della matrice uniforme che riesce a garantire prestazioni meccaniche elevate .

Nel seguito, vengono illustrate nel dettaglio le fasi del procedimento di Figura 1.

Con riferimento alla Figura 2, nella fase A viene realizzata una preforma a partire da tessuto di fibre di carbonio. In particolare, in una sottofase A.1 (indicata con il numero di riferimento 11), il tessuto di carbonio viene tagliato in una pluralità di strati delle dimensioni richieste che vengono disposti uno sull'altro fino a raggiungere lo spessore ed il peso desiderato, mantenendo l'orientamentodelle fibre desiderato, ottenendo un assemblato di strati sovrapposti. Un telaio, e.g. comprendente o consistente in una cornice e/o dei riferimenti rigidi, garantisce il corretto orientamento delle fibre di carbonio degli strati di tessuto e la forma desiderata per il materiale composito finale: la forma rimarrà infatti inva- riata durante le fasi successive.

Il tessuto di fibre di carbonio per la realizzazione della preforma può essere tessuto secco che viene impregnato (manualmente od automaticamente) con resina in polvere, e.g. resina fenolica per la realizzazione di strutture in carbon/carbon, oppure può essere tessuto pre-impregnato (e.g. ancora mediante

polvere di resina fenolica).

In una sottofase A.2 successiva (indicata con il numero di riferimento 12), gli strati sovrapposti di tessuto di fibre di carbonio impregnati vengono posti in un sacco a vuoto (*vacuum bag*), applicando uno strato pelabile (*peel ply*), opzionalmente in materiale plastico (usualmente nylon), all'assemblato di detti strati sovrapposti, allo scopo di consentire il distacco e la rimozione del materiale (opzionalmente plastico) in cui è realizzato il sacco a vuoto dopo la fase B (indicata con il numero di riferimento 20) di cura, opzionalmente realizzata in autoclave.

Il ciclo di cura in autoclave effettuato durante la fase B dipende dalla specifica resina di cui è impregnato il tessuto di fibre di carbonio dell'assemblato ed i parametri del ciclo di cura sono dati dal produttore della resina, opzionalmente a seguito di un'analisi termogravimetrica in grado di individuare le trasformazioni chimiche dei componenti e la natura del residuo. Usualmente, la temperatura del ciclo di cura è variabile da 120°C a 180°C e viene mantenuta a tale valore per una durata variabile da 60 minuti a 100 minuti, opzionalmente pari a 80 minuti. A titolo esemplificativo, e non a titolo limitativo, la Figura 3 mostra l'andamento della temperatura 200 nel sacco, della pressione 201 nella camera e della pressione 202 nel sacco a vuoto durante un ciclo di cura in autoclave.

Le fasi da D a G (in cui la fase G può essere ripetuta in funzione dell'esito del controllo effettuato nella fase I) della preferita forma di realizzazione del procedimento secondo l'invenzione costituiscono cicli di densificazione del materiale composito.

In particolare, i cicli LPI effettuati nelle fasi D e G non richiedono una regolazione accurata dei parametri di processo, poiché i cicli CVI delle fasi E e F rendono meno critico l'effetto del ciclo LPI (come visto meno prevedibile) sulla densificazione del materiale composito e sulle conseguenti proprietà meccaniche e termiche di quest'ultimo.

Nelle fasi E e F che effettuano il primo ed il secondo ciclo di infiltrazione per vapore chimico (CVI), gas idrocarburi sono infiltrati nella struttura porosa del

manufatto e riscaldati fino ad una temperatura variabile da 900°C a 1400°C, opzionalmente da 1000°C a 1400°C, più opzionalmente da 1100°C a 1300°C, ancora più opzionalmente da 1150°C a 1250°C, persino più opzionalmente pari a 1200°C. In ogni ciclo CVI, il carbonio gassoso inizialmente viene depositato sulla superficie del substrato poroso del manufatto a causa della complessa interazione tra la fase gassosa omogenea e le reazioni superficiali eterogenee. Inoltre, la deposizione di carbonio o di carburo di silicio sulla superficie è significativamente influenzata dai processi di trasporto del gas (convezione e diffusione). Il carbonio pirolitico viene opzionalmente depositato utilizzando metano (CH_4) come secondo precursore e/o come terzo precursore, mentre il carburo di silicio pirolitico viene opzionalmente depositato utilizzando metiltriclorosilano (CH_3SiCl_3) od una miscela di tetraclorosilano ($SiCl_4$) e metano (CH_4) come secondo precursore e/o come terzo precursore; inoltre, il carbonio pirolitico ed il carburo di silicio pirolitico vengono opzionalmente depositati ad una temperatura variabile da 900°C a 1200°C con idrogeno come gas portante (che partecipa alle reazioni chimiche quando viene utilizzata una miscela di tetraclorosilano e metano come secondo precursore e/o come terzo precursore) ed argon come gas diluente. Il tempo ne- cessario per l'infiltrazione è opzionalmente variabile da 2 a 6 ore. La reazione chimica di deposizione nel caso in cui il (secondo e/o terzo) precursore è metano è

$$CH_4\ (g) \rightarrow C(s) + 2H_2\ (g),$$

mentre nel caso in cui il (secondo e/o terzo) precursore è metiltriclorosilano è

$$CH_3SiCl_3 \rightarrow SiC + HCl;$$

nel caso in cui il (secondo e/o terzo) precursore sia una miscela di tetraclorosilano ($SiCl_4$) e metano (CH_4), le reazioni chimiche che conducono alla deposizione di carburi di silicio pirolitico sono molteplici e ad esse partecipa anche l'idrogeno (H_2).

Altre forme di realizzazione del procedimento secondo l'invenzione possono avere che le fasi E ed F utilizzano gas idrocarburi differenti da metano, da metiltriclorosilano e dalla miscela di tetraclorosilano e metano per depositare

carbonio pirolitico e carburo di silicio pirolitico.

Come descritto ad esempio da John D. Buckley e Dan D. Edle in "*Carbon-carbon materials and composites*", Noyes Publications, New Jersey U.S.A., 1993, e da Peter Morgan in "*Carbon fibers and their composites*", Taylor & Francis Group, U.S.A. , 2005, per effettuare un ciclo CVI può essere utilizzata una came- ra, spesso cilindrica, di dimensioni opportune che garantisca temperature di esercizio fino a 1700°C con pressioni fino a 1000 Torr (dove 1 Torr = 133,3223684 Pascal). Le tecniche di infiltrazione CVI utilizzabili nel procedimento secondo l'invenzione possono essere di tipo isotermo, a gradiente termico o con gradien- te di pressione, od anche combinazioni di due o più di queste tre tecniche.

La tecnica isoterma prevede una camera riscaldata, e.g. tramite resistenza, a temperatura uniforme. In questo caso, il manufatto all'interno della camera, per la sua inerzia termica, tenderà a riscaldarsi prima in superficie favorendo l'infiltrazione di carbonio o silicio (quando il secondo e/o terzo precursore è carburo di silicio) solo negli strati superficiali. E' una tecnica con limitati costi di impianto adatta per pezzi a basso spessore. Le altre due tecniche invece prevedono un gradiente di pressione o temperatura in modo da favorire un'infiltrazione uniforme. In particolare, per il gradiente di temperatura si ha un mandrino suscettore che favorisce il riscaldamento anche sul pezzo oltre che il riscaldamento della camera. Il gradiente di pressione può essere ottenuto in vario modo, ad esempio sigillando un lato del manufatto ed immettendo a pressione positiva il (secondo e/o terzo) gas precursore.

L'apparato in cui vengono effettuati i cicli CVI è provvisto di controlli (manuali o automatici) per i gas coinvolti nel ciclo. A titolo esemplificativo, e non a titolo limitativo, nel caso in cui venga utilizzato metano (CH_4) come (secondo e/o terzo) gas precursore, la portata (i.e. la velocità di flusso o *flow rate*) totale dei gas, precisamente il (secondo e/o terzo) gas precursore (ovvero il gas reagente CH_4), il gas portante (H_2) ed il gas diluente (Ar), è controllata da quattro control- lori di flusso di massa (*Mass-Flow Controller*) secondo la seguente tabella (in cui la colonna "range" indica il massimo valore che può assumere il flusso del relati-

vo gas):

Gas	Range
CH4	20000 SCCM
H2	20000 SCCM
Ar	20000 SCCM
Ar (purificante)	50000 SCCM

dove “SCCM” significa “centimetro cubo standard per minuto” (“*standard cubic centimeter per minute*”).

I cicli CVI forniscono i migliori risultati in termini di protezione delle fibre dall’ossidazione e quindi delle proprietà meccaniche complessive del materiale composito finale. Infatti, un ciclo CVI è particolarmente adatto per depositare sottili strati interposti tra fibre e matrice ceramica, riducendo quindi le delaminazioni del materiale composito dovute alla mancanza di infiltrazione di carbonio. In proposito, nel procedimento secondo l’invenzione, il primo e/o il secondo cicloCVI opzionalmente comprende o consiste di due o più sotto-cicli isotermi (di du- rata opzionalmente variabile da 100 ore ad 1 ora, più opzionalmente variabile da 60 ore a 1 ora, ancora più opzionalmente variabile da 30 ore a 2 ore, persino più opzionalmente pari a 4 ore) proprio per creare una sottile interfaccia di carbonio, per cui le fibre di carbonio vengono rivestite con una interfase di carbonio pirolitico avente spessore variabile da 0,01 a 0,5 μm, opzionalmente variabile da 0,05 a 0,3 μm, più opzionalmente variabile da 0,1 a 0,2 μm. In particolare, lo spessore dell’interfaccia è estremamente importante per il comportamento meccanico del materiale composito ceramico poiché uno spessore elevato (maggiore di 0,5 μm) danneggia le proprietà meccaniche del materiale composito, mentre uno spesso- re troppo basso (minore di 0,05 μm) non è sufficiente per assicurare un comportamento resistente. Il rivestimento aggiunto alle fibre di rinforzo tramite i cicli CVI ha una doppia funzione:

- consentire un debole legame tra fibre di rinforzo e matrice ceramica persino se è presente una fessurazione nella matrice;
- proteggere le fibre dall'attacco di agenti ossidanti ed evitare la degradazione delle proprietà meccaniche e termiche del materiale composito.

Le fasi C e H di pirolisi sono opzionalmente effettuate utilizzando quali precursori pirolitici: resine epossidiche, pece, resine fenoliche, policarbosilani, organosilani. Più opzionalmente, quale precursore pirolitico viene utilizzata resina fenolica nel caso di produzione di materiale composito C/C e policarbosilani nel caso di produzione di materiale composito C/SiC.

Nella fase G, il laminato (ottenuto dalla fase F) viene impregnato tramite LPI utilizzando una soluzione contenente un quarto precursore della matrice ceramica. La fase di infiltrazione può essere eseguita in diversi modi, essi possono prevedere l'applicazione della resina a pressione e temperatura ambiente o possono essere eseguiti tramite l'applicazione di temperatura e/o pressione che rendono meno viscoso il quarto precursore in fase liquida. Successivamente, nella fase H il manufatto ottenuto dalla fase G viene pirolizzato in atmosfera inerte; nella fase H, oligomeri a basso peso molecolare ed idrocarburi sono perduti dalla matrice ceramica.

A titolo esemplificativo e non a titolo limitativo, per effettuare il ciclo di pirolisi della fase C può essere utilizzato un forno a muffola di vuoto, di dimensioni utili opportune, che garantisca un'atmosfera inerte (quale ad esempio satura di argon o altro gas inerte) ed una temperatura di esercizio fino a 1400°C (in realtà, anche una temperatura più bassa è appropriata per il ciclo di pirolisi).

Il controllo dell'atmosfera inerte può essere effettuato direttamente attraverso rilevatori di ossigeno oppure indirettamente tramite una leggera sovrappressione della camera del forno da pirolisi rispetto alla pressione ambiente (ad esempio, forni da pirolisi sono disponibili dall'azienda britannica Carbolite Ltd.). Il controllo della temperatura viene vantaggiosamente effettuato almeno in tre punti nella sezione utile del forno; a tale scopo, termocoppie idonee sono quelle di tipo K, N, R ed S. Se il forno prevede dei ripiani, questi possono essere

realizzati in grafite per la loro capacità di mantenere la planarità anche alle alte temperature.

Nel caso il procedimento produca materiale composito C/C, i cicli di pirolisi delle fasi C e H avvengono ad una temperatura massima opzionalmente variabile da 300°C a 1400°C, più opzionalmente variabile da 600°C a 1300°C, ancora più opzionalmente variabile da 800°C a 1200°C, persino più opzionalmente pari a 1100°C. La velocità di rampa (*ramp rate*) della pirolisi è regolata in modo da evitare di causare danni strutturali al materiale; a titolo esemplificativo e non a titolo limitativo, la velocità di rampa può essere pari a 100°C/ora dalla temperatura ambiente Ta fino a 500°C, e pari a 60°C/ora da 500°C fino a 1100°C. Il manufatto viene poi mantenuto alla temperatura massima per un periodo variabile da 1 a 10 ore, opzionalmente da 2 a 8 ore, più opzionalmente pari a 8 ore. Dopo ogni sequenza di fasi G e H (che come detto possono essere ripetute più volte a seconda dell'esito del controllo della fase I), il manufatto viene pesato, opzionalmente dopo essere stato pulito per rimuovere il materiale in eccesso, più opzionalmente tramite una spazzola metallica e/o carta abrasiva. In particolare, gli inventori hanno accertato che dopo la prima esecuzione della sequenza di fasi G e H il manufatto ha valori di porosità variabili dal 20% al 40%. Allo scopo di incrementare la densità e la resistenza meccanica del manufatto, questo ha bisogno di una o più ulteriori sequenze di una fase G di infiltrazione LPI e di una fase H di pirolisi, che vengono ripetute finché la variazione di peso del manufatto dopo la fase H di pirolisi è inferiore ad una soglia percentuale (opzionalmente non superiore al 5% in peso, più opzionalmente non superiore al 2% in peso, ancora più opzionalmente pari a 1% in peso) del peso del manufatto ottenuto dalla fase F. Gli inventori hanno verificato che, generalmente, sono necessarie da 2 a 15 ripetizioni della sequenza di fasi G e H, opzionalmente almeno 4 ripetizioni, più opzionalmente almeno 5 ripetizioni, ancora più opzionalmente 8 ripetizioni.

Nel caso il procedimento produca materiale composito C/SiC, che è geometricamente simile ad un materiale composito C/C, l'unica differenza del procedimento è nella lavorazione della preforma. Infatti, in tal caso la matrice in

carburo di silicio viene opzionalmente ottenuta da una o più infiltrazioni della preforma con polimero liquido seguita da una fase B di cura. Le fasi C e H di pirolisi sono opzionalmente effettuate in atmosfera inerte ad una temperatura massima opzionalmente variabile da 300°C a 1400°C, più opzionalmente variabile da 600°C a 1300°C, ancora più opzionalmente variabile da 800°C a 1200°C, persino più opzionalmente pari a 1100°C. Anche in questo caso, la velocità di rampa della pirolisi è regolata in modo da evitare di causare danni strutturali al materiale; a titolo esemplificativo e non a titolo limitativo, la velocità di rampa può ancora essere pari a 100°C/ora dalla temperatura ambiente Ta fino a 500°C, e pari a60°C/ora da 500°C fino a 1100°C. Anche in questo caso, il manufatto viene poi mantenuto alla temperatura massima per un periodo variabile da 1 a 10 ore, op- zionalmente da 2 a 8 ore, più opzionalmente pari a 8 ore.

In quel che precede sono state descritte le preferite forme di realizzazione e sono state suggerite delle varianti della presente invenzione, ma è da intendersi che gli esperti del ramo potranno apportare modificazioni e cambiamenti senza con ciò uscire dal relativo ambito di protezione, come definito dalle rivendicazioni allegate.

RIVENDICAZIONI

1. Procedimento di produzione di materiali compositi a matrice ceramica rinforzati con fibre ceramiche, in cui la matrice ceramica è selezionata dal gruppo comprendente o consistente di matrice carboniosa e matrice in carburo di silicio e le fibre ceramiche sono selezionate dal gruppo comprendente o consistente di fibre di carbonio e fibre in carburo di silicio, il procedimento comprendendo le seguenti fasi:

A. realizzare (10) una preforma di dette fibre ceramiche,

B. effettuare (20) una cura della preforma,

C. effettuare (30) un primo ciclo di pirolisi sul manufatto ottenuto dalla fase B,

D. impregnare (40) il manufatto ottenuto dalla fase C con resina liquida contenente un primo precursore di detta matrice ceramica tramite infiltrazione di fase liquida (LPI),

E. effettuare (50) un primo ciclo di infiltrazione per vapore chimico (CVI) per infiltrare almeno un primo gas, selezionato dal gruppo comprendente gas idrocarburi e gas contenenti silicio, quale secondo precursore di detta matrice ceramica nel manufatto ottenuto dalla fase D,

F. effettuare (60) un secondo ciclo di infiltrazione per vapore chimico (CVI) per infiltrare almeno un secondo gas, selezionato dal gruppo comprendente gas idrocarburi e gas contenenti silicio, quale terzo precursore di detta matrice ceramica nel manufatto ottenuto dalla fase E, ottenendo un laminato,

G. impregnare (70) il laminato ottenuto dalla fase F con resina liquida contenente un quarto precursore di detta matrice ceramica tramite infiltrazione di fase liquida (LPI),

H. effettuare (80) un secondo ciclo di pirolisi sul manufatto ottenuto dalla fase G,

I. controllare (90) se la variazione di peso del manufatto ottenuto dalla fase H rispetto al manufatto ottenuto dalla fase F è minore di una soglia per-

centuale del peso del laminato ottenuto dalla fase F,

J. se l'esito del controllo della fase I è negativo, ritornare ad eseguire la fase G (70) seguita dalla fase H (80), altrimenti terminare (100) il procedimento.

2. Procedimento secondo la rivendicazione 1, caratterizzato dal fatto che detta soglia percentuale è non superiore al 5% in peso, opzionalmente non superiore al 2% in peso, più opzionalmente pari a 1% in peso.

3. Procedimento secondo la rivendicazione 1 o 2, caratterizzato dal fatto che almeno una tra la fase E e la fase F è effettuata ad una temperatura variabile da 500°C a 1400°C, opzionalmente da 800°C a 1200°C, per una durata temporale variabile da 10 ore a 2 ore, più opzionalmente variabile da 8 ore a 2 ore, ancora più opzionalmente variabile da 6 ore a 2 ore.

4. Procedimento secondo una qualsiasi delle precedenti rivendicazioni, caratterizzato dal fatto che le fasi D e G utilizzano resina liquida contenente un medesimo materiale, per cui il primo precursore di detta matrice ceramica è identico al quarto precursore di detta matrice ceramica, e/o dal fatto che detto almeno un primo gas utilizzato nella fase E è identico a detto almeno un secondo gas utilizzato nella fase F, per cui il secondo precursore di detta matrice ceramica è identico al terzo precursore di detta matrice ceramica.

5. Procedimento secondo una qualsiasi delle precedenti rivendicazioni, caratterizzato dal fatto che la fase D è effettuata utilizzando quale primo precursore almeno un materiale selezionato dal gruppo comprendente o consistente di resine epossidiche, pece, resine fenoliche, resine furaniche, polistirolo ossidato, policarbosilani, organosilani e tetraetossisilano e/o dal fatto che la fase G è effettuata utilizzando quale quarto precursore almeno un materiale selezionato dal gruppo comprendente o consistente di resine epossidiche, pece, resine fenoli- che, resine furaniche, polistirolo ossidato, policarbosilani, organosilani e tetraetossisilano.

6. Procedimento secondo una qualsiasi delle precedenti rivendicazioni, caratterizzato dal fatto che nella fase D micropolveri e/o nanopolveri, opzional-

mente composte da nanotubi in carbonio (CNT – Carbon NanoTubes) e/o da nanofibre in carbonio (CNF – Carbon NanoFibres) e/o da nanopiastrine di grafene (GNP - Graphene NanoPlatelets), sono miscelate con il primo precursore, e/o dal fatto che nella fase G micropolveri e/o nanopolveri, opzionalmente composte da nanotubi in carbonio (CNT – Carbon NanoTubes) e/o da nanofibre in carbonio (CNF – Carbon NanoFibres) e/o da nanopiastrine di grafene (GNP - Graphene NanoPlatelets), sono miscelate con il quarto precursore.

7. Procedimento secondo una qualsiasi delle precedenti rivendicazioni, caratterizzato dal fatto che nella fase E viene utilizzato metano (CH_4) oppure metiltriclorosilano (CH_3SiCl_3) oppure una miscela di tetraclorosilano ($SiCl_4$) e metano (CH_4) come secondo precursore di detta matrice ceramica, idrogeno (H_2) come gas portante ed argon (Ar) come gas diluente, e/o dal fatto che nella fase F viene utilizzato metano (CH_4) oppure metiltriclorosilano (CH_3SiCl_3) oppure una miscela di tetraclorosilano ($SiCl_4$) e metano (CH_4) come secondo e terzo precursore di detta matrice ceramica, idrogeno (H_2) come gas portante ed argon (Ar) come gas diluente.

8. Procedimento secondo una qualsiasi delle precedenti rivendicazioni, caratterizzato dal fatto che almeno uno tra il primo ciclo di infiltrazione per vapore chimico (CVI) della fase E ed il secondo ciclo di infiltrazione per vapore chimico (CVI) della fase F è realizzato mediante una tecnica isoterma e/o una tecnica a gradiente termico e/o una tecnica con gradiente di pressione.

9. Procedimento secondo la rivendicazione 8, caratterizzato dal fatto che almeno uno tra il primo ciclo di infiltrazione per vapore chimico (CVI) della fase E ed il secondo ciclo di infiltrazione per vapore chimico (CVI) della fase F comprende o consiste di due o più sotto-cicli isotermi, aventi durata temporale opzionalmente variabile da 100 ore ad 1 ora, più opzionalmente variabile da 60 ore a 1 ora, ancora più opzionalmente variabile da 30 ore a 2 ore, persino più opzional- mente pari a 4 ore.

10. Procedimento secondo una qualsiasi delle precedenti rivendicazioni, caratterizzato dal fatto che per una o più delle fasi D, G e H vengono individuati

parametri ottimi di processo comprendenti o consistenti dei valori di temperatura e durata temporale mediante un algoritmo genetico che risolve un modello matematico rappresentato da un sistema di quattro equazioni integrali alle derivate parziali trovando le sue soluzioni ottime, detto modello matematico assumendo che

- il composito è costituito da quattro fasi chimiche: fibre, resina fenolica, char, e gas;
- le fibre non reagiscono durante la pirolisi e la loro concentrazione volumetrica è costante;
- il char è composto principalmente da pirene e fenantrene;
- il gas è costituito da idrogeno; e
- la pressione si mantiene costante,

il sistema di quattro equazioni integrali alle derivate parziali determinando la variazione di concentrazione volumetrica di ognuna delle quattro fasi.

11. Procedimento secondo una qualsiasi delle precedenti rivendicazioni, caratterizzato dal fatto che ognuna delle fasi C e H è effettuata utilizzando quale precursore pirolitico almeno un materiale selezionato dal gruppo comprendente o consistente di resine epossidiche, pece, resine fenoliche, policarbosilani, ed organosilani.

12. Procedimento secondo una qualsiasi delle precedenti rivendicazioni, caratterizzato dal fatto che almeno una tra la fase C e la fase H è effettuata in atmosfera inerte.

13. Procedimento secondo una qualsiasi delle precedenti rivendicazioni, caratterizzato dal fatto che almeno una tra la fase C e la fase H è effettuata ad una temperatura massima variabile da 300°C a 1400°C, opzionalmente variabile da 600°C a 1300°C, più opzionalmente variabile da 800°C a 1200°C, ancora più opzionalmente pari a 1100°C, il manufatto su cui viene effettuata la pirolisi essendo mantenuto alla temperatura massima per un periodo opzionalmente variabile da 1 a 10 ore, più opzionalmente variabile da 2 a 8 ore, ancora più opzionalmente pari a 8 ore.

14. Procedimento secondo una qualsiasi delle precedenti rivendicazioni, caratterizzato dal fatto che la fase I comprende altresì, prima del controllo della variazione di peso del manufatto ottenuto dalla fase H, pulire il manufatto, opzionalmente tramite una spazzola metallica e/o carta abrasiva.

15. Procedimento secondo una qualsiasi delle precedenti rivendicazioni, caratterizzato dal fatto che nella fase A la preforma è realizzata a partire da un tessuto di fibre ceramiche, la fase A comprendendo le seguenti sotto-fasi:

A.1 tagliare (11) il tessuto di fibre ceramiche in una pluralità di strati e disporre detti strati di tessuto uno sull'altro, mantenendo un orientamento delle fibre ceramiche, in un telaio, opzionalmente comprendente o consistente in una cornice e/o dei riferimenti rigidi, ottenendo un assemblato di strati sovrapposti, detti strati di tessuto essendo impregnati, opzionalmente con resina in polvere nel caso in cui dette fibre ceramiche siano fibre di carbonio oppure con polimero liquido nel caso in cui dette fibre ceramiche siano fibre in carburo di silicio,

A.2 porre (12) detti strati sovrapposti di tessuto in un sacco a vuoto, applicando uno strato pelabile all'assemblato di strati sovrapposti,

la fase B, opzionalmente realizzata in autoclave, comprendendo altresì, dopo la cura, la rimozione del sacco a vuoto, la cura della fase B essendo opzionalmente effettuata ad una temperatura variabile da 120°C a 180°C che viene più opzionalmente mantenuta per una durata variabile da 60 minuti a 100 minuti, ancora più opzionalmente pari a 80 minuti.

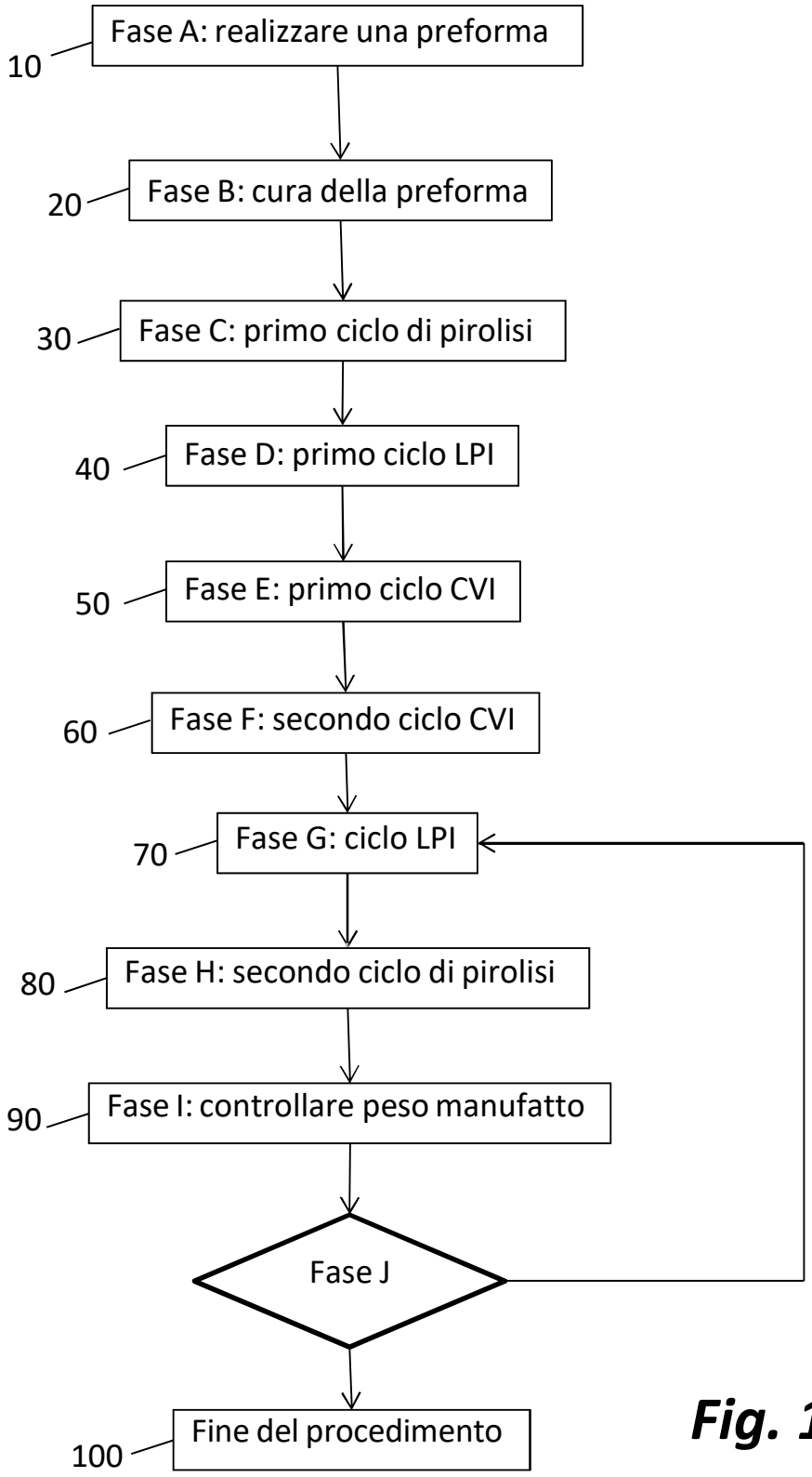
Fase A: realizzare una preforma
10
Fase B: cura della preforma
20
Fase C: primo ciclo di pirolisi
30
Fase D: primo ciclo LPI
40
Fase E: primo ciclo CVI
50
Fase F: secondo ciclo CVI
60
Fase G: ciclo LPI
70
Fase H: secondo ciclo di pirolisi
80
Fase I: controllare peso manufatto
90
Fase J
Fine del procedimento
100

Fig. 1

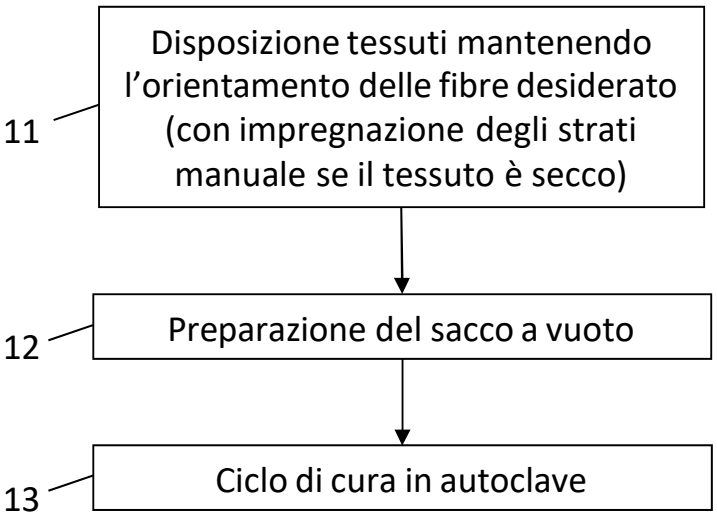
Disposizione tessuti mantenendo l'orientamento delle fibre desiderato (con impregnazione degli strati manuale se il tessuto è secco)
11
Preparazione del sacco a vuoto
12
Ciclo di cura in autoclave
13

Fig. 2

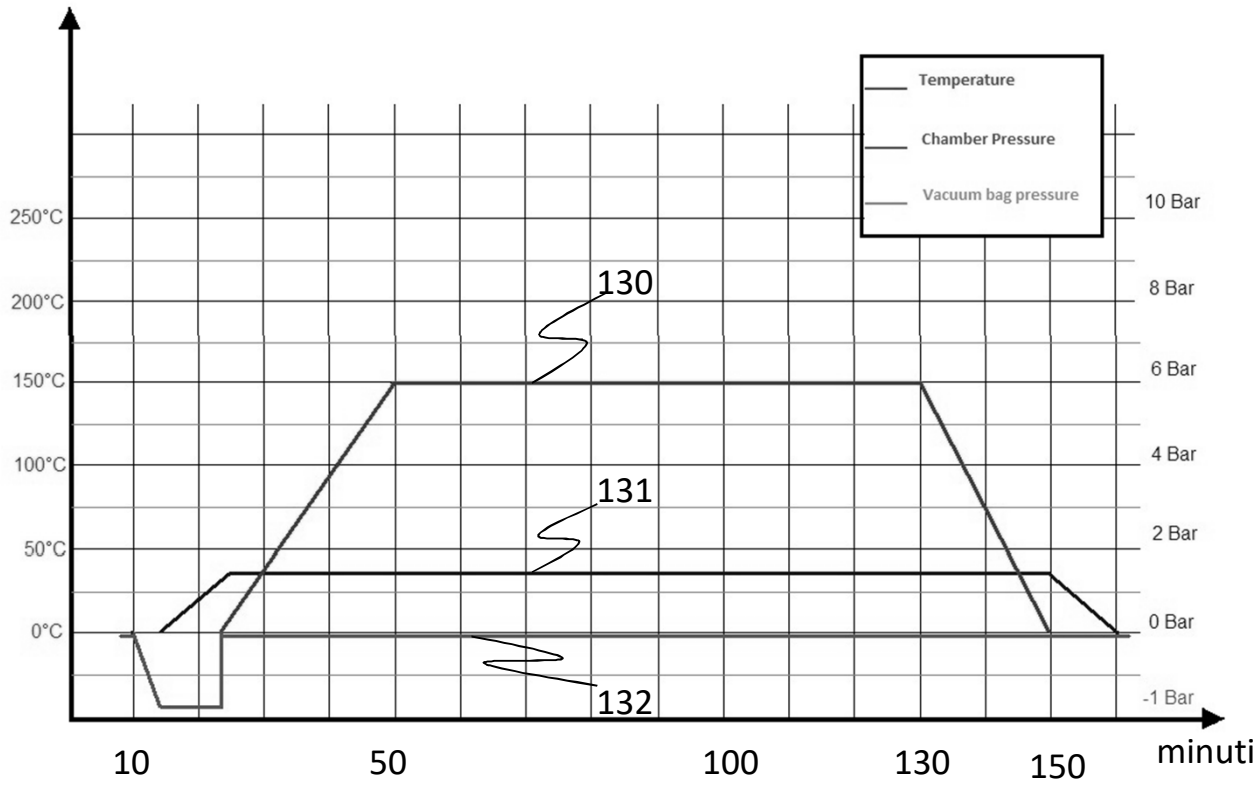
Temperature
Chamber Pressure
Vacuum bag pressure
250°C
200°C
150°C
100°C
50°C
0°C
10 Bar
8 Bar
6 Bar
4 Bar
2 Bar
0 Bar
-1 Bar
130
131
132
10
50
100
130
150
minuti

Fig. 3

WORLD INTELLECTUAL PROPERTY ORGANIZATION

Document No.

WO2021/176289A1

Publication Date

20210910

Applicants

ISTITUTO NAZIONALE DI ASTROFISICA E AGENZIA SPAZIALE ITALIANA

Title

METHOD AND SYSTEM FOR MONITORING THE PRECIPITATION OF PARTICLES IN THE MAGNETOSPHERE

Further details available here

(12) INTERNATIONAL APPLICATION PUBLISHED UNDER THE PATENT COOPERATION TREATY (PCT)

(19) World Intellectual Property Organization
International Bureau

(43) International Publication Date
10 September 2021 (10.09.2021)

WIPO | PCT

(10) International Publication Number
WO 2021/176289 A1

(51) International Patent Classification:
G01V 3/08 (2006.01) *G01V 1/00* (2006.01)
G01T 1/00 (2006.01)

(21) International Application Number:
PCT/IB2021/051335

(22) International Filing Date:
17 February 2021 (17.02.2021)

(25) Filing Language: Italian

(26) Publication Language: English

(30) Priority Data:
102020000004339 02 March 2020 (02.03.2020) IT

(71) Applicants: **ISTITUTO NAZIONALE DI ASTROFISICA-INAF** [IT/IT]; Vial Del Parco Mellini, 84, 00136 Roma (IT). **AGENZIA SPAZIALE ITALIANA** [IT/IT]; Via del Politecnico, snc, 00133 Roma (IT).

(72) Inventors: **ARGAN, Andrea**; c/o Istituto Nazionale Di Astrofisica-inaf, Viale del Parco Mellini, 84, 00136 Roma (IT). **TAVANI, Marco**; c/o Istituto Nazionale Di Astrofisica-inaf, Viale del Parco Mellini, 84, 00136 Roma (IT). **TROIS, Alessio**; c/o Istituto Nazionale Di Astrofisica-inaf, Viale del Parco Mellini, 84, 00136 Roma (IT).

(74) Agent: **CARANGELO, Pierluigi** et al.; c/o Jacobacci & Partners SpA, Via Tomacelli, 146, 00186 Roma (IT).

(81) Designated States *(unless otherwise indicated, for every kind of national protection available)*: AE, AG, AL, AM, AO, AT, AU, AZ, BA, BB, BG, BH, BN, BR, BW, BY, BZ, CA, CH, CL, CN, CO, CR, CU, CZ, DE, DJ, DK, DM, DO, DZ, EC, EE, EG, ES, FI, GB, GD, GE, GH, GM, GT, HN, HR, HU, ID, IL, IN, IR, IS, IT, JO, JP, KE, KG, KH, KN,

(54) Title: METHOD AND SYSTEM FOR MONITORING THE PRECIPITATION OF PARTICLES IN THE MAGNETOSPHERE

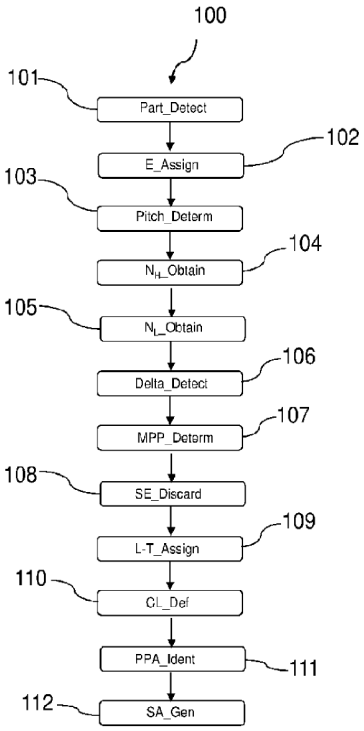

FIG. 3

(57) Abstract: A method (100) for monitoring the precipitation of magnetospheric particles, comprising the steps of: detecting (101) charged magnetospheric particles by at least one particles detector (10) installed on board at least one satellite vehicle (1) in orbit (2) associating the detected particles with respective detection data; processing (102) the detection data to associate a respective estimate or measurement of kinetic energy with the detected magnetospheric particles; obtaining a first count value NH (104) correlated to the number of charged particles, detected in a period of time, which is associated with a relatively higher estimate or measurement of kinetic energy included in a first energy range; obtaining a second count value NL (105) correlated to the number of charged particles, detected in said period of time, which is associated with a relatively lower

WO 2021/176289 A1

[Continued on next page]

KP, KR, KW, KZ, LA, LC, LK, LR, LS, LU, LY, MA, MD, ME, MG, MK, MN, MW, MX, MY, MZ, NA, NG, NI, NO, NZ, OM, PA, PE, PG, PH, PL, PT, QA, RO, RS, RU, RW, SA, SC, SD, SE, SG, SK, SL, ST, SV, SY, TH, TJ, TM, TN, TR, TT, TZ, UA, UG, US, UZ, VC, VN, WS, ZA, ZM, ZW.

(84) **Designated States** *(unless otherwise indicated, for every kind of regional protection available)*: ARIPO (BW, GH, GM, KE, LR, LS, MW, MZ, NA, RW, SD, SL, ST, SZ, TZ, UG, ZM, ZW), Eurasian (AM, AZ, BY, KG, KZ, RU, TJ, TM), European (AL, AT, BE, BG, CH, CY, CZ, DE, DK, EE, ES, FI, FR, GB, GR, HR, HU, IE, IS, IT, LT, LU, LV, MC, MK, MT, NL, NO, PL, PT, RO, RS, SE, SI, SK, SM, TR), OAPI (BF, BJ, CF, CG, CI, CM, GA, GN, GQ, GW, KM, ML, MR, NE, SN, TD, TG).

Published:

— *with international search report (Art. 21(3))*

estimate or measurement of kinetic energy included in a second energy range; detecting a relative variation (106) of the second count value NL with respect to the first count value N_H; determining (110) that in the aforementioned period of time an impulsive event of precipitation of charged particles in the magnetosphere occurred MPP event comparing the aforementioned variation with a threshold value; assigning (109) to the MPP event a geomagnetic longitude and a time in which the MPP event occurred; defining (110) one or more groups of MPP events, each group comprising MPP events which occurred in a time range at the same geomagnetic longitude or at relatively close geomagnetic longitudes; identifying (111) a group of MPP events as indicative of an activity of terrestrial origin, such as a pre-seismic o seismic activity, for example, based on the number of MPP events included in the group and/or based on the associated variations found in the detecting step (109).

"Method and system for monitoring the precipitation of particles in the magnetosphere"

FIELD OF THE INVENTION

[0001] The present invention relates to the technical field of satellite systems for monitoring particles in space and, in particular, for acquiring and processing data relating to the activity of particles. Specifically, the invention relates to a method and a system for monitoring the precipitation of particles in the magnetosphere, which may be implemented using a particles detector. Such method and such monitoring system may be used, for example, to identify possible active regions for pre-seismic activity and to provide alerts for latent activity linked to earthquakes. The monitoring system and method may be used to monitor, in general, electromagnetic perturbations of the Earth magnetosphere induced by terrestrial phenomena.

PRIOR ART

[0002] Demonstrating, with high and reliable statistical significance, a method for correlating physical signals, detectable by means of the current technology, and earthquakes is a difficult problem to solve. Previous attempts during the last few decades have involved several research groups in many countries affected by strong seismic activity, including groups in Italy, Greece, the USA, Japan and China. The methods used have involved ground measurements and, more recently, measurements with space instruments.

[0003] Several cases of anomalous emission of electromagnetic signals with peculiar properties have been reported, temporally and spatially coincident with energetic earthquakes, i.e., earthquakes of a particularly great intensity. Such results,

while interesting, are limited to the determination of occasional evidence between earthquakes and ground or space measurements. The causes thereof are many: lack of a systematic study of such effects over a sufficiently long period of time (years), result reproducibility issues, high background noise influencing the measurement processes, weak overall statistical evidence. No correlation attempt obtained so far has been supported by a highly statistically significant post-trial determination of the probability of occurrence of such results.

[0004] Studies of possible correlations between peculiar magnetospheric particles events and earthquakes have been carried out since the late 1980s. The first works on this topic are by Galper A. M. et al. (1989) as described, for example, in:

- Aleksandrin, S. Yu.; Galper, A. M.; Grishantzeva, L. A.; Koldashov, S. V.; Maslennikov, L. V.; Murashov, A. M.; Picozza, P.; Sgrigna, V.; Voronov, S. A., "High-energy charged particle bursts in the near-Earth space as earthquake precursors", Annales Geophysicae, 21, 597-602 (2003); and
- Galper, A.M., et al., "Connection of the fluxes of charged particles of high energy in radiation belt with the Earth seismicity", Cosmic Research, 27, 789-792 (1989).

[0005] In such studies an attempt was made to develop a method for obtaining a correlation between seismic events and electromagnetic perturbations. The method of Galper et al. is based on:

- a magnetosphere and lithosphere coupling model based on the propagation of electromagnetic waves which propagate along the magnetic L-shells (defined as the field lines identified by the distance in units of terrestrial rays at

which the magnetic field lines intersect the equatorial plane of the Earth magnetosphere) and on the interaction of these waves with the particles trapped in the L-shell, a phenomenon which leads to the precipitation of particles;

- a selection of earthquakes with magnitude (in MMS scale) M ≥ 5 (which is a rather low value, and which therefore leads to correlations between the precipitation of magnetospheric particles and earthquakes of a low statistical significance);
- an identification of the precipitation of particles based on increases or bursts of high-energy particles produced by wave-particle resonance. These precipitations of particles are observed by satellites with appropriate equipment for detecting magnetospheric particles;
- a temporal correlation between the precipitation of magnetospheric particles and seismic events based on the time difference between the precipitation of magnetospheric particles and seismic events occurring on the same L-shells within a narrow range.

[0006] However, due to the methods chosen and the earthquake population selected (of too low magnitude), the results of the above studies are marginal from a statistical point of view. In recent years, there have been no substantial improvements since these first attempts.

[0007] A general description of the above methods is presented, for example, by Pulinets & Boyarchuk in Pulinets, S. & Boyarchuk, K., "Ionospheric Precursors of Earthquakes", Springer (2004). In this publication, the section devoted to the detection of the precipitation of magnetospheric particles is based on the aforementioned articles by Galper et al.

[0008] An informed description of electromagnetic waves possibly associated with earthquakes may be found in Hayakawa M., "Earthquake Prediction with Radio Techniques", (Singapore, John Wiley & Sons, 2015). In this publication and in further publications:

- Hayakawa, M., Yoshino, T. & Morgounov, V.A., "On the possible influence of seismic activity on the propagation of magnetospheric whistlers at low latitudes", Phys. Earth and Planet. Interiors, 77, 97-108 (1993);

- Hayakawa, M., Hobara, Y., Ohta, K., &Hattori, K., "The ultra-low frequency magnetic disturbances associated with earthquakes", Earthquake Sci., 24(6), 523-534 (2011);

- Ohta, K., Izutsu, J., Schekotov, A. & Hayakawa, M., "The ULF/ELF electromagnetic radiation before the 11 March 2011 Japanese earthquake", Radio Science, 48, 589-596 (2013);

circumstantial evidence is presented regarding the emission of low-frequency electromagnetic waves observed in relation to earthquakes of great magnitude. These ground-based observations focus on the detection of ULF and VLF waves using instruments positioned on the ground, with emissions possibly coincident with powerful earthquakes. See also publications:

- Currie, J.L & Waters, J.L., "On the use of geomagnetic indices and ULF waves for earthquakes precursor signatures", J. Geophys. Res. Space Physics, 119, 992-1003 (2014);

- Park, S.A., Johnston, M.J.S., Madden, T.R., Morgan, F.D. & Morrison, H.F., "Electromagnetic precursors to earthquakes in the ULF band: a review of observations and mechanisms", Rev. Geophys., 31, 117-132 (1993).

[0009] Furthermore, some cases of magnetospheric anomalies regarding the so-called total electron content (TEC) have also been discussed given the proximity in space and time thereof with some earthquakes, for example, in the above publication: Hayakawa, M., Earthquake Prediction with Radio Techniques, (Singapore, John Wiley & Sons).

[0010] However, none of the aforementioned studies present a systematic research and no global statistical analysis of the possible correlations between ULF/VLF signals and/or TEC anomalies with earthquakes was discussed, even if it were possible to identify candidates therefrom.

[0011] The DEMETER satellite group (operational in the period 2004-2010) has published observations of wave perturbations in the ionosphere in spatial and temporal proximity to earthquakes of great magnitude. See for example publications:

- Onishi, T., Parrot, M. & Berthelier, J.-J., "The DEMETER mission, recent investigations on ionospheric effects associated with man-made activities and seismic phenomena", Comptes Rendus Physique, 12, 160-170 (2011); and

- Parrot, M., Berthelier, J.~J., Lebreton, J.~P., Sauvaud, J.~A., Santolik, O., and Blecki, J., "Examples of unusual ionospheric observations made by the DEMETER satellite over seismic regions", Physics and Chemistry of the Earth, 31, 486-495 (2006).

[0012] These observations from space (from a height of about 700 km) show interesting detections of VLF and LF waves. However, a global analysis of DEMETER data in temporal proximity to earthquakes does not support the existence of a correlation with a high statistical significance between these wave emissions and earthquakes.

[0013] In practice, so far, no satisfactory demonstration (based on a rigorous and complete statistical analysis) of a systematic correlation between events of magnetospheric particles and earthquakes has been provided. The existence of such a correlation would imply that earthquakes emit electromagnetic and plasma waves capable of propagating along the magnetic field lines and of interacting, by resonance, with electrons and positrons (secondary albedo particles) in the inner Earth magnetosphere. Only circumstantial evidence has been presented in the above literature, and evidence of possible correlations has so far been discussed with completely unsatisfactory statistical analyzes.

[0014] One of the main issues of the method of Galper et al. is linked to the use of L-shells to locate the geographic area potentially affected by the seismic event. Conventionally, the area identified by the aforementioned method consists of two "bands", almost horizontal in longitude, which correspond to the points of intersection of the magnetic field lines, corresponding to given L-shells, with the surface of the Earth, one above the magnetic equator and another one below, both extending to the entire circumference of the Earth. This feature produces great uncertainty about the geographical area where the seismic event may occur.

[0015] Another major limitation of the method of Galper et al. is the low statistical significance and the great number of false correlations (false positives) induced by the choice of correlating magnetospheric events with earthquakes of a magnitude with relatively low threshold (M=5).

[0016] With regard to the magnetospheric anomalies which have been proposed in correlation with earthquakes (such as the phenomena affecting the TEC), this evidence has always been

presented as events of a "post-factum" nature without a full discussion of the global context in which such anomalies are normally revealed, without mentioning the missing discussion of "false positive" events. Similar conclusions may be deduced for the results of the DEMETER satellite, which aim at highlighting ionospheric perturbations and/or anomalous electromagnetic signals in the lower magnetosphere.

[0017] It is therefore possible to conclude that the current magnetospheric measurements of particle bursts associable with earthquakes through magnetic L-shells, anomalies of the TEC type, and ionospheric perturbations constitute, at best, only circumstantial evidence for a possible correlation with earthquakes. Therefore, investigations based on these assumptions, or on the methods proposed so far, are not based on satisfactory statistical evidence.

[0018] The need is therefore still felt to develop a monitoring method which allows to fully, or at least partially, overcome the drawbacks and limitations of the methods of the prior art described above. It is therefore a general object of the present description to provide a monitoring method which allows to satisfy the aforementioned need.

[0019] Such general object is achieved by means of a monitoring method as defined in general in claim 1. Preferred and advantageous embodiments of the aforementioned monitoring method are defined in the appended dependent claims.

[0020] The invention will be better understood from the following detailed description of particular embodiments, provided by way of example and consequently not limiting in any manner, with reference to the accompanying drawings which are briefly described in the following paragraphs.

BRIEF DESCRIPTION OF THE DRAWINGS

[0021] Figure 1 shows a diagrammatic view of a non-limiting embodiment of an example of a system adapted and configured to implement a method for monitoring the precipitation of particles in the magnetosphere according to the present invention.

[0022] Figure 2 shows a possible embodiment of a particles detector which may be employed in the system of Figure 1.

[0023] Figure 3 shows a non-limiting embodiment of a flow chart of the method for monitoring the precipitation of particles in the magnetosphere according to the present invention.

[0024] Figure 4 shows acquired data relating to the precipitation of particles in a two-dimensional time-longitude diagram.

[0025] Figure 5a shows a timing histogram of data acquired with the monitoring method according to the present invention.

[0026] Figure 5b shows a timing histogram of historical data relating to seismic events in the same period of time as the diagram of Figure 5a.

DETAILED DESCRIPTION

[0027] Figure 1 shows a non-limiting embodiment of a monitoring system 1, 2 adapted and configured to implement a method 100 for monitoring the precipitation of particles in the magnetosphere according to the present invention. Figure 3 shows a flow chart of a possible exemplary and non-limiting embodiment of the aforementioned monitoring method 100.

[0028] With reference to Figure 1, the monitoring system 1, 2 comprises a space segment comprising at least one satellite vehicle 1, or, more briefly, an artificial satellite 1 or satellite 1, movable on an orbit 3 with respect to planet Earth

4. On board the satellite vehicle 1, at least one particles detector 10 is installed, adapted and configured to detect charged magnetospheric particles, preferably charged particles with kinetic energy lower than 1 GeV.

[0029] In accordance with an advantageous embodiment, the aforementioned space segment comprises a plurality of satellite vehicles 1, i.e., a constellation of satellite vehicles 1, on each of which a respective particles detector 10 is installed.

[0030] The monitoring system 1, 2 comprises at least one ground segment comprising at least one ground station 2 adapted and configured to operatively connect, directly or indirectly, with the satellite vehicle 1 to receive telemetry data transmitted by the satellite vehicle 1. The ground station 2 comprises, in a manner *per se* known, satellite data reception apparatuses and one or more processors adapted and configured to process received data to produce processed data. The aforementioned operative connection may be direct or take place by means of other satellite vehicles 1 or, in general, space vehicles or stations. The ground station may comprise several stations, geographically distributed and operatively connected to one another. The monitoring system 1, 2 preferably comprises a display system (not shown in the Figures), such as, for example, at least one display, adapted and configured to display the processed data. The display system is, for example, accommodated in the ground station 2 or in another station or processing center operatively connected to the ground station 2.

[0031] In accordance with a particularly advantageous embodiment, the orbit 3 of the satellite vehicle 1 is an equatorial orbit, preferably an equatorial low Earth orbit (LEO). Since the charged particles of interest for the monitoring method 100 according to the present invention are

charged particles in resonance with magnetospheric plasma waves (the latter being a physical phenomenon which occurs in an efficient manner only with particles such as electrons and positrons), several advantages may be obtained by choosing equatorial LEO orbits with respect to polar orbits, and in particular:

- in an equatorial LEO orbit, the flow of particles in the energy range between 0.01 GeV and 0.10 GeV is dominated by electrons and positrons (which appear to be secondary albedo particles, with respect to primary cosmic rays). The flow thereof is between 10^3 - 10^4 $(m^2\ s\ sr\ GeV)^{-1}$ at a height of about 500 km;
- an equatorial orbit allows to avoid the background due to the high flow of solar particles as well as the background induced by the flow of cosmic protons in the kinetic energy range below 1 GeV;
- an equatorial orbit is the best for acquiring signals according to geomagnetic longitude. On the contrary, polar orbits would not be adapted for this purpose since they lead to acquire signals mainly according to L-shells and not longitudes.

[0032] In accordance with a particularly preferred but not limiting embodiment, the satellite vehicle 1 is, for example, the satellite called AGILE, described, for example, in the article by Tavani, M. et al., "The AGILE Mission, Astron. & Astrophys.", 502, 995-1013 (2009).

[0033] The AGILE satellite is, in fact, in a unique condition to study the phenomenon of the precipitation of particles in the inner magnetosphere since the orbit thereof is not affected by solar storms or by external magnetic perturbations. The AGILE

satellite currently orbits the Earth in an equatorial orbit about 500 km high. On the AGILE satellite, a particles detector 10 is installed which, in particular, is an imaging gamma detector (GRID), which, in addition to detecting cosmic gamma rays with an energy of over 20 MeV, is also capable of efficiently detecting charged magnetospheric particles. This is, for example, accurately described in the article by Argan, A., Piano, G., Tavani, M. & Trois, A., "AGILE as a particle detector", Journal Geophys. Res., 121, 3223-3239 (2016). This latter paper, with regard, in particular, to the structure and operation of the particles detector GRID, is herein entirely incorporated as a reference for describing the structure and operation of a non-limiting example of particle detector 10 suitable for being employed in the monitoring method 100 according to the present invention.

[0034] In the case of the AGILE satellite, the flow of charged particles in the orbit of about 95 min. is dominated by electrons and positrons with kinetic energies lower than one GeV. The charged particles detection rate by the particles detector GRID (after crossing the anticoincidence system of the aforementioned detector) is relatively low (a few Hz). The orbit 3 of the AGILE satellite is not subject to transient increases in the number of charged particles induced by solar activity or magnetic perturbations which instead strongly affect other satellites on inclined or polar orbits.

[0035] In the case of the AGILE satellite, the acceptance of the particles detector GRID for detecting particles is approximately 50 cm^2sr, with an instrumental response which depends on the angle of incidence of the particle with respect to the axis of the particles detector GRID; the detection of cosmic gamma photons therefore coexists with an efficient

acquisition of data of charged particle events. These latter events trigger the on-board data acquisition system and are transmitted to the ground station 2 with precise data preferably regarding acquisition time, local magnetic field and information on the orbital position.

[0036] With reference now to Figure 3, the monitoring method 100 comprises a step 101 of detecting ("Part_Detect") charged magnetospheric particles by the particles detector 10 installed on board the satellite vehicle 1 in orbit, associating the detected charged particles with respective detection data.

[0037] As already explained, a possible example of particles detector 10 is the particles detector GRID installed on board the AGILE satellite, and in such case it is a gamma ray imaging detector which is also such as to detect charged magnetospheric particles, for example, charged with kinetic energy below 1 GeV. In alternative embodiments, the particles detector 10 may, for example, be a simpler and less bulky particles detector, for example, configured to detect and track exclusively charged particles.

[0038] In accordance with a general embodiment, the particles detector 10 comprises a particles imaging tracker and/or an imaging calorimeter.

[0039] In accordance with a particularly advantageous embodiment, the particles detector 10 comprises a multilayer structure 11 or a segmented structure 11, for example, comprising a plurality of solid-state planar sub-detectors and, for example, made of silicon-tungsten, arranged to form a stack of sub-detectors aligned along an axis z. Each of the aforementioned sub-detectors allows, for example, to detect, for each charged particle, the coordinates x, y on an impact

plane and preferably a quantity of charge deposited by the charged particle on the sub-detector. The aforementioned multilayer structure therefore allows to trace in 3D the path of the charged particles inside the particles detector 10. Charged particles with a relatively high amount of kinetic energy may cross the entire multilayer structure 11 and affect all the sub-detectors, also according to the direction, while charged particles with a relatively small amount of kinetic energy may stop after the impact with one or more of the sub-detectors. In the particular example shown in Figure 2, which corresponds to the particles detector GRID installed on board the AGILE satellite, the particles detector 10 comprises a multilayer structure 11 and preferably also a calorimeter 12, for example in cesium iodide, in which the multilayer structure 11 is above the calorimeter 12. The particles detector 10 may comprise, for example, an anticoincidence screen 13.

[0040] For example, the detection data associated with each charged particle in step 101 of the monitoring method 100 include data related to the path, for example in 3D, of the charged particle inside the particles detector 10 and/or the quantity of charge deposited by the particle in the detector 10 and/or the time in which the detection of the charged particle occurred and/or the geomagnetic longitude at which the detection of the particle occurred.

[0041] The monitoring method 100 further comprises a step 106 ("E_Assign") of processing the detection data to associate, i.e. assign, the detected magnetospheric particles to a respective estimate or measurement of kinetic energy. Estimate or measurement of kinetic energy means any data of the quantitative type corresponding, or correlated, to the kinetic energy of the charged particle. This estimate or measurement may be obtained

according to various methodologies known to the skilled in the art, for example, by counting the number of sub-detectors crossed by the charged particle and/or by analyzing the geometric path of the charged particle in the multilayer structure (for example, the deviations of such path) and/or by measuring the quantity of charge deposited by the particle, for example, on each of the sub-detectors involved, and/or by using the data provided by the calorimeter 12 (if provided).

[0042] In accordance with an advantageous embodiment, the monitoring method 100 further comprises a step of determining 103 the pitch of the arrival directions of the charged magnetospheric particles with respect to the local magnetic field, and of selecting (for subsequent processing) particles having a pitch included in one or more pitch ranges. Thereby, it is possible to discard detection events which are not, absolutely or statistically, of interest for subsequent processing. For example, charged particles, the arrival direction of which is perpendicular or almost perpendicular to the local magnetic field, may be discarded, since charged particles characterized by these arrival directions are not statistically particles for which a precipitation phenomenon is in progress.

[0043] The monitoring method 100 further comprises:

- a step of obtaining 104 ("N_H_Obtain") a first count value N_H correlated to the number of charged particles, detected in a period of time, which is associated with a relatively higher estimate or measurement of kinetic energy included in a first energy range;

- a step of obtaining 105 ("N_L_Obtain") a second count value N_L correlated to the number of particles, detected in said period

of time, which is associated with a relatively lower estimate or measurement of kinetic energy included in a second energy range.

[0044] The first energy range and the second energy range may be defined as a high-energy channel and a low-energy channel, respectively.

[0045] In accordance with a particularly advantageous embodiment, the first energy range and the second energy range are selected so that under normal conditions the first count value N_H and the second count value N_L are mutually equal or approximately mutually equal.

[0046] Conveniently, the first energy range comprises energies greater than 60 MeV and the second energy range comprises energies lower than 40 MeV. Advantageously, the second energy range comprises energies higher than 5 MeV, for example, higher than 10 MeV and lower than 40 MeV.

[0047] In accordance with a possible embodiment, the two energy ranges are adjacent to each other and have an extreme in common, equal to, or equal to about, 50 MeV. For example, the first energy range includes energies lower than (or lower / equal to) about 55 MeV and the second energy range includes energies greater / equal to (or greater than) 55 MeV.

[0048] For the purposes of the present description, when the word "about" is associated with a numerical value, it is intended to designate both the exact numerical value as well as variations of up to 10% above or below said numerical value.

[0049] Again with reference to Figure 3, the monitoring method 100 further comprises the steps of:

- detecting a relative variation 106 ("Delta_Detect") of the

second count value N_L with respect to the first count value N_H;

- determining 107 ("MPP_Determ") that in the aforementioned period of time an impulsive event of precipitation of particles in the magnetosphere occurred - or "MPP event" - comparing the aforementioned variation with a threshold value.

From a practical point of view, an MPP event is an event indicative of an impulsive precipitation of charged particles due to resonance phenomena between charged particles and radiation, such as, for example, plasma waves, which propagate in the Earth magnetosphere. Said radiation may, for example, be caused by natural and/or artificial phenomena affecting the Earth atmosphere and/or lithosphere.

[0050] According to a particularly advantageous embodiment, the aforementioned threshold value is established correlating historical data of said variations to historical data relating to events of seismic or pre-seismic activity comprising geolocation and intensity information of said events.

[0051] The aforementioned MPP event constitutes an event representative of impulsive precipitations of charged magnetospheric particles with respect to precipitations of charged particles which are generally detectable in the absence of perturbations.

[0052] The aforementioned time range may be a large or small range at will and, for example, it may be of the order of one second or of the order of ten seconds.

[0053] In accordance with an advantageous embodiment, the step of detecting a relative variation 106 comprises an operation of calculating a ratio HR - Hardness Ratio - between the first

count value N_H and the second count value N_L, or vice versa. The step of determining 107 ("MPP_Determ") that an MPP event has occurred therefore comprises an operation of verifying whether said HR ratio is above, or below, or equal to said threshold value.

[0054] For example, in the case where $HR=N_H/N_L$, the threshold value beyond which it may be determined that an MPP event has occurred is greater than or equal to ten, for example, equal to about fifteen, for example equal to fourteen. It has been shown that it is advantageous to select the energy ranges for which the N_H and N_L values are counted, so that such values, under normal conditions, are equal to or almost equal to each other, so that the HR ratio is generally equal to or about equal to one.

[0055] In accordance with an advantageous embodiment, the monitoring method 100 further comprises a step of eliminating and/or identifying 108 ("SE_Discard") spurious events, correlating said variation detected in the detecting step 106 with indices of magnetospheric and solar activity. In fact, it is known that some types of events, such as, for example, solar storms, may cause anomalous precipitations of charged magnetospheric particles.

[0056] The monitoring method 100 further comprises the steps of:

- assigning 109 ("L-T-Assign") to each MPP event a geomagnetic longitude and a time in which the MPP event occurred;

- defining 110 ("CL_Def") one or more groups of MPP events, or clusters of MPP events, each group comprising MPP events which occurred in a time range at a same geomagnetic longitude or at relatively close geomagnetic longitudes.

[0057] For example, the aforementioned time range is of the order of a few weeks, and, for example, it is equal to 3-5 weeks, for example, it is equal to 4 weeks.

[0058] For example, relatively close geomagnetic longitudes are longitudes included in a range of longitudes having an amplitude equal to a maximum of 20° and, for example, equal to, or equal to about, 15° or 10°.

[0059] The monitoring method 100, following the step of defining 110 one or more groups of MPP events, comprises a step of identifying 111 ("PPA_Ident") a group or cluster of MPP events as indicative of a natural or artificial terrestrial activity, such as, for example, a pre-seismic o seismic activity, based on the number of MPP events included in the group and/or based on the associated variations found in the detecting step 106. Such number is greater than or equal to one and preferably greater than or equal to two. For example, if a very high HR is associated with the MPP event, it may be decided that the cluster is a degenerate cluster and includes only one MPP event. For MPP events with lower HR, for example, equal to ten, it may be established that a group of MPP events, in order to be indicative of a pre-seismic or seismic activity, must contain a minimum number of events equal to two, or three or four. It should be noted that the aforementioned activities are not limited to seismic or pre-seismic activities, since they may also include other natural activities (for example, of a meteorological nature, such as terrestrial gamma-ray flashes) or artificial activities which may influence the precipitation of particles.

[0060] Preferably, the monitoring method 100 further comprises a step 112 ("SA_GEN") of generating a seismic or pre-seismic alert. Said alert may, for example, be displayed on a screen

and/or sent by means of a data message, to, for example, a text message or an email.

[0061] For example, in Figure 4, MPP events for which the calculated HR (Hardness Ratio) value is greater than or equal to fourteen are mapped on a two-dimensional longitude-time diagram. In these MPP events, in practice, a significant depletion occurred in the precipitation of low-energy charged particles with respect to the precipitation of high-energy charged particles. In Figure 4, six groups of MPP events, or clusters, identified in the step 111 of the monitoring method 100 have been marked with respective dashed circles.

[0062] It should be noted that the steps of the monitoring method 100 described above may be performed in a different order from that of the diagram of Figure 3, for example, the counting steps 104 and 105 may be inverted or carried out simultaneously. Furthermore, it is necessary to perform the step of detecting particles 101 on board the satellite vehicle 1 while the subsequent processing steps may be performed on the ground after storing the data on board the satellite vehicle 1 and transmitting the data acquired in step 101 to the ground station 2, although the execution of some of said steps on board the satellite vehicle 1 may be advantageous for discarding, already on board the satellite, particles and/or MPP events which are not of interest for the subsequent processing steps, so as to reduce the bandwidth resources required for transmitting data to the ground.

Experimental results

[0063] The experimental results obtained by processing data acquired by the AGILE satellite by means of a processing system based on specially developed software will be described below.

[0064] The focus has been on detecting, by the particles detector GRID of the AGILE satellite, with high statistical significance, impulsive decreases of particles detected in the low-energy channel with respect to those detected in the high-energy channel. "Hardness" is defined as the Hardness Ratio (HR) defined as the number of high-energy events divided by the number of low-energy events, both determined during the same time range δt. An impulsive MPP event is defined in terms of the associated hardness HR during a time range δt. HR(N) is the value of the hardness relative to the MPP event for HR values greater than or equal to N. The measured rates of the particle counts in the two energy ranges (and therefore the HR(N) values) are subject to the Poisson statistic as well as to possible other effects affecting the existence thereof.

[0065] The particle data flow provided by the AGILE satellite along the equatorial orbit continuously provides HR values according to time T and geomagnetic longitude LG. Given the detection capabilities of AGILE, an appropriate binning for the analysis of the longitude and time features of the HR are given by time bins of one day and by geomagnetic longitude bins of one degree. As an example, Figure 4 shows the longitude and time distribution of the MPP events measured with HR(14) during the acquisition of the data of the present analysis (April 16, 2015 - November 30, 2017). It is very important to appreciate that the MPP event measurements in this case were not affected by solar events or by atmospheric flash-induced magnetospheric effects. The local and global lack of homogeneity, which may be seen in the distribution of MPP events in Figure 4, are therefore not caused by external solar or meteorological effects or by the properties of the particles detector on board the AGILE satellite.

[0066] The developed processing system allows to correlate the distributions of the detected MPP events with the occurrence of earthquakes, i.e., seismic events. The data of interest for such earthquake analysis (time of the seismic event, geographical position, magnitude and physical parameters) are obtained from the public archives of the USGS. In order to minimize the influence of random statistical fluctuations, this analysis only considers earthquakes of magnitude $M > 6$ (in MMS scale), with a special emphasis on earthquakes with $M > 7$.

[0067] The processing system has allowed to verify the existence of a "global" time correlation between MPP events and earthquakes by considering summed quantities for time bins of one hundred days. Such choice is motivated by the need to initially check the possible correlation between apparently random values of the MPP events and a quantity proportional to the total seismic energy for the most energetic earthquakes. For this purpose, the temporal behavior of two amplitudes was compared. The first amplitude is a quantity proportional to the negative of the logarithm of the joint probability according to the Poisson statistic of having MPP events within the bin of one hundred days. The second amplitude is a quantity proportional to the negative of the logarithm of the joint probability of having earthquakes within the same time bin, assuming the probability of occurrence of earthquakes anticorrelated with the energy thereof. These quantities are summed over the entire range of longitudes (excluding values in the South Atlantic anomaly, SAA) and within time bins of one hundred days and are then plotted as histograms of the normalized values for the MPP events (HR) and for the cumulative energies of the earthquakes (Ψ_N), separately. Figures 5a and 5b show the result of such analysis for the HR(14) and for the

earthquakes of magnitude M > 6 of the Northern geomagnetic hemisphere. The similarity of the two distributions of MPP events and earthquakes is evident at first glance, with maxima and minima falling within the same time ranges. A joint statistical analysis of the two distributions aimed at testing the hypothesis of a correlation between the two provides the value of the Kolmogorov-Smirnov coefficient equal to 0.97, and a Pearson coefficient equal to 0.928.

[0068] As a next step, the geo-localization of the MPP events has been considered, taking into consideration the fact that a value of the geomagnetic longitude L_G may be attributed to each MPP event. At this point, the MPP events may be mapped into a two-dimensional longitude-time diagram, and it is possible to identify groups of MPPs (clusters) comprising statistically significant MPPs.

[0069] A correlation between prominent MPP events and high-intensity earthquakes may be expected, not only in relation to time but also to geomagnetic longitude, if a fraction of the MPP events are directly correlated with electromagnetic signals originating in earthquake-affected regions and are channeled along the North-South magnetic meridians; such electromagnetic signals propagate along the magnetic field lines (as expected from VLF/ELF and whistler waves). Given the statistics of the MPP events and the coverage of the AGILE satellite per unit of longitude and time, possible correlations between MPP events and earthquakes have been studied on a day-week scale for longitude ranges given by the Dobrovolsky radius R_D (which measures the radius of the region affected by the seismic phenomenon; R_D depends on the magnitude of the seismic event). For each earthquake, a two-dimensional "active region" (AR) is determined, centered on the position of the seismic event

defined in geomagnetic longitude by the range $\Delta L' = 2R_D$ and in time by the time range $\Delta T'$. This latter quantity is determined by the distributions of time delays $\Delta T = T_{MPP} - T_{EQ}$ (with seven-day bins) between MPPs with HR(15) and earthquakes (EQ) in the Northern geomagnetic hemisphere of magnitudes $M \geq 6.4$ and $M > 7$, which occur within regions in the range $\Delta L'$. Both distributions show an excess of peak events in the first negative time bin (implying that a subset of MPP events anticipate seismic events) with a non-symmetric amplitude of the distribution around the peak. From the distributions observed, the time range defining the active regions is obtained from the set of the three bins which precede the seismic event and a bin following it. The total time range defining the active regions is therefore $\Delta T' =$ four weeks, consisting of three weeks before the EQ and one week after the EQ. A complete simulation was performed so as to determine the statistical significance of such procedure (see below the section "Statistical Discussion").

[0070] After defining the regions of the seismic events, the active regions were then assigned to the MPP clusters in the two-dimensional map, identifying them as regions of possible pre-seismic activity (PPA).

[0071] For future events, in the case of significant clustering above the MPP event threshold, the developed processing system produces a pre-seismic warning by specifying the geomagnetic longitude range, the time range and the probability of occurrence of the cluster of MPP events observed.

[0072] The processing system also produces MPP event maps obtained for different threshold parameters and may make them available for electronic transmission (computers and smartphones by means of dedicated pages/applications).

Statistical analysis

[0073] MPP events with large Hardness Ratio values (HR) and active regions for large magnitude earthquakes are correlated not only in time but also in geomagnetic longitude. The two-dimensional distributions of MPPs with HR(15) and of the active regions for earthquakes of magnitude M > 7 are considered herein. A first estimate of the probability of random occurrence of the similarity of the two distributions is based on the binomial probability $p = 2x10^{-8}$ that the observed MPP events overlap in time and longitude the active regions. Such value is confirmed by a complete simulation, as shown below.

[0074] The statistical significance of the results obtained was determined by carrying out a complete simulation of the HR signals, reproducing the random fluctuations induced by the Poisson statistic influencing the MPP events. Three conditions were imposed to select cases of interest for randomly generated distributions. The first condition (C1) is based on the global temporal correlation shown in Figures 5a and 5b: a simulated distribution of MPP events must satisfy the requirement of reproducing a correlation similar to that shown in Figures 5a and 5b. The second condition (C2) is imposed by the two-dimensional distributions: the total number of HR(15) falling within the active regions for seismic events with M > 7 must be equal to or greater than 17 (as determined by the observations). The third condition (C3) is dictated by imposing that the number of active regions with at least one HR(15) therein is greater than or equal to 10 out of the 13 in total, obtained from the observations. A first estimate of the pre-trial probability may be obtained from the product of the three conditional probabilities of C1-C2-C3, $P_{tot-pre} = P(C1,C2,C3) = P(C1)\ P(C2|C1)\ P(C3|C1,C2)$.

[0075] The estimate $P(C1) = 7.3 \times 10^{-5}$, based on the value of the Pearson coefficient of Figures 5a and 5b, had already been obtained. A binomial estimate of the (unconditional) probability $P(C2) = 2 \times 10^{-8}$ was also obtained. Furthermore, it holds $P(C3|C1,C2) = 0.22$. The product of these probabilities is therefore $P(C1)\ P(C2)\ P(C3|C1,C2) = 3.2 \times 10^{-13}$.

[0076] However, due to the difficulty in determining the conditional probability $P(C2|C1)$, only a complete simulation with a sufficiently large number of iterations may provide the final value of the total pre-trial probability $P_{tot\text{-}pre}$. A complete simulation was then carried out with a total number of iterations equal to 6.267×10^{12}. Such simulation produces 25 cases of simulated configurations which satisfy the conditions C1-C2-C3 for the case of HR(15) and of EQ in the Northern geomagnetic hemisphere with M > 7. As a result of this simulation, the pre-trial probability for this case is therefore $P_{tot\text{-}pre} = 3.99 \times 10^{-12}$.

[0077] The final probability is obtained by considering the number of trials performed. The conservative estimate of the number of trials is $N_{trial} = 2.6 \times 10^{4}$. The final post-trial total probability that the detected distributions occur randomly is therefore given by the product of $P_{tot\text{-}pre}$ *with* N_{trial}, which yields $P_{tot\text{-}post}$ [HR(15), M > 7]= 1.04×10^{-7}. This value corresponds to a statistical significance greater than 5 sigma in units of equivalent standard deviations of a bilateral Gaussian distribution.

[0078] An independent simulation for the case of HR(15) and earthquakes with M ≥ 6.4 (6.058×10^{12} iterations) produces 84 cases which satisfy the conditions C1-C2-C3, and a value $P_{tot\text{-}pre} = 1.39 \times 10^{-11}$, which implies $P_{tot\text{-}post}$ [HR(15), M ≥ 6.4]= 3.6×10^{-7}; such value is slightly below the significance of 5 sigma

in units of equivalent standard deviations of a bilateral Gaussian distribution.

Conclusions

[0079] From the above, it is apparent that the monitoring method 100 and the monitoring system 1, 2 described above allow to fully achieve the preset objects in terms of overcoming the drawbacks of the prior art. By virtue of the analysis of the variations of the precipitation of charged particles, respectively in a relatively high-energy channel and a relatively low-energy channel, if such variations are considered as significant, it is possible to obtain a high degree of correlation between groups of MPP events and seismic events of relatively high magnitude ($M > 6$) and therefore generate seismic or pre-seismic alerts.

[0080] Having established with unprecedented statistical significance the existence of a correlation between MPP events and energetic earthquakes in the Northern geomagnetic hemisphere, it is possible to attribute the causes of the phenomenon of impulsive precipitation of charged particles, observed by means of the monitoring method described, to the wave-particle resonance in the range of the electromagnetic waves of the ELF type. This interpretation is in accordance with what is expected from the propagation of electromagnetic waves in the lithosphere which must pass through rocks and saline water.

[0081] Without prejudice to the principle of the invention, the embodiments and the constructional details may be broadly varied with respect to the above description disclosed by way of non-limiting example, without departing from the scope of the invention as defined in the appended claims.

CLAIMS

1. A method (100) for monitoring the precipitation of magnetospheric particles comprising the steps of:

- detecting (101) charged magnetospheric particles by at least one particles detector (10) installed on board at least one satellite vehicle (1) in orbit (2) associating the detected particles with respective detection data;
- processing (102) the detection data to associate a respective estimate or measurement of kinetic energy with the detected magnetospheric particles;
- obtaining a first count value N_H (104) correlated to the number of charged particles, detected in a period of time, which is associated with a relatively higher estimate or measurement of kinetic energy included in a first energy range;
- obtaining a second count value N_L (105) correlated to the number of charged particles, detected in said period of time, which is associated with a relatively lower estimate or measurement of kinetic energy included in a second energy range;
- detecting a relative variation (106) of the second count value N_L with respect to the first count value N_H;
- determining (110) that in the aforementioned period of time an impulsive event of precipitation of charged particles in the magnetosphere occurred – MPP event - comparing the aforementioned variation with a threshold value;
- assigning (109) to the MPP event a geomagnetic longitude and a time in which the MPP event occurred;
- defining (110) one or more groups of MPP events, each group

comprising MPP events which occurred in a time range at the same geomagnetic longitude or at relatively close geomagnetic longitudes;

- identifying (111) a group of MPP events as indicative of an activity of terrestrial origin, such as for example a pre-seismic o seismic activity, based on the number of MPP events included in the group and/or based on the associated variations found in the detecting step (109).

2. A method (100) according to claim 1, comprising a step of generating (112) an alert of a pre-seismic or seismic activity.

3. A method (100) according to any one of the preceding claims, wherein said step of detecting a relative variation (106) includes an operation of calculating a HR ratio - Hardness Ratio - of the first count value N_H to the second count value N_L, or vice versa, and the determining step (109) includes an operation of verifying whether said HR ratio is higher, or lower, or equal to said threshold value.

4. A method (100) according to any one of the preceding claims, wherein said at least one satellite vehicle (1) is in equatorial orbit (3), preferably in an equatorial low Earth orbit (LEO).

5. A method (100) according to any one of the preceding claims, comprising a step of eliminating and/or identifying (108) spurious events correlating said detected variation with indices of magnetospheric and solar activity.

6. A method (100) according to any one of the preceding claims, wherein the charged particles detector (10) allows detecting charged magnetospheric particles distinguishing them from gamma rays.

7. A method (100) according to any one of the preceding claims, wherein the particles detector (10) comprises a particles imaging tracker and/or an imaging calorimeter.

8. A method (100) according to any one of the preceding claims, wherein the first energy range and the second energy range are selected so that under normal conditions the first count value N_H and the second count value N_L are mutually equal or approximately mutually equal.

9. A method (100) according to any one of the preceding claims, wherein said charged magnetospheric particles are mostly electrons and/or positrons.

10. A method (100) according to any one of the preceding claims, wherein said particles detector (10) is adapted and configured to detect and trace particles having energy less than 1 GeV.

11. A method (100) according to any one of the preceding claims, comprising a step of storing said detection data on board the satellite vehicle (1) and a step of directly or indirectly transmitting at least part of said data to a ground station (2) which is operatively connectable to said satellite vehicle (1).

12. A method (100) according to claim 11, comprising a step of at least partially processing said detection data on board the satellite vehicle and wherein the transmitting step comprises transmitting said processed data.

13. A method (100) according to any one of the preceding claims, wherein the threshold value is established correlating historical data of said variations to historical data related to seismic events comprising geolocation and intensity information of said seismic events.

14. A method (100) according to any one of the preceding claims, further comprising a step of determining (103) the pitch of the charged magnetospheric particles with respect to the local magnetic field and selecting particles having a pitch included in one or more pitch ranges.

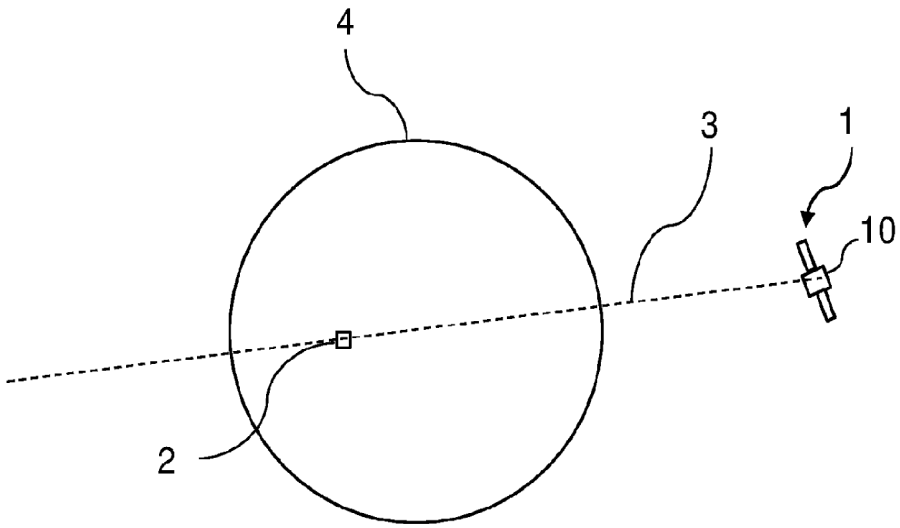

FIG. 1

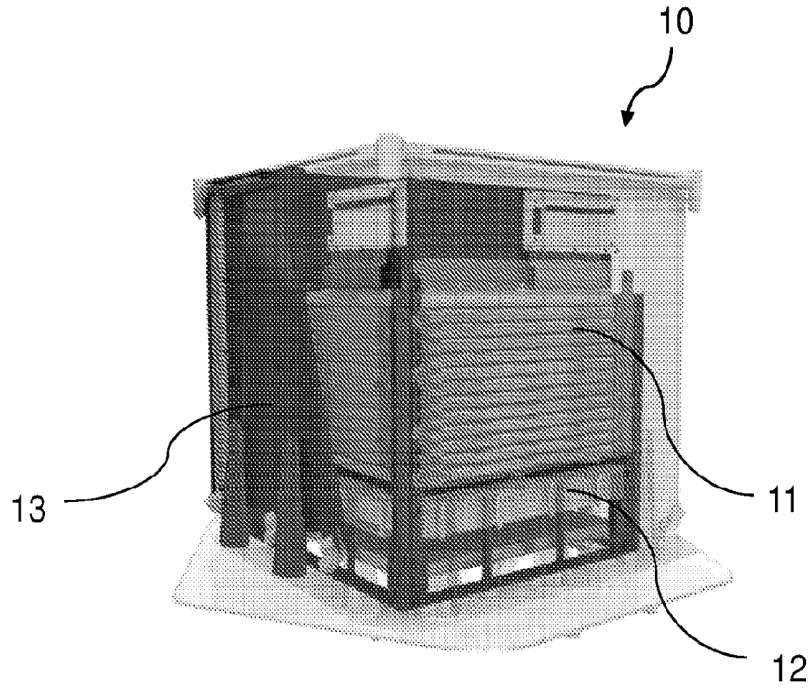

FIG. 2

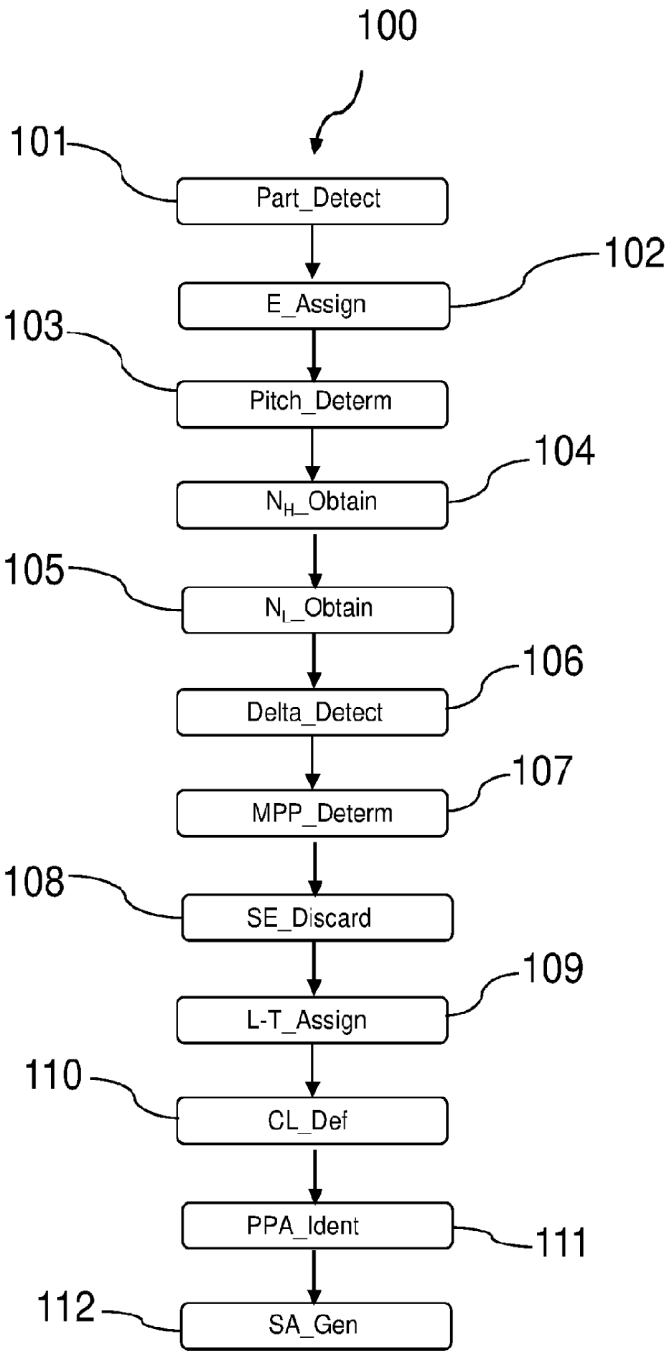
100
101
Part_Detect
102
E_Assign
103
Pitch_Determ
104
N_H_Obtain
105
N_L_Obtain
106
Delta_Detect
107
MPP_Determ
108
SE_Discard
109
L-T_Assign
110
CL_Def
PPA_Ident
111
112
SA_Gen

FIG. 3

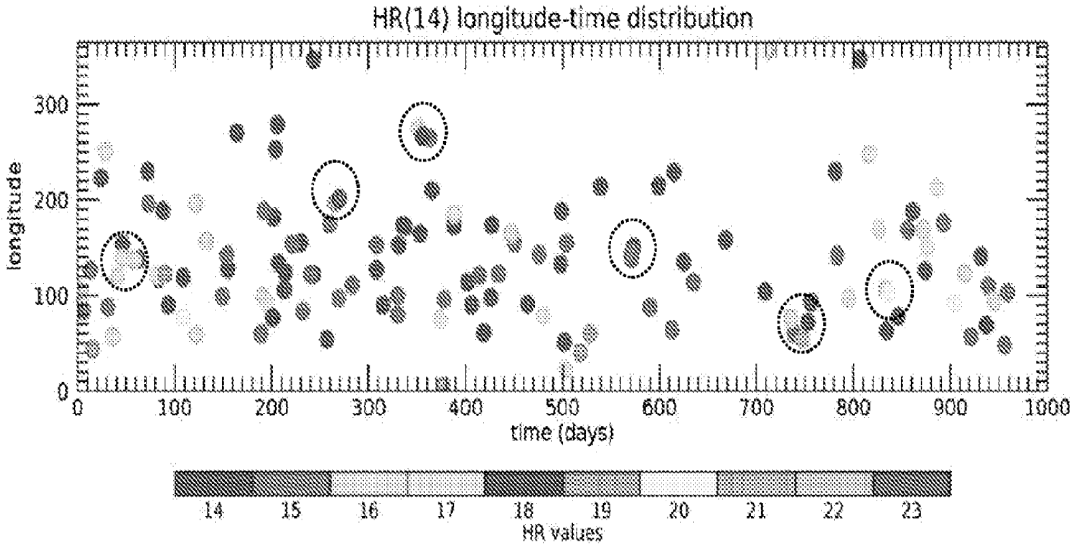

FIG. 4

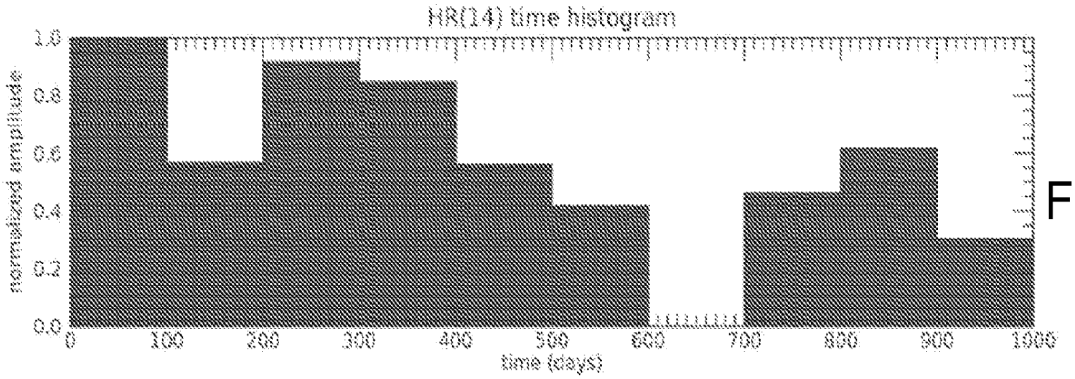

FIG. 5a

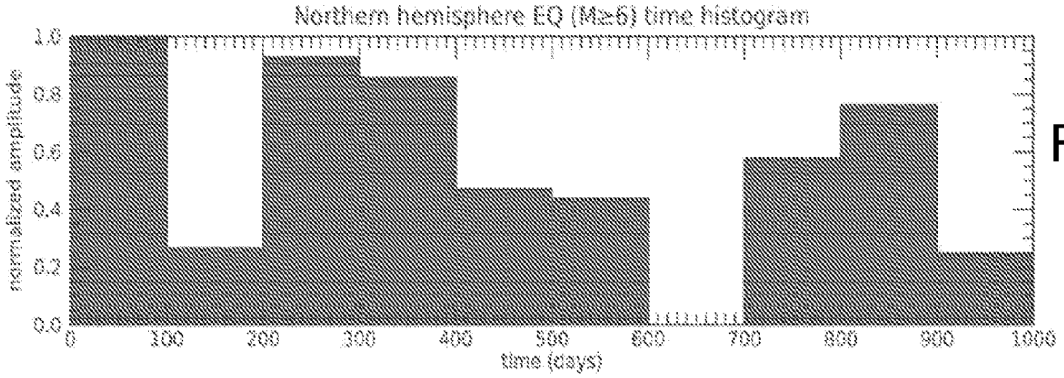

FIG. 5b

INTERNATIONAL SEARCH REPORT

International application No
PCT/IB2021/051335

A. CLASSIFICATION OF SUBJECT MATTER
INV. G01V3/08 G01T1/00 G01V1/00
ADD.

According to International Patent Classification (IPC) or to both national classification and IPC

B. FIELDS SEARCHED

Minimum documentation searched (classification system followed by classification symbols)
G01V G01T

Documentation searched other than minimum documentation to the extent that such documents are included in the fields searched

Electronic data base consulted during the international search (name of data base and, where practicable, search terms used)

EPO-Internal

C. DOCUMENTS CONSIDERED TO BE RELEVANT

Category*	Citation of document, with indication, where appropriate, of the relevant passages	Relevant to claim No.
A	SGRIGNA V ET AL: "Correlations between earthquakes and anomalous particle bursts from SAMPEX/PET satellite observations", JOURNAL OF ATMOSPHERIC AND SOLAR-TERRESTRIAL PHYSICS, PERGAMON, AMSTERDAM, NL, vol. 67, no. 15, 1 October 2005 (2005-10-01), pages 1448-1462, XP027847600, ISSN: 1364-6826 [retrieved on 2005-10-01] paragraph [0003] - paragraph [0004] tables 2-4 ----- -/--	1-14

[X] Further documents are listed in the continuation of Box C. [ ] See patent family annex.

* Special categories of cited documents :

"A" document defining the general state of the art which is not considered to be of particular relevance

"E" earlier application or patent but published on or after the international filing date

"L" document which may throw doubts on priority claim(s) or which is cited to establish the publication date of another citation or other special reason (as specified)

"O" document referring to an oral disclosure, use, exhibition or other means

"P" document published prior to the international filing date but later than the priority date claimed

"T" later document published after the international filing date or priority date and not in conflict with the application but cited to understand the principle or theory underlying the invention

"X" document of particular relevance; the claimed invention cannot be considered novel or cannot be considered to involve an inventive step when the document is taken alone

"Y" document of particular relevance; the claimed invention cannot be considered to involve an inventive step when the document is combined with one or more other such documents, such combination being obvious to a person skilled in the art

"&" document member of the same patent family

Date of the actual completion of the international search	Date of mailing of the international search report
10 May 2021	21/05/2021

Name and mailing address of the ISA/	Authorized officer
European Patent Office, P.B. 5818 Patentlaan 2 NL - 2280 HV Rijswijk Tel. (+31-70) 340-2040, Fax: (+31-70) 340-3016	Breccia, Luca

1

Form PCT/ISA/210 (second sheet) (April 2005)

C(Continuation). DOCUMENTS CONSIDERED TO BE RELEVANT

Category*	Citation of document, with indication, where appropriate, of the relevant passages	Relevant to claim No.
A	XIANGXIANG YAN ET AL: "Multiparameter seismo-ionospheric anomaly observation before the 2008 Wenchuan, China, Mw7.9 earthquake", JOURNAL OF APPLIED REMOTE SENSING, SOCIETY OF PHOTO-OPTICAL INSTRUMENTATION ENGINEERS, 1000 20TH ST. BELLINGHAM WA 98225-6705 USA, vol. 7, no. 1, 1 January 2013 (2013-01-01) , page 73532, XP060026650, DOI: 10.1117/1.JRS.7.073532 paragraph [02.4] -----	1-14
A	CHILINGARIAN A ET AL: "Correlated measurements of secondary cosmic ray fluxes by the Aragats Space-Environmental Center monitors", NUCLEAR INSTRUMENTS & METHODS IN PHYSICS RESEARCH. SECTION A, ELSEVIER BV * NORTH-HOLLAND, NL, vol. 543, no. 2-3, 11 May 2005 (2005-05-11), pages 483-496, XP027782903, ISSN: 0168-9002 [retrieved on 2005-05-11] paragraph [0003] -----	1-14

WORLD INTELLECTUAL PROPERTY ORGANIZATION

Document No.

WO2023/126455A1

Publication Date

20230706

Applicant

CONSIGLIO NAZIONALE DELLE RICERCHE E AGENZIA SPAZIALE ITALIANA

Title

PHOTOACOUSTIC SPECTROSCOPY SENSOR FOR TRACE GAS DETECTION AND METHOD FOR TRACE GAS DETECTION

Further details available here

(12) INTERNATIONAL APPLICATION PUBLISHED UNDER THE PATENT COOPERATION TREATY (PCT)

(19) World Intellectual Property Organization
International Bureau

(43) International Publication Date
06 July 2023 (06.07.2023)

WIPO | PCT

(10) International Publication Number
WO 2023/126455 A1

(51) International Patent Classification:
G01N 21/17 (2006.01) *G01N 29/24* (2006.01)
G01N 21/27 (2006.01)

(21) International Application Number:
PCT/EP2022/087976

(22) International Filing Date:
28 December 2022 (28.12.2022)

(25) Filing Language: English

(26) Publication Language: English

(30) Priority Data:
102021000033143 30 December 2021 (30.12.2021) IT

(71) Applicants: **CONSIGLIO NAZIONALE DELLE RICERCHE** [IT/IT]; Piazzale Aldo Moro 7, 00185 Roma (IT). **A.S.I. AGENZIA SPAZIALE ITALIANA** [IT/IT]; Via del Politecnico snc, 00133 Roma (IT).

(72) Inventors: **SICILIANI DE CUMIS, Mario**; Via Cesare Sinopoli 55, 88100 Catanzaro (IT). **BORRI, Simone**; c/o Cosiglio Nazionale delle Ricerche, Piazzale Aldo Moro 7, 00185 Roma (IT). **CANINO, Mariaconcetta**; c/o Consiglio Nazionale delle RIcerche, Piazzale Aldo Moro 7, 00185 Roma (IT). **CANCIO PASTOR, Pablo**; c/o Consiglio Nazionale delle RIcerche, Piazzale Aldo Moro 7, 00185 Roma (IT). **DE NATALE, Paolo**; c/o Consiglio Nazionale delle RIcerche, Piazzale Aldo Moro 7, 00185 Roma (IT). **LOPEZ GARCIA, Inaki**; c/o Consiglio Nazionale delle RIcerche, Piazzale Aldo Moro 7, 00185 Roma (IT). **RONCAGLIA, Alberto**; c/o Consiglio Nazionale delle RIcerche, Piazzale Aldo Moro 7, 00185 Roma (IT).

(54) Title: PHOTOACOUSTIC SPECTROSCOPY SENSOR FOR TRACE GAS DETECTION AND METHOD FOR TRACE GAS DETECTION

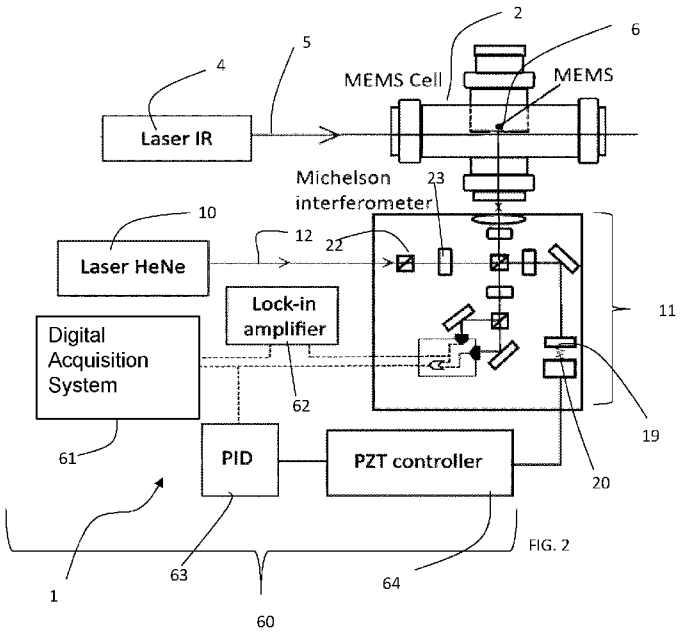

FIG. 2

(57) Abstract: A photoacoustic sensor for spectroscopic gas detection, comprising a chamber adapted to contain the gas to be analysed, an excitation laser source adapted to emit a modulated laser beam, which is absorbed by the gas present in the chamber and creating a pressure wave, a transducer, the transducer being located inside the chamber, and being adapted to be put into oscillations by the pressure wave, the transducer having a reflective portion, an interferometer having a first and a second arm and an output able to detect the oscillations of the transducer, with the first arm ending in the transducer, and the second arm including an optical path changer element and an actuator connected to the optical path changer element to change the optical path defined by the second arm of the interferometer, a first polarizing beam splitter, a second laser source for interferometer reading, adapted to emit a second laser beam impinging onto the first polarizing beam splitter, the first polarizing beam splitter being adapted to split the second laser beam in the

WO 2023/126455 A1

[Continued on next page]

(74) **Agent: MORABITO, Sara** et al.; Cantaluppi & Partners S.r.l., Piazzetta Cappellato Pedrocchi, 18, 35122 Padova (IT).

(81) **Designated States** *(unless otherwise indicated, for every kind of national protection available)*: AE, AG, AL, AM, AO, AT, AU, AZ, BA, BB, BG, BH, BN, BR, BW, BY, BZ, CA, CH, CL, CN, CO, CR, CU, CV, CZ, DE, DJ, DK, DM, DO, DZ, EC, EE, EG, ES, FI, GB, GD, GE, GH, GM, GT, HN, HR, HU, ID, IL, IN, IQ, IR, IS, IT, JM, JO, JP, KE, KG, KH, KN, KP, KR, KW, KZ, LA, LC, LK, LR, LS, LU, LY, MA, MD, MG, MK, MN, MW, MX, MY, MZ, NA, NG, NI, NO, NZ, OM, PA, PE, PG, PH, PL, PT, QA, RO, RS, RU, RW, SA, SC, SD, SE, SG, SK, SL, ST, SV, SY, TH, TJ, TM, TN, TR, TT, TZ, UA, UG, US, UZ, VC, VN, WS, ZA, ZM, ZW.

(84) **Designated States** *(unless otherwise indicated, for every kind of regional protection available)*: ARIPO (BW, CV, GH, GM, KE, LR, LS, MW, MZ, NA, RW, SD, SL, ST, SZ, TZ, UG, ZM, ZW), Eurasian (AM, AZ, BY, KG, KZ, RU, TJ, TM), European (AL, AT, BE, BG, CH, CY, CZ, DE, DK, EE, ES, FI, FR, GB, GR, HR, HU, IE, IS, IT, LT, LU, LV, MC, ME, MK, MT, NL, NO, PL, PT, RO, RS, SE, SI, SK, SM, TR), OAPI (BF, BJ, CF, CG, CI, CM, GA, GN, GQ, GW, KM, ML, MR, NE, SN, TD, TG).

Declarations under Rule 4.17:

— *of inventorship (Rule 4.17(iv))*

Published:

— *with international search report (Art. 21(3))*

— *in black and white; the international application as filed contained color or greyscale and is available for download from PATENTSCOPE*

first and the second arm of the interferometer, so that the split beam travelling in the first arm is back- reflected by the reflective portion of the transducer, and the split beam travelling in the second arm is back-reflected by the optical path changer element, so that the resulting back-reflected split beams interfere in the interferometer, a second polarizing beam splitter adapted to split the interfering light at the output of the interferometer in two beams which are orthogonally polarized, a first detector adapted to detect one of the two orthogonally polarized beam exiting the interferometer and to generate a corresponding first electric signal, a second detector adapted to detect the other of the two orthogonally polarized beam exiting the interferometer and to generate a corresponding second electric signal, an electronic circuit configured to obtain a difference signal, the difference signal being function of the difference between the signal generated by the first detector and the signal generated by the second detector, and a feedback loop adapted to command the movements of the actuator in order to change and stabilize the optical path of the second arm, so that the difference signal is kept equal to a desired constant value during the gas concentration measurements.

Photoacoustic spectroscopy sensor for trace gas detection and method for trace gas detection

The present invention relates to a photoacoustic sensor to detect traces of selected molecular species in a gas. Furthermore, the invention relates to a method to detect traces of a gas using a photoacoustic phenomenon.

In molecular trace gas analysis, researchers are constantly pushing towards more sensitive, affordable and robust instruments as required by the industry and the scientific community. For example, the SCAR technique has been developed, described in WO 2017/055606, which achieves few parts per quadrillion-ppq (10^{-15}) record sensitivities. However, such accurate measurements are possible at the expense of a relatively high cost, a limited portability and highly sophisticated components. Modern photo-acoustic spectroscopic (PAS) techniques, such as cantilever-enhanced photo-acoustic spectroscopy (CEPAS), quartz-enhanced photo-acoustic spectroscopy (QEPAS) and variants of cavity-enhanced photo-acoustic spectroscopy are also techniques known in the art which can achieve high sensitivities. For example, for the standard QEPAS sensor sensitivity of 50 parts per trillion-ppt (10^{-12}) on SF_6 has been obtained, as described in V. Spagnolo, P. Patimisco, S. Borri, G. Scamarcio, B. E. Bernacki, and J. Kriesel, Opt. Lett. 37, 4461 (2012) with cost-effective elements, non-critical optical alignment, and possibility of fabricating very compact systems. Furthermore, this technique is suitable for several implementations, which can improve its performance. Commercial sensors are available, as produced by companies like Thorlabs.

The CEPAS sensors developed so far present an almost unique design of the cantiveler (rectangular shape) and of the detection scheme, using a standard interferometric reading. The variants on which research groups have worked concern the design of the acoustic cell and the cantilever support. These sensors are commercialized by the Finnish company GASERA, and some aspects of the sensors are described for example in US 7,738,116 and US 9,170,397.

Recently, a CEPAS sensor has demonstrated sub-ppt detection on HF in T. Tomberg, M. Vainio, T. Hieta and L. Halonen, Sci. Rep. 8, 1848 (2018), though obtained with the use of a very complex high power optical source (Optical Parametric Oscillator). However, this result demonstrates the high potential of both the CEPAS technique and its possible implementations.

An example of a Michelson interferometeric optophone is described in the document CHU J H ET AL: "Michelson interferometric detection for optoacoustic spectroscopy", OPTICS COMMUNICATIONS, ELSEVIER, AMSTERDAM, NL, vol. 89, no. 2-4, 1 May 1992 (1992-05-01), pages 135-139.

The present invention relates to a photoacoustic sensor and a method to detect gas traces that achieve a relatively high sensitivity. In particular, the sensor and the method of the invention allows solving – at least partially – some of the instability problems over time (drifts) of the sensor. Furthermore, the sensor and the

method of the invention allow averaging the signal obtained by the measurements over longer timescales, improving sensitivity and avoiding systematic effects in the determination of the concentration of the trace species in the gas sample.

According to a first aspect, the invention relates to a photoacoustic sensor for spectroscopic gas detection, comprising:

- A chamber adapted to contain the gas to be analysed;
- An excitation laser source adapted to emit a frequency- or amplitude-modulated laser beam, which is absorbed by the gas present in the chamber and creating a pressure wave;
- A transducer, the transducer being located inside the chamber, and being adapted to be put into oscillations by the pressure wave, the transducer having a reflective portion;
- An interferometer having a first and a second arm and an output, with the first arm ending in the transducer, and the second arm including an optical path changer element and an actuator connected to the optical path changer element to change the optical path defined by the second arm of the interferometer;
- A first polarizing beam splitter;
- A second laser source for interferometer reading, adapted to emit a second laser beam impinging onto the first polarizing beam splitter, the first polarizing beam splitter being adapted to split the second laser beam in the first and the second arm of the interferometer, so that the split beam travelling in the first arm is back-reflected by the reflective portion of the transducer, and the split beam travelling in the second arm is back-reflected by the optical path changer element, so that the resulting back-reflected split beams interfere in the interferometer;
- A second polarizing beam splitter adapted to split the interfering light at the output of the interferometer in two beams which are orthogonally polarized;
- A first detector adapted to detect one of the two orthogonally polarized beam exiting the interferometer and to emit a corresponding first interference signal;
- A second detector adapted to detect the other of the two orthogonally polarized beam exiting the interferometer and to emit a corresponding second interference signal;
- An electronic circuit configured to obtain a difference signal, the difference signal being function of the difference between the signal generated by the first detector and the signal generated by the second detector;
- A feedback loop adapted to command the movements of the actuator in order to change the optical path of the second arm, so that the difference signal is kept equal to a desired constant value during the gas concentration measurements.

According to a different aspect, the invention relates to a method to detect a gas concentration by means of a photoacoustic phenomenon, the method comprising:

- Providing a chamber where a gas is located, the concentration of which is to be measured;
- Providing a transducer in the chamber, the transducer comprising a reflective portion;
- Generating a pressure wave in the chamber by means of a modulated excitation laser beam directed into the chamber, according to the photo-acoustic phenomenon, the pressure wave putting the transducer in oscillation;
- Impinging with a second laser beam onto the reflective portion of the transducer;
- providing an interferometer, having a first arm terminating into the transducer and a second arm terminating into an optical path changer element adapted to vary the path length of the second arm;
- Directing a second laser beam towards the interferometer, the second laser beam forming a first back-reflected beam when reflected by the transducer and a second back reflected beam when reflected by the optical path changer element;
- Creating an interference between the first and the second back-reflected beams;
- Splitting the interfering back-reflected beams in a first and a second interference beam;
- Polarizing the first and/or the second interference beam so that their polarization axes are mutually perpendicular;
- Detecting the first interference beam and the second interference beam generating a first and a second signal;
- generating a difference signal function of the difference between the first signal and the second signal;
- Defining a working point value of the difference signal;
- Adapting the optical path length of the second arm actuating the actuator so that the difference signal is kept equal to the working point value during the gas concentration measurement.

According to an embodiment of the invention, a different device able to control the interferometer optical path can be substituted to the actuators, e.g. a liquid crystal or electro-optic element or any device able to change the phase of the radiation.

It should be noted that the feature of “the second detector adapted to detect the other of the two orthogonally polarized beam exiting the interferometer and to emit a corresponding second interference signal” represents a differential detection scheme, centered on the zero, that is obtained when the two beams have perfectly orthogonal polarization. Any unbalance in polarization gives a nonzero signal.

According to an embodiment of the invention, the feedback look is made of an electronic circuit taking the difference signal, comparing it to a desired fixed value, and producing an error signal to be sent to the actuator.

According to an embodiment of the invention, the step of "defining a working point value of the difference signal" provides for setting the working point value to zero.

In the invention, the sensor and the method are used to detect the gas concentration in the gas chamber. A gas, called gas sample, is located in the gas chamber, normally containing different molecular species, and the purpose of the invention is to measure the concentration of one or more target molecules eventually present in the gas sample in traces. Therefore with "measuring the gas concentration", measuring a specific (target) molecular species among the species present in the gas sample is meant. In addition, some gaseous promoters (e.g. water vapor) may be added, in a known concentration, to the gas sample to be analyzed, in order to enhance the photoacoustic effect.

The gas chamber defines an air-tight enclosure. It can be made of any material suitable in the art. The gas chamber can be used in flow or in static gas conditions.

Furthermore, a first laser source, called excitation laser source, is provided. The first laser source is adapted to emit a first laser beam. Preferably, the first laser source emits a first laser beam. Preferably, the first laser beam is in the infrared (IR) range. The wavelength of the IR beam is selected so that it resonates with roto-vibrational molecular transitions. The infrared beam is an electromagnetic beam having a wavelength in the range 700 nm (frequency 430 THz) - 1 mm (300 GHz). However, any other wavelength, that is resonant with rotational, vibrational, electronic transitions, alone or in combination and exploiting overtones, can be used, if radiation absorption is sufficiently intense to generate detectable acoustic waves.

The first laser source may be located inside the gas chamber, or it may be external to the same. If the first laser source is located outside the gas chamber, a window is preferably present in the gas chamber, which is substantially transparent for the first laser beam, so that this laser beam can pass through the window and reach the inner part of the chamber.

The wavelength of the first laser beam is so selected that it can interact with the target molecules present in the gas of the gas sample. In particular, the wavelength is selected in a way that it excites a molecular transition in the molecules of the gas to be analysed inside the gas chamber. The first laser beam is thus selected so that it is resonant with a selected molecular transition of the gas, the concentration of which is to be measured. Furthermore, the first laser beam is a modulated laser beam. The first laser is (frequency

or amplitude) modulated at a frequency *f*, so that it excites the transition, and the subsequent molecular relaxation produces an acoustic wave.

The infrared laser beam, absorbed by the gas to be analysed, generates heat waves, which result in pressure fluctuations within the gas chamber, substantially forming pressure waves in the chamber. This process is a very well known phenomenon and therefore no further detailed in the following.

Preferably, the pressure inside the chamber is comprised between 1 mbar and atmospheric pressure, more preferably above 10 mbar.

Furthermore, in the gas chamber a transducer is located. The transducer may be connected to a substrate. The substrate may be a silicon wafer. The substrate may be internal or external to the gas chamber. The transducer extends into the gas chamber, that is, it is subject to the pressure wave which develops due to the excitation laser beam. The substrate is then connected, for example by means of a support, to the gas chamber.

According to the invention, the transducer comprises a main component which is adapted to be put into oscillations by a pressure wave. The main component comprises a reflective element with at least a reflective portion forming a mirror of the interferometer.

Preferably, the reflective element defines a triangular surface, a rectangular surface or a squared surface.

Preferably, the reflective element defines a regular polygonal surface or an irregular polygonal surface.

Preferably, the reflective element defines a circular surface or an oval surface.

Preferably, the reflective element is thin compared to the substrate, i.e. the reflective element has a maximum thickness of tens of microns whereas the substrate has a maximum thickness of hundreds of microns.

According to an embodiment of the invention, the reflective element is directly connected (i.e. without other elements) to the chamber, in particular to the substrate. In this case, the main component may be considered as a self-supporting member.

Preferably, the main component, in particular the reflective element, is a membrane or an equivalent structure.

According to another embodiment of the invention, the main component comprises a first suspension structure between the reflective element and the chamber, in particular the substrate. The first suspension structure is made of one or more elongated elements having two opposite longitudinal ends connected to the reflective element and the chamber (in particular the substrate), respectively. Therefore, the reflective

element is connected to the chamber (in particular to the substrate) via the first suspension structure. The first suspension structure supports the reflective element and allows the main component to oscillate. In should be noted that at least one of the number, size and shape of elongated elements of the first suspension structure determines the mechanical resonance spectrum of the main component. For instance, the elongated element of the first suspension structure may have shape of one of beam, arc, L, S, Z and spiral or combination thereof.

Preferably first suspension structure is arranged so that it have no optical function for the photoacoustic sensor.

In addition to the first suspension structure, the transducer may comprise a damping and insulation structure between the first suspension structure and the chamber, in particular the substrate. In this case, a longitudinal end of each elongated element of the first suspension structure is connected to the main component and the other one of each elongated element is connected to damping and insulation structure. Therefore, the main component is connected to the chamber (in particular to the substrate) via the damping and insulation structure. It should be noted that a purpose of the damping and insulation structure is to filter the ambient noise during the use of the photoacoustic sensor.

Preferably, the damping and insulation structure at least partially surrounds the main component. The damping and insulation structure can surround the main component in a symmetrical or asymmetrical way.

Preferably, the mass of the damping and insulation structure is ten times greater than the mass of the main component.

Preferably, the mass and/or size and/or shape of the damping and insulation structure allows to filter out selected frequency components. Moreover, the mechanical modes of the damping and insulation structure do not overlap the modes of the main component nor the working frequency of the photoacoustic sensor (if different).

Preferably, the damping and insulation structure is arranged so that it has no optical function for the photoacoustic sensor.

In addition to the damping and insulation structure, the transducer may comprise a second suspension structure between the damping and insulation structure and the chamber, in particular the substrate. The second suspension structure is made of one or more elongated elements having two opposite longitudinal ends connected to the damping and insulation structure and the chamber (in particular the substrate), respectively. Therefore, the main member is connected to the damping and insulation structure, the latter being connected to the chamber (in particular to the substrate) via the second suspension structure. The second suspension structure supports the damping and insulation structure.

Preferably, the second suspension structure is designed in such a way that the transmission of mechanical frequencies interfering with the working mode of the main component are minimized. For instance, the elongated element of the second suspension structure may have shape of one of beam, arc, L, S, Z and spiral or combination thereof.

Preferably, the second suspension structure is arranged so that they have no optical function for the photoacoustic sensor.

According to another embodiment of the invention, the main component lacks of the first suspension structure and the reflective element is directly connected to the damping and insulation structure which is connected to the chamber, in particular to the substrate. In this case, the transducer may also comprise the second suspension structure so that the damping and insulation structure is connected to the chamber (in particular to the substrate) via the second suspension structure.

The transducer is preferably a microelectromechanical system (MEMS) transducer. MEMS are also referred to as micromachines or microsystem technology (MST). MEMS transducers preferably range in size from 10 µm to a couple of centimeters. With "size", the maximum dimension of the MEMS is meant.

As mentioned, the transducer may be attached to a substrate. The attachment may be a single-point attachment, that is, there is a single connection between the substrate and the MEMS transducer, or multiple-points attachments, where there are multiple connections. The number of connections may be chosen depending on the geometry of the transducer.

Preferably, the transducer has a geometry such that two of its dimensions are much bigger than its third dimension. That is, generally the thickness of the transducer is much smaller than its length or width.

Preferably, three main types of transducer may be considered.

The first type of transducer refers to a transducer whose reflective element is a membrane. The membrane performs a movement similar to the movement of a drum. This is achieved due to a connection between the membrane and the substrate which is symmetrical to an axis. In other words, the membrane has a symmetry axis and the connections between the membrane and the support are symmetric with respect to this axis. This means that a membrane always includes at least two connections between itself and the substrate. The membrane may define a triangular surface, a rectangular or squared surface, it may define a regular or an irregular polygonal surface (preferably, the regular or irregular polygon has a number of sides comprised between 3 and 20), it may define a circular or an oval surface. The thickness of the membrane is preferably comprised between 30 nm and 50 micrometres. Preferably, the thickness depends on the material in which the membrane is formed. The maximum lateral dimension is preferably comprised between 100 micrometres and 2 cm.

With maximum transverse dimension, the maximum dimension of the side of a rectangle circumscribed to the membrane is meant.

Preferred membranes geometries and materials are listed in TABLE 1.

Material	***Further details***	***Thickness***	***Maximum transverse dimension***	***Frequencies of oscillation***
Silicon	polysilicon, crystalline silicon (crystal directions: 100, 110,111)	200 nm- 30 micron	100 micron – 15 mm	10 Hz- 500 kHz
Silicon nitride	Stoichiometric or Non-stoichiometric compound	10 nm-2 micron	100 micron – 10 mm	100 Hz- 1 MHz
Silicon oxide	Stoichiometric or Non-stoichiometric compound	50 nm-2 micron	100 micron – 10 mm	350 Hz- 250 kHz
Multilayer SiO_2+Si_3N_4	Stoichiometric or Non-stoichiometric compound	10 nm-2 micron	100 micron – 10 mm	250 Hz- 350 kHz
SiC – 3C		10 nm-10 micron	100 micron – 10 mm	350 Hz- 250 kHz
SU8		50 nm-30 micron	100 micron – 10 mm	250 Hz- 200 kHz

Indium Tin Oxide (ITO)		10 nm-500 nm	100 micron – 10 mm	250 Hz- 150 kHz

TABLE 1

The second type of transducer refers to a transducer whose main component comprises a first suspension structure between the reflective element and the substrate. In this case, the reflective element may be described as a central element (triangular, rectangular, regular or irregular polygons - side numbers between 3 and 20 – circles). Differently from the membranes, however, the reflective element is connected to the substrate asymmetrically. The transducer can oscillate therefore “anchored on one side”. Also in this case multiple connections may be present between the reflective element and the first suspension structure. The number of connections is preferably comprised between 1 and 20. In particular, the connections between the reflective element and the first suspension structure correspond to the connections between the reflective element and the elongated elements of the first suspension structure.

The shape of the elongated elements of the first suspension structure may be of 4 types:

-right rectangular beams, in this case it is therefore said that there is a single element forming the elongated element;

-L- shape (composition of two perpendicular elements);

- Z – shape (composition of three elements perpendicular to two by two);

- S – shape (composition of at least two z-shape elongated elements).

Preferred geometries and materials of the elongated elements are listed in TABLE 2.

Material	***Further details***	***Thickness***	***Maximum transverse dimension***	***Number of elongated elements***	***Maximum convex hull dimension of an elongated element***	***Oscillation frequencies***

Silicon	polysilicon, crystalline silicon (crystal directions: 100, 110,111)	200 nm-30 micron	100 micron – 15 mm	1-20	100 micron – 10 mm	10 Hz- 900 kHz
SiC – 3C		10 nm-2 micron	100 micron – 10 mm	1-20	100 micron – 10 mm	350 Hz- 250 kHz
SU8		50 nm-30 micron	100 micron – 10 mm	1-20	100 micron – 10 mm	250 Hz- 150 kHz
SU8+Si/Si_3N_4/SiO_2	Silicon, silicon oxide, silcion nitride	50 nm-20 micron	100 micron – 10 mm	1-20	100 micron – 10 mm	400 Hz- 750 kHz

TABLE 2

The third type of transducer refers to a transducer whose main component comprises a first suspension structure between the reflective element and the substrate. Different from the second type-transducer, the first suspension structure has a spiral like shape. The spiral is formed by a plurality of elements connected to each other in series (that is, one after the other). The reflective element is connected to the spiral and forms a central element of the transducer. The central element can have any shape, the same shape detailed when it comes to the membrane.

In this case, the first suspension structure is a composition of bar-like elements with a relative angle between 15 and 179 degrees. The first suspension structure creates “loops” around the central element.

Preferred first suspension structure geometries and materials are listed in TABLE 3.

Material	*Further details*	*Thickness*	*Maximum transverse dimension*	*Number of elements*	*Number of loops*	*Oscillation frequencies*
Silicon	polysilicon, crystalline silicon (crystal directions: 100, 110,111)	200 nm- 30 micron	100 micron – 15 mm	1-20	0.05-3	10 Hz- 500 kHz
SiC – 3C		10 nm-2 micron	100 micron – 10 mm	1-20	0.05-3	350 Hz- 250 kHz
SU8		50 nm-30 micron	100 micron – 10 mm	1-20	0.05-3	250 Hz- 150 kHz
SU8+Si/Si_3N_4/SiO_2	Silicon, silicon oxide, silcion nitride	50 nm-20 micron	100 micron – 10 mm	1-20	0.05-3	400 Hz- 400 kHz

TABLE 3

The pressure wave caused by the excitation of the molecular transition and propagating in the chamber forces the transducer to oscillate. The transducer is thus put into motion by the propagating pressure wave in the chamber. The motions are oscillations.

The frequency of the oscillations of the transducer depends on the modulation frequency of the first laser, the laser that excites the gas molecular transition. The amplitude of the oscillations depend on many factors, including the power of the exciting laser, the modulation depth of the first laser, the gas pressure, the target molecule concentration, the cross section of the selected molecular transition, the presence of gas promoters or interfering molecules. Due to the fact that all these parameters are known, with the

exception of the concentration of the target molecules in the gas, the amplitude of the oscillations of the transducer is measured and from it the concentration is derived.

The amplitude of the photoacoustic wave is given by

$$S = K \cdot P \cdot \sigma \cdot n \qquad (1)$$

where *K* is a constant depending on the transducer geometry, material and dimension, chamber geometry, and modulation frequency, *P* is the optical power of the excitation laser source, σ is the absorption cross-section of the measured transition, and *n* is the density number of absorbing molecules (proportional to their concentration). The constant *K* is usually defined by calibration, and depends on the shape of the cell and on the modulation frequency *f* of the (first) excitation laser:

$$K \propto \frac{1}{f}$$

The acoustic wave forces the transducer to oscillate, at the same frequency *f* and with and amplitude which is proportional to *S*. The acoustic wave can eventually excite also higher-order resonances. The amplitude of the acoustic wave carries the information about the concentration of the target molecules. This information is transferred to the transducer, specifically to its oscillation amplitude, and can be detected interferometrically.

In order to measure such amplitude, the transducer comprises, at least partially, a reflective portion. The reflective portion is reflective for electromagnetic radiation with the features described below. The transducer can be, for example, at least partly, coated by a reflective material or be formed, at least partly, by a reflective material.

Coating materials depend on He-Ne laser (or equivalent) wavelength, transducer material and gas sample. Possible materials are for example one or more of gold, aluminum, silver, dielectric multilayers, polymers and metal oxides.

In order to measure the oscillations of the transducer, an interferometer is provided. The interferometer is part of the sensor. Thanks to the reflecting surface, the transducer forms one of the mirrors of the interferometer.

Interferometry makes use of the principle of superposition to combine waves in a way that will cause the result of their combination to have some meaningful property that provides information on the original state of the waves and on the path/length travelled. This works because when two waves with the same frequency combine, the resulting intensity pattern is determined by the phase difference between the two waves—waves that are in phase will undergo constructive interference while waves that are out of

phase will undergo destructive interference. Waves which are not completely in phase nor completely out of phase will have an intermediate intensity pattern, which can be used to determine their relative phase difference.

In order to obtain interferometric data, a second laser source is provided, called also “reading” laser. This second laser source is adapted to emit a beam of coherent electromagnetic radiation. Usually the reading laser emits in the visible region, which makes alignment of the interferometer easy and where good-quality and cost-effective optical and electronic components are available. One of the common choices for the second laser source is a He-Ne laser, emitting at 633 nm wavelength, due to its good stability, good mode profile, robustness and good quality over price ratio. When compact dimensions are important, visible diode lasers may be preferred

The second laser source may be located outside the chamber. If the second laser source is located outside the chamber, the chamber includes a window transparent to the electromagnetic radiation emitted by the second laser source so that the electromagnetic radiation emitted by the second laser source can enter the chamber. Preferably, the transducer defines a first and a second surface, one opposite to the other. Preferably, the second laser beam impinges onto the first or the second surface of the transducer perpendicularly.

Preferably, inside the chamber, the beam (electromagnetic radiation) emitted by the excitation laser and the beam emitted by the second laser are substantially perpendicular to each other.

The electromagnetic radiation emitted by the second laser source is split in two split beams. This split can be performed for example by a first beam splitter. Each split beam is directed into one of the two different arms of the interferometer, each arm defining an optical path for the electromagnetic radiation. The first arm of the interferometer includes the transducer, where the electromagnetic radiation is back- reflected inside the first arm. The second arm terminates with an optical path changer element, where the split beam is back-reflected into the second arm. The beams of electromagnetic radiation from the two arms are recombined in a standard manner known in the art as interferometer.

The optical path changer, better detailed below, is for example a movable reflecting surface or a device able to control the interferometer optical path can be substituted to the actuators, e.g. a liquid crystal or electro-optic element or any device able to change the phase of the second laser radiation. In this way, the optical path defined by the second arm of the interferometer may be changed. The change is operated via an actuator. The actuator is adapted to operate on the optical path changer element and force the latter to change the optical path defined by the second arm.

The interferometer is designed to get balanced detection, that is, the intensity of the beam exiting the first and the second arm is the same.

The interferometer used is preferably a Michelson interferometer, mounted in a balanced arrangement which ensures the best signal-to-noise ratio possible for a given laser power. Alternatively, a Mach-Zender type interferometer can be used as well.

The proposed balanced arrangement is realized via polarization control of the second laser beam. The second laser radiation has preferably a linear polarization. Alternatively, in order to obtain a linear polarization, proper phase-retarder plates and polarizers are located downstream the second laser to obtain a linearly polarized radiation. Instead of linearly polarized light, perfectly circular polarization can be used as well as the second laser radiation beam. A first polarizing beam splitter divides the second laser beam into two parts, with orthogonal polarizations, each part travelling along one of the two arms of the interferometer. The same first polarizing beam splitter is used to recombine the radiation from the two arms of the interferometer. Another (second) polarizing beam splitter divides the recombined radiation in two parts, again with orthogonal polarizations, each part impinging on one of the two detectors.

As known, the two back-reflected beams of electromagnetic radiation interfere and form an interference pattern. The interference pattern, or interference fringes, give information about the difference in optical path lengths between the two arms of the interferometer.

Due to the oscillations of the transducer, the optical path defined by the first arm of the interferometer changes in length. Therefore, an analysis of the interference fringes can be used to determine the amplitude of the oscillations of the transducer and then, in turn, it is possible to obtain the concentration of the gas to be analysed inside the chamber.

The fringes caused by the interference between the electromagnetic radiation traveling in the first arm and in the second arm of the interferometer can be detected by a suitable detector, such as a photodetector known in the field. The detector preferably has a sufficiently high bandwidth to detect the oscillation frequency of the transducer. Further, preferably, the detector performs the detection, with the lowest possible background noise. Preferably, the detector has a bandwidth larger than the oscillation frequency working point.

The back-reflected beams travelling in the interferometer (and interfering) can be split in two at the output of the interferometer. The split may be performed, for example, by the second beam splitter. The second beam splitter can be a polarization beam splitter. If the second beam splitter is not a polarization beam splitter *per se*, further polarizers may be present in the interferometer, so that the two beams divided by the second beam splitter have mutually orthogonal polarization. In both cases, the second beam splitter is called “polarization beam splitter”, i.e. both in case in which it is in itself a polarization beam splitter or in

case polarizers are added. The direction of the polarization axis is arbitrary, but the two split beams are preferably orthogonally polarized. The two split beams are then impinging onto the first and the second detector, part of the sensor of the invention.

Calling D1 and D2 the detectors, both beams are focused into the two detectors D1 and D2. Assuming plane waves, the electric field of the interfering back-reflected laser beams before the second beam splitter can be written using Jones formalism:

$$\overrightarrow{E_7} = \frac{E_A}{\sqrt{2}}\begin{bmatrix}1\\1\end{bmatrix} e^{(\varphi_A - i\omega t)} + \frac{E_B}{\sqrt{2}}\begin{bmatrix}1\\-1\end{bmatrix} e^{(\varphi_B - i\omega t)}$$

where the two components of the vector represent the field components along the horizontal and the vertical axes. Here E_A and E_B are the amplitudes of the back-reflected beams coming from the transducer and the optical path changer element paths (e.g. A being the first arm and B the second arm of the interferometer), respectively, with phases φ_A and φ_B. Assuming that the emerging beams from the beam splitter are horizontally and vertically polarized, respectively, the vertical polarization components of one of the beams which is impinging onto the first detector can be calculated by multiplying the Jones-matrix representing the polarizing beam splitter $\begin{bmatrix}0 & 0\\0 & 1\end{bmatrix}$:

$$\overrightarrow{E_8} = \overrightarrow{E_7}\begin{bmatrix}0 & 0\\0 & 1\end{bmatrix} = \frac{E_A}{\sqrt{2}}\begin{bmatrix}0\\1\end{bmatrix} e^{(\varphi_A - i\omega t)} - \frac{E_B}{\sqrt{2}}\begin{bmatrix}0\\1\end{bmatrix} e^{(\varphi_B - i\omega t)}$$

The detector D1 detects the field intensity:

$$I_1 = \overrightarrow{E_8} \cdot \overrightarrow{E_8} = \frac{{E_A}^2 + {E_B}^2}{2} - E_A E_B cos(\varphi_A - \varphi_B) \qquad (2)$$

Similarly, the horizontal polarization components at the exit of the beam splitter can be calculated by multiplying the Jones-matrix representing the polarizing beam splitter $\begin{bmatrix}1 & 0\\0 & 0\end{bmatrix}$:

$$\overrightarrow{E_9} = \overrightarrow{E_7}\begin{bmatrix}1 & 0\\0 & 0\end{bmatrix} = \frac{E_A}{\sqrt{2}}\begin{bmatrix}1\\0\end{bmatrix} e^{(\varphi_A - i\omega t)} + \frac{E_B}{\sqrt{2}}\begin{bmatrix}1\\0\end{bmatrix} e^{(\varphi_B - i\omega t)}$$

and the detector D2 detects the field intensity:

$$I_2 = \overrightarrow{E_9} \cdot \overrightarrow{E_9} = \frac{{E_A}^2 + {E_B}^2}{2} + E_A E_B cos(\varphi_A - \varphi_B) \qquad (3)$$

Therefore, the fringes of interference between the back-reflected beams that carry the information on the oscillations of the transducer can be analyzed either studying a signal emitted by the first detector, signal

function the detected beam of equation (2), or a signal emitted by the second detector, signal function of the detected beam of equation (3).

If it is assumed that, at rest conditions, i.e. when there is no transducer displacement, the two arms of the interferometer are set so that

$$\varphi_A - \varphi_B = \frac{3\pi}{2} \qquad (4)$$

the following applies.

Assuming that the oscillation of the transducer is a harmonic signal $u(t) = Ssin(2\pi f \cdot t)$, oscillating at the laser modulation frequency f, the two outputs of the detectors D1 and D2 give an oscillating signal proportional to $u(t)$ with a fixed background equal to the total field intensity $\frac{{E_A}^2+{E_B}^2}{2}$:

$$I_{1,2} = \frac{{E_A}^2 + {E_B}^2}{2} \mp E_A E_B sin\left(\frac{2\pi u(t)}{\lambda}\right) \approx \frac{{E_A}^2 + {E_B}^2}{2} \mp \frac{2\pi E_A E_B}{\lambda} u(t) \qquad (5)$$

The harmonic displacement $u(t)$ of the transducer has an amplitude S proportional to the gas concentration, according to Eq. (1). In order to retrieve the value of the oscillation amplitude S, a demodulation may be performed. For example, a lock-in amplifier may be used to demodulate the detector signal at the reference frequency f. This operation can be done on the D1 (or D2) signals. Thus, analyzing the signal detected by the first or the second detector, the oscillations of the transducer can be measured.

The above sensor operates according to the method of the invention.

Preferably, the excitation laser is operated at a given current and temperature so that the frequency of the laser light matches the molecular transition. The modulation of the excitation laser beam operates as follows. A modulation at the frequency f is added to the driving current of the first laser and, in addition, a slow triangular ramp (with a frequency much slower than f) is added to the current in order to scan the excitation laser optical frequency across the molecular transition.

As the excitation laser optical frequency enters in resonance with the molecular transition of the gas of interest, a molecular excitation modulated at the frequency f is induced, followed by the molecular non-radiative relaxation, which produces the modulated pressure wave in the gas sample.

Such wave hits the transducer and induces a modulated displacement at the frequency f and with an amplitude proportional to the amplitude of the pressure wave.

Preferably, the modulation frequency is so selected that f matches the resonance frequency of the transducer, or one of the higher-order resonances.

Anyway, the modulation frequency could be out of the mechanical resonance.

The transducer displacement is measured via the Michelson interferometer, described above.

Preferably, a specific working point is set, in other words a value for $\varphi_A - \varphi_B$ is set, as well as the power level impinging onto the detectors. For example, the conditions according to eq. (4) are set. In this way, any displacement of the transducer is measured with the highest sensitivity of the interferometer, corresponding to the maximum slope of the sinusoidal signal. This is true for the two signal outputs at the first and second detectors D1 and D2, according to eq.(5).

Preferably, the signal output from the first detector, D1, or the second one, D2, is demodulated by a lock-in amplifier around the modulation frequency f to retrieve the amplitude of the cantilever oscillation. The lock-in amplifier filters the signals coming from the first or the second detector (and/or their difference signal) with a bandwidth set by the lock-in parameters, and demodulates it at the frequency f, thus extracting only the signal amplitude modulated at the frequency f, averaged with a time constant τ. Vibrations of the transducer at frequencies sufficiently outside the set bandwidth are filtered out and do not contribute to the noise of the final measurement. In this way, on one side, the background noise contributions affecting the signal are largely suppressed and, on the other side, a measurable DC signal proportional to the amplitude of the transducer oscillation is obtained.

Preferably, before performing the measurement with an unknown gas, a measurement is made with known gases, to calibrate the sensor of the invention. The sensor is calibrated by using gas samples with certified concentration of the target molecules: for a given concentration of the gas sample, the amplitude of the measured interferometric signal is recorded and associated to the known concentration. This procedure is repeated for different gas concentrations and a one-to-one function is set between the measured interferometric signal and the gas concentration. This function allows retrieving any unknown concentration (of the same molecule) provided that the sensor operating conditions are the same of those set during the calibration.

Given this configuration, the measured signal demodulated by the lock-in amplifier is affected by several noise contributions which may decrease the final signal-to-noise ratio of the single acquisition and/or affect the repeatability of the measurements, thus decreasing the final sensitivity. These noise contributions are mainly related to instabilities of the interferometer and to environmental noise, and may include:

- *slow drifts of the relative length of the two arms*, not due to the transducer displacement. This produces a deviation from the selected working point, such as the condition set by eq. (4), making the interferometer

exiting the optimal maximum-slope operating condition. This produces slow variations in time of the amplitude of the interferometric signal, invalidating the sensor calibration and affecting both the single acquisition (if the drift time is comparable with the slow ramp spanning the excitation laser frequency and the lock-in time constant τ) and the repeated acquisitions (because repeated acquisitions occur at different operating points of the interferometer). As a consequence, the single acquisition may be distorted, repeated acquisitions produce different measured amplitudes and, finally, the calibration is no more valid;

- *fast mechanical/acoustical noise* inducing vibrations of the interferometer components. This noise produces fast variations of the length of the two arms, makes the working point of the interferometer to rapidly change and thus introduces noise in the measured interferometric signal.

These noise contributions are not filtered out by the lock-in amplifier, because they induce variations in the amplitude of the signal $u(t) = S\,sin(2\pi f \cdot t)$ oscillating at f (in other terms they affect the S value) and directly translate into amplitude noise in the measured spectra. This decreases the final detection sensitivity.

According to the invention, in order to overcome this problem, a differential detection scheme, centered on the working point (which is preferably the zero) is applied. This differential detection scheme is obtained because the two beams have perfectly orthogonal polarization when the transducer is not moving.

Any unbalance in polarization gives a nonzero signal, as better detailed below. .An electronic locking loop which fixes the interferometer operating point to a desired working point such as, for example, the condition set by Eq. (4), is considered. This is made by using a differential signal I_D as reference, as detailed below.

The sensor includes a circuit board or any other suitable circuitry which is adapted to create a signal which is equal to the difference of the signals obtained by the two detectors detecting the two different interfering back-reflected beams outlined above. Thus, the difference signal is the signal generated by subtracting the value of one signal detected by the first detector from the value of the other signal detected by the second detector. For example, still assuming planar waves, the differential component $I_D = I_2 - I_1$ is thus given by:

$$I_D = 2E_A E_B cos(\varphi_A - \varphi_B)$$

The difference signal, therefore, is an oscillating function and depends on the difference of the phases $\varphi_A - \varphi_B$.

Any displacement of the transducer $u(t)$ produces an unbalancing of the signals and a non-null value for I_D:

$$I_D(t) = 2E_A E_B cos\left(\frac{3\pi}{2} + \frac{2\pi u(t)}{\lambda}\right) = 2E_A E_B sin\left(\frac{2\pi u(t)}{\lambda}\right) \qquad (6)$$

Where it has been considered that eq. (4) applies. It is to be understood that the use of equation (4) is one of the possible choices; indeed, any value of the phase difference can be selected.

If the displacement is small enough compared to λ, the previous equation can be approximated with:

$$I_D(t) \approx \frac{4\pi E_A E_B}{\lambda} u(t)$$

Where, as detailed above, $u(t) = Ssin(2\pi f \cdot t)$.

In practice, in a more intuitive view, the interferometer translates a displacement of the transducer into a measurable amplitude signal, while the slope of the sinusoidal interferometric signal sets the value of the displacement-to-amplitude *conversion factor*. By setting the two arms in the condition of Eq.(4), this conversion factor is set at its maximum value (i.e. maximum slope of the sinusoidal signal) and the measured amplitude is maximized.

According to the invention, it is desired to keep fixed the working point of the interferometer, that is, it is desired to satisfy eq. (4), where the difference of the two signals coming from the first and the second detectors remains equal to zero. This working point (which means, the value of the difference between the two currents) is kept fixed during the measurement of gas concentration, while the transducer is oscillating. As said, Eq. (4) is just one possible choice for setting the working point and other choices are possible. To this purpose, the optical path changer element comes into play. In order to keep the working point fixed, then the optical path defined by the second arm of the interferometer needs to change. The optical path is for example changed operating on the actuator which in turn operates on the optical path changer element. For example, if the optical path changer element is a movable reflecting element, the latter is displaced. This induces a variation of the optical path of the second arm of the interferometer. In order to "lock" the value of the difference signal I_D to the desired value, therefore, the actuator is used, which changes the optical path defined by the second arm of the interferometer. The actuator may be, for example, a piezoelectric element which physically displaces the movable reflecting element. The locking point is fixed at the zero value of I_D, and this value is maintained by acting on the movable reflecting element, thus adjusting the corresponding path length. This locking can be performed for example by using a proportional–integral–derivative controller (PID controller), which defines a locking bandwidth. This solution has several advantages:

- It cancels out the noise contributions within the locking bandwidth, thus reducing the noise floor;

- It cancels out the slow drifts of the working point, thus solving the problem of measurements repeatability over time and calibration.

When the frequency of the transducer (i.e. the modulation frequency of the infrared laser) is much higher than the locking bandwidth, the locking circuit is unable to "correct" the phase variations induced by the transducer oscillations. This means that the locking circuit does not perturb the signal due to gas absorption, which can be retrieved by analyzing one of the two detectors outputs (D1 or D2), and only maintains the interferometer stable over time in the optimal conditions. Therefore, in a first embodiment of the invention, the desired spectroscopic information are obtained from the signal emitted by the first detector or the second detector in response to the detection of the first or the second interference beam. In this embodiment, therefore, the D2-D1 signal is used for the locking circuit and the D1 (or D2) output is sent to the lock-in amplifier for the spectroscopic analysis. In order to achieve this condition, instead of using the fundamental transducer resonance frequency (if too low), one of the higher resonant modes can be used. A further advantage of using a high-*f* resonant mode is the lower contribution from ambient noise at higher frequencies, which increases the final signal-to-noise ratio.

In a second embodiment, a different signal is used to obtain spectroscopic information. The first embodiment described above applies when the locking bandwidth is much smaller than the modulation frequency *f*, which can be achieved for example by using a higher resonant mode of the transducer. Alternatively, another option is using a locking bandwidth larger than the modulation frequency. This may happen, for example, when a low-*f* resonant mode, e.g. the fundamental one, is used. This option may be particularly advantageous when the ambient noise is low, and does not affect too much the measurement. An advantage of using a low-frequency mode is that usually it is stronger than higher-order modes, so the oscillation amplitude of the transducer is larger. In this case, the locking bandwidth may be of the same order of magnitude or even higher than the modulation frequency. It means that the locking circuit not only maintains the interferometer working point at the zero value of D2-D1, but also "corrects" the oscillation of the cantilever. As a consequence, the signal from D1 or D2 is suppressed by the locking loop (partially or totally, depending on the parameters of the locking circuit). In this case, instead of using the D1 (or D2) signal for the spectroscopic analysis, it is convenient to use the error signal sent to the actuator connected to the optical path changer element. Assuming that the locking circuit is strong and fast enough to completely cancel out the interference signal, it means that the locking loop is fast enough to follow the transducer oscillations and it acts on the actuator to correct the phase variations induced by the transducer oscillations. As a consequence, the D1 (or D2) signals are kept to a constant value, usually zero, and they cannot be used for the spectroscopic analysis. Nonetheless, the spectroscopic information is not lost, because it is now transferred to the signal moving the actuator acting on the optical path changer element (for example displacing the movable reflecting element): this signal, which is for example the error

signal of the PID, now contains the contributions from the external noise and slow drifts of the interferometer plus the contribution from the transducer. The latter is the only contribution oscillating at *f*, and thus can be easily separated from the "noise" contributions. In this case, the error signal is split in two parts: one is sent to the PID circuit for the locking loop, the other is sent to the lock-in amplifier for the demodulation. The demodulated signal from the lock-in amplifier reproduces the oscillation amplitude of the transducer and can be used for the spectroscopic analysis. Also in this case the locking circuit improves the signal-to-noise ratio of the measurement because it removes the slow drifts and maintains the interferometer working point to the optimal condition.

The interference fringes reaching the detector may be further processed, for example a demodulation can take place. Preferably, a Fourier Transform of the signal obtained from the detector is performed. From the Fourier Transform analysis, information on the gas concentration can be obtained.

Preferably, the transducer is realized in one of such materials: Silicon, SiO_2, Si_3N_4, SiC and polymers including their amorphous or crystalline forms or in non-stoichiometric forms. The material constituting the transducer is deposited on a silicon wafer substrate. The transducer can be coated by a metal, a metal oxide or a dielectric multilayer.

These materials allow the use of the transducer also in "harsh" environment.

Preferably, the sensor includes a damping and insulation structure located between the chamber and the transducer, the transducer being connected to the chamber only via the damping and insulation structure. In order to isolate the mechanical mode resonant at a given frequency from the external acoustic noise, which may degrade the signal by increasing the background noise and by creating locking issues, a damping and insulating structure is provided. The structure is interposed between the transducer and the chamber. The structure surrounds the transducer or, alternatively, holds it at least from one side. Preferably, the mass of this structure is much bigger than the mass of the transducer.

Preferably, the desired constant value is equal to zero.

Preferably, the working point of the interferometer, that is, the value of I_D, which is set and "locked" is the value written in equation (4). In this way, it maintains the working point at the maximum slope of the interferometric signal, thus maximizing the conversion factor.

Preferably, wherein the dimension of the transducer ranges between 10 μm and 2 cm.

Said dimension is defined as the segment having the maximum length and connecting two different points of the transducer.

Sizes are directly linked to the frequency resonances of the transducer. The resonances are tailored depending on application/environment/target molecules.

Preferably, the method comprises the step of putting the transducer into oscillation at a frequency equal to the resonance frequency of the transducer or to a higher-order resonance.

The transducer has a mechanical resonant frequency and higher-order resonances. Preferably, either the resonance frequency or a higher-order resonance are selected due to the fact that large oscillations are obtained. Larger oscillations are easier to detect and with a higher signal-to-noise ratio.

Preferably, the method comprises the step of obtaining the gas concentration from the step of detecting the first interference beam or from the step of detecting the second interference beam if the frequency of the movements of the optical path changer element is much slower than the modulation frequency of the excitation laser.

Alternatively, preferably the method comprises the step of obtaining the gas concentration by:

- Operating the actuator so as to change the optical path length of the second arm so that the difference signal is kept equal to the working point value;
- obtaining the gas concentration by demodulating the error signal.

The invention will be now better described with non-limiting reference to the appended drawings, where:

- Fig. 1 shows a schematic representation of a sensor for the measurement of a gas concentration according to the invention;
- Fig. 2 is a more detailed representation of the sensor of figure 1;
- Fig. 3 is another more detailed representation of the sensor of figure 1 and 2;
- Fig. 4 is a schematic representation of the polarization of the signal travelling in the sensor of figure 3;
- Figs. 5 – 8 are perspective views of four different embodiments of a transducer included in the sensor of figures 1 – 3;
- Figs. 9 and 10 are a top view and a perspective view of an additional embodiment of a transducer included in the sensor of figures 1 – 3;
- Figs. 11 – 14 show top view of different embodiments of a detail of figures 9 and 10;
- Figs. 15 shows a graph which is the result of a measurement performed with the sensors of figure 1 – 3;
- Figs. 16 and 17 are graphs showing a comparison between a measurement (fig. 16) performed not according to the invention and a measurement (fig. 17) performed according to the invention;

- Figs. 18 and 19 are graphs showing a comparison between a further measurement (fig. 18) performed not according to the invention and a further measurement (fig. 19) performed according to the invention;
- Fig. 20 shows a series of steps of the method of forming a transducer in heteroepitaxial 3C-SiC according to the invention;
- Fig. 21 shows a series of steps of the method of forming a transducer in silicon according to the invention;
- Figs. 22, 23 and 24 show different embodiments of a transducer included in the photoacoustic sensor according to the invention,
- Figs. 25a, 25b, 26a and 26b refer to spectroscopic acquisitions of a N_2O line.

With initial reference to figure 1, a sensor for gas realized according to an embodiment of the invention is schematically depicted and globally indicated with 1.

The sensor 1 is used to measure the concentration of the selected gas. Preferably, therefore, using sensor 1, the concentration of the selected molecular species can be measured and the composition of the gaseous sample analyzed.

The sensor 1 includes a chamber 2 where the gas 3 to be measured is located. The chamber 2 may work in static conditions or under a constant flow regime. In the first case, the chamber is filled with the gas of interest, at the desired pressure, and sealed or closed with a valve, in other word it is gas-impermeable for the gas 3 of interest. In the second case, a constant flux of the gas of interest is maintained in the chamber for all the time duration of the measurement. The gas 3 of interest is depicted as moving balls in figure 1.

The sensor 1 further includes a first laser 4, called excitation laser. The laser may be for example an Infrared laser ("IR Laser" in figure 2), and must emit a radiation resonant, in frequency, with the desired transition of the target molecule. This excitation laser is adapted to produce an excitation laser beam, depicted with an arrow 5 in figure 1 and 2, which enters in the chamber 2 and interacts with the gas 3. The excitation laser beam can be modulated in frequency and/or amplitude.

The excitation laser beam 5 interacts with one (or more, when tuned in frequency) gas molecular species in the chamber 2, which absorb part of the light and re-emit the energy in form of collisional energy to the other gas molecules in the chamber. This creates a pressure wave propagating in the gas sample 3. The absorption, and the consequent generation of the pressure wave, can be modulated over time by modulating the interaction between the excitation laser beam 5 and the gas 3. Therefore, as above mentioned, the excitation laser 4 is adapted to generate a laser beam 5 which can be modulated in frequency or amplitude.

The chamber 2 further comprises a transducer 6, for example a MEMS-structure. The transducer 6 is in contact with the gas 3 so that the pressure wave created by the excitation laser beam 5 can hit the transducer itself. In the depicted embodiment, the transducer 6 is attached to a wall 2a of the chamber via a pedestal 7. Preferably, the transducer 6 is located in the chamber 2 at a distance from the excitation laser beam 5 which maximizes the effect of the pressure wave on the transducer. The pressure wave generated by the excitation laser beam moves the transducer 6. Modulating the excitation laser beam 5 as detailed above, the pressure wave at the resonant frequency of the transducer 6 can be created. Preferably, therefore, the transducer is put into oscillation by the pressure wave at a frequency equal to the resonant frequency of the transducer 6 or a lower harmonic of the resonant frequency.

One surface of the transducer 6 is coated by a reflective coating, so that the coated surface can act as a mirror. The coating material and thickness are determined in order to resist in the gas ambient and maximize the reflectance at the readout laser wavelength.

The transducer 6 comprises a main component 6c. The main component 6c comprises a reflective element 6d with at least a reflective portion forming a mirror of the interferometer.

The transducer 6 can have any shape. Some possible shapes are depicted in figures 5 – 8. A first example of transducer is a rectangular MEMS 6a. The rectangular MEMS may be connected to the chamber 2, such as to wall 2a, in a single location 9 (see figure 6) or the same structure 6a can be connected to the wall 2a in more locations, such as 2 locations 9a, 9b of figure 5. Any number of locations can be considered as well. In the example of figures 7 and 8, a circular MEMS 6b is used as the transducer 6. As in the case of the rectangular MEMS 6a, the circular MEMS 6b may be connected to the chamber 2, such as to wall 2a, in a single location 9 (see figure 8) or the same structure 6b can be connected to the wall 2a in more locations, such as 2 locations 9a, 9b of figure 7. Any number of locations can be considered as well.

Furthermore, the transducer 6, regardless of its shape, can be connected to the chamber 2 in multiple stages, as depicted in figures 9 and 10. Figures 9 and 10 refer only to the circular MEMS 6b, however the same principle can be applied to any shape of the transducer 6. In other words, the reflective element 6d of the transducer 6 may be connected directly to the chamber or a “stage” can be interposed in between. For example, the sensor 1 may further comprise a damping and insulation structure 15 positioned between the main component 6c and the chamber 2. That is, the connection between the chamber 2 and the main component 6c is made via a damping and insulation structure 15. The role of the damping and insulation structure is to isolate the mechanical mode resonant at a given frequency in the transducer 6 from the external acoustic noise, which may degrade the signal by increasing the background noise and by creating locking issues (see below in the description of the interferometric detection method). Essentially, the main component 6c is “isolated” by using a multi-stage structure (in Figs. 9 and 10, single-stage transducers 6 are

represented for simplicity). The damping and insulation structure 15 can be circular or polygonal symmetry (for example rectangular). The geometrical shape of the damping and insulating structure 15 may depend on the geometry of the main component 6c and from the manufacturing process. The damping and insulation structure 15 has a mass much bigger than the mass of the main component 6c. The damping and insulation structure connects the chamber to the main component 6c. The main component 6c is not otherwise connected to the chamber, that is, the main component 6c is connected to the chamber only via the damping and insulating structure 15. In principle, a large mass (with respect to the main component 6c and the supporting structures detailed below) isolates the main component 6c, filtering out the low frequency noise. Various geometries for the suspension structures are possible (see point c below). In this way, the overall structure transducer + damping and insulation structure 15 has several mechanical modes, including at least one in which only the main component 6c moves. The frequency of this mode is far from the fundamental mode of the global structure. For this reason, it is possible to obtain a good mechanical insulation and to work with a good signal-to-noise ratio for the interferometer.

Preferably, the damping and insulation structure 15 surrounds the main component 6c.

Preferably, the connections between the damping and insulation structure 15 and the transducer are made via one or more first suspension structure, all named 16 in the figures. The first suspension structure is a special type of connection between the reflective element 6d and the chamber or the reflective element 6d and the damping and insulation structure 15. The first suspension structure comprises elongated elements (named also as suspensions) that reduce the length of the outer perimeter of the reflective element 6d in connection to the damping and insulation structure 15.

Second suspension structure 18, similar to the first suspension structure 16, may also be present, to connect the damping and insulation structure 15 to the chamber 2.

The suspension structures 16, 18 can have four different embodiments, depicted in figures 11 – 14. In the following, only the first suspension structure is indicated in the figures, but the same shape applies also to the second suspension structure 18 as well. In figure 11, a beam shaped suspension 16 is shown. The suspension is substantially rod-like and it extends along a single direction for a given length. In figure 12, a L-shaped suspension 16 is shown. The suspension extends in a first direction for a first given length, then it makes a 90° turn and it extends for a second given length along a second direction. In figure 13, a Z-shaped suspension is shown. The suspension extends in a first direction for a first given length, then it makes a turn < 90° and it extends for a second given length along a second direction, it makes a second turn < 90° and it extends for a third length along a third direction, preferably parallel to the first direction. In figure 14, an S-shaped suspension is shown.

A combination of the above shapes can be used as well to form a suspension 16, 18. For example, in order to form a suspension having a spiral structure, beams and L-shapes can be suitably combined. Furthermore, two or more S-shaped structures can be combined in succession.

The choice of the suspension structure shape depends on the torsional rigidity of the transducer 6. Further, the choice of the suspension structure shape depends on the type of movement performed by the transducer 6. Further, the choice of the suspension structure shape depends on the operative frequency of the transducer.

In case of transducers having a relatively complex geometry, structures of similar dimensions could be resonant at quite different frequencies with different displacements, in particular with different kind of displacements. It is possible to have transducers having substantially the same dimension (where the dimension is meant as the maximum dimension of the transducer, as above defined) but very different resonance frequency. The range of achievable resonance frequencies spans from hundreds of Hz to few MHz. This is obtained by choosing the number of anchoring points where to connect the reflective element 6d to the damping and insulation structure 15 via the suspenders 16. It also depends on the number of anchoring points where to connect the damping and insulation structure 15 to the chamber 2 via the suspenders 18. It also depends on the shape of the suspenders.

Furthermore, the sensor 1 comprises an interferometer 11 (visible in figures 2 and 3) and a second laser 10, called a reading laser. The interferometer 11 is used, together with the second laser 10, to detect the oscillation of the transducer 6 by interferometry. The second laser 10 is preferably a low power laser, for example a HeNe laser or a diode laser. The interferometer 11 is for example a Michelson type specifically designed to have balanced detection through laser beam polarization control.

The detailed diagram of the interferometer is shown in the Figs. 2 and 3.

The second laser 10 is configured to emit a second “reading” laser beam 12, depicted with arrows in figures 1 – 3. Furthermore, the interferometer 11 comprises a first arm 13 and a second arm 14, having equal length (with reference to figure 3 the first arm goes from P2 – MEMS – P2 and the second arm is P2 – M2 – P2). The first arm 13 ends with the MEMS transducer 6. The latter, as written above, has a reflective coating and acts as a partially reflecting mirror. The second arm 14 includes a movable mirror 19 and an actuator 20. The first arm 14 ends on the moving mirror 19 mounted on the actuator 16, for example a piezoelectric crystal.

The interferometer 11 comprises a first polarizer 22. After being emitted, the second laser beam 12 impinges on the first polarizer 22, which acts as a filter for the initial polarization of the laser beam, so that the second laser beam 12 exiting the first polarizer has linear polarization, for example vertical. Thus, with

reference to figures 3 and 4, the beam exiting the first polarizer and detected in point P1 is linearly polarized.

The interferometer 11 comprises a first waveplate 23, and a first beam splitter 24, a movable mirror 19, an actuator 20 moving the mirror 19. The second beam exiting the first polarizer 22 and impinging on the waveplate 23 rotates its polarization (23 is preferably a quarter-wave plate). Thus, a measurement of the second beam in point P2 would result in a linearly polarized state forming an angle with the vertical direction. The interferometer 11 then comprises a first beam splitter 24, which splits the linearly polarized second beam 12 into a first and a second split second beam 50, 51. The first split second beam 50 is directed towards the transducer 6 and the second split second beam 51 is directed towards the movable mirror 19.

The movable mirror 19 is mounted on a moving stage (not shown) that enables its movements in the longitudinal direction with respect to the second split second beam (in this way it is possible to adjust the length of the second arm 14). The movements are actuated by the actuator 20, for example a piezoelectric transducer. The piezoelectric transducer allows fine movements (micrometric or sub-micrometric) of the movable mirror 19. In this way, the optical path defined by the second arm 14 can be varied.

Following now the first split second beam 50, it impinges on the transducer 6. A suitable optic (not visible in the drawings) may be located in front of the transducer 6 to focalize the first split second beam 50 onto the transducer 6.

After the first beam splitter 24, the first split second beam is horizontally polarized, as for example detectable in point P3A, as visible in figures 3 and 4. In its path towards the transducer 6, the first split second beam 50 impinges on a second waveplate 25 (quarter-wave plate), which rotates its polarization again. It then impinges onto the transducer 6 and it forms a back-reflected first split second beam 50'.

The back-reflected first split second beam 50' returns back along the first arm 13 of the interferometer 11 and goes again through the second waveplate 25, so that its polarization is rotated again (see point P5A in figures 3 and 4). When it reaches the first beam splitter 24, back-reflected first split second beam 50' does not return towards the second laser, but it continues along the interferometer.

The second portion of the second beam 51 travels through the second arm 14 of the interferometer 11. After the first beam splitter 24, the second split second beam is vertically polarized, as for example detectable in point P3B, as visible in figures 3 and 4. In its path towards the movable mirror 19, the second split second beam 51 impinges on a third waveplate 26 (quarter-wave plate), which rotates its polarization again (see point P4B). It then impinges onto a further mirror 27 and finally onto the movable mirror 19, where it forms a back-reflected second split second beam 50'.

The back-reflected second split second beam 51' returns back along the second arm 14 of the interferometer 11 and goes again through the third waveplate 26, so that its polarization is rotated again (see point P5B in figures 3 and 4). When it reaches the first beam splitter 24, the back-reflected second split second beam 51' does not return towards the second laser, but it continues along the interferometer.

The waveplates 25 and 26 are quarter-wave plates, so that the back-reflected first split second beam 50' that is reflected by transducer 6 and the back-reflected second split second beam 51' that is reflected by the movable mirror 19 returns to the first beam splitter 24 with linear polarization, rotated by 90°.

At this point, the first beam splitter 24 recombines the back-reflected first split second beam 50' and the back-reflected second split second beam 51' from the two arms 13, 14 and directs it towards the detectors, detailed below. After recombining, the recombined back-reflected beam passes through a fourth waveplate 28, which rotates its polarization. The recombined beam impinges on a second beam splitter 29, so that the second beam splitter divides the recombined beam into two parts, with equal intensity. The first part is called first interference beam 52 and the second part is called second interference beam 53. The polarization of the two beams 52, 53 is one orthogonal to the other, for example, as depicted in points P8 and P9, one polarization is vertical and the other horizontal.

The interferometer 11 comprises a first and a second detector 30, 31. Preferably, the first and second detector are used for balanced detection. The first and second interference beams 52, 53 impinge on the first and second detector 30, 31, respectively. Mirrors 32, 33 may be used to direct the beams 52, 53 onto the detectors 30, 31.

The sensor 1 further comprises an electronic board 40. The first and second detectors 30, 31 are mounted on the electronic board 40.

The detectors 30, 31 emit signals that can be extracted and acquired. The signals of interest are the following: the signal from each detector (first and second detector) and the difference signal called D2-D1. The latter is the direct subtraction of the two photocurrents from the first and second detector 30, 31.

The analysis is as follows. The signals from the first and second detector 30, 31 are used as monitors of the two single arms 13, 14 of the interferometer 11, both during the alignment phase and during the spectroscopic measurement. The difference signal (D2-D1), in perfectly balanced conditions, is a zero background signal and can be used both for recording the spectroscopic absorption lines and as reference signal for electronic locking, as detailed below.

The sensor 1 includes therefore a detection system 60 shown in figure 2. The detection system 60 includes a digital acquisition system 61, for example an oscilloscope, to which the signal from one of the two detectors 30, 31 is sent to check the alignment; the signal from the other detector is sent to a lock-in

amplifier 62 that demodulates it. The lock-in amplifier 62 gives at the output either the first-derivative (1*f* demodulation) or the second-derivative (2*f* demodulation) signal of the molecular absorption of interest of the gas 3. This is the signal that is used in the spectroscopic analysis of the gas concentration. An example of such a demodulated signal is for example given in figure 15.

The difference signal D2-D1 is used to stabilize the interferometer 11 by means of a locking circuit. The elements of the locking circuit are: a Proportional-Integral-Differential gain circuit (PID) 63, and a voltage controller 64 for the piezoelectric actuator 20. The locking circuit drives the piezoelectric 20 acting on the movable mirror 19 and adjusts the optical path of the second split second beam 51 and the back reflected second split second beam 51', in order to have, on the detectors 30, 31, an interference that corresponds to a desired working point.

A preferred embodiment sets the working point at half the fringe. This condition corresponds to the maximum linearity and maximum dynamic response of the interferometer and allows for effective detection of oscillations of the transducer 6: any variation occurs with respect to the point of maximum slope of the signal (point of maximum slope of the sinusoidal interference signal). The locking enables the stabilization of the interferometer in the optimal response condition and, at the same time, corrects the slow drifts (due to temperature fluctuations, for example) which would lead to a progressive misalignment over time. It is therefore an ideal system for maintaining stable optimal working conditions, thus enabling applications in the field or requiring long acquisition times (for a higher detection sensitivity). The locking parameters are optimized at the chosen working point (resonance frequency and mechanical resonance modes) in order to obtain the maximum signal to noise ratio taking advantages from the lower background and from a minor sensitivity to the acoustic and environmental noise.

Figure 22 shows different embodiments of the transducer 6, wherein the reflective element 6d is a membrane directly connected to the chamber, i.e. without a first suspension structure.

Figure 23 shows further embodiments of the transducer 6, wherein the main component 6c comprises a first suspension structure 16 between the reflective element 6d and the chamber.

Figure 24 shows an example of embodiment of the transducer 6, wherein the first suspension structure 16 has the shape of a spiral and connects the reflective element 6d to the chamber.

Figures 25a and 25b refer to a spectroscopic acquisition of a N_2O line.

In particular, Fig. 25a shows an acquisition in resonance (frequency modulation equal to the first cantilever resonance) meanwhile Fig. 25b shows an acquisition out of resonance, wherein:

- Gas conditions: N_2O 200 ppm in N_2

- P=20 mbar
- Integration time: 30 ms

Figures 26a and 26b refer to a spectroscopic a further acquisition of a N_2O line.

In particular, Fig. 26a shows an acquisition in resonance (frequency modulation equal to the third cantilever resonance) meanwhile Fig. 26b shows an acquisition out of resonance, wherein:

- Gas conditions: N_2O 200 ppm in N_2
- P=20 mbar
- Integration time: 30 ms

Example 1

The following gas has been studied.

QCL operating at 4526 nm tunable in the range 4520 – 4530 nm . The laser is scanned around the transition of N_2O at 4526.86 nm (2209.523 cm^{-1}) in a cell containing the gas sample at a fixed pressure (13 mbar in this case) for the whole time duration of the measurement. For these measurements, a rectangular silicon cantilever with size 2mm x 4mm and 10 µm depth has been used, and the third-order mechanical resonance has been chosen. The Locking point of the Michelson (differential signal) is set at zero. A gas sample on N_2O (200 ppm concentration) in dry N2 has been used for the test. The second laser probing the Michelson interferometer is a HeNe laser emitting at 633 nm wavelength.

Example of repeated measurements in standard unlocked (figure 16) and locked (figure 17) conditions are reported. The dashed lines represent the triangular ramp spanning the laser frequency of the excitation laser beam over the molecular transition of the gas of interest. This comparison shows the benefit of the locking condition in terms of stability of the signal amplitude over repeated measurements. The strong variation of the signal amplitude over repeated acquisitions in standard unlocked operation (fig.16), which also invalidates the calibration, is corrected by the locking condition (fig.17).

Example 2

QCL operating in the same conditions as in example 1. The cell is closed at a gas pressure of 15 mbar. For these measurements, too, the third-order mechanical resonance has been chosen. The locking point of the Michelson is, again, set to zero (differential signal).

Demonstrative comparison between repeated measurements in standard unlocked (Fig. 18) and locked (Fig. 19) conditions. The signal-to-noise ratio over a single acquisition of the graph in fig. 18 is 40, to be compared of the signal-to-noise ratio equal to 180 for a single acquisition of the graph of fig. 19.

Example 3

The transducer 6 may be realized in the 3C-polytype of silicon carbide heteroepitaxially grown on a silicon wafer by using the method of figure 20.

An heteroepitaxial layer of 3C-SiC 71 grown on a wafer 70 of silicon that has two surfaces 70a and 70b. The surface 70a is made up of Si and the surface 70b is made up of 3C-SiC. The surface 70b is etched through a mask prepared via photolithography using a suitable photoresist 72 to give the desired shape to the SiC layer. The Si surface 70a is etched through a mask 73. The remaining portions of the silicon carbide 70b are then covered by a reflective coating 74 so that the transducer 6 has a reflective surface.

The SiC 70b surface can be etched in a plasma of CHF_3 and O_2; the silicon surface 70a can be anisotropically etched via dry etching using the standard silicon etching chemistry (e.g. fluorine- and chlorine-based gas mixtures); silicon can be anisotropically etched via wet etching, e.g. TMAH, KOH, NaOH solutions.

The steps marked with a star are not performed in the fabrication of a membrane.

Example 4

A silicon on insulator (SOI) wafer (75) has two surfaces: 75a is made up of a thin silicon device layer on a buried SiO_2 layer (75c); 70 b is a several hundred-micron thick silicon handle substrate. A SiO_2 layer 76 is deposited on top of the surface 75a. The SiO_2 layer 76, the surface 75a and the buried SiO_2 layer 75c are etched through a suitable photoresist mask layer 77. A conformal SiO_2 layer 78 is deposited to cover the surface and the vertical walls of the device layer 75a, and the top surface of the handle substrate 75b. The layer in the groves / on the top on the handle surface is 78a. A dry etching is performed in order to remove the layer from 78a. The remaining SiO_2 is the etch stop for the etching of the handle substrate from the back side 75b. The handle 75b is etched via photolithography through a suitable photoresist 79. The remaining etch stop layer 78 and buried SiO_2 layer 75c are wet etched. The MEMS surface 75a is coated by a suitable metal layer.

The silicon layer 75a and 75b can be etched via a Bosch process reactive ion etching. The Si handle 75c can be either etched via wet etching in TMAH, KOH or NaOH. The SiO_2 75c, 76, and 78 can be etched by wet etching in HF or by dry etching in a fluorine-based (e.g. SF_6, CHF_3) gas mixture.

The steps marked with a star are not performed in the fabrication of a membrane.

Claims

1. A photoacoustic sensor for spectroscopic gas detection, comprising:
   - A chamber adapted to contain the gas to be analysed;
   - An excitation laser source adapted to emit a modulated laser beam, which is absorbed by the gas present in the chamber and creating a pressure wave;
   - A transducer, the transducer being located inside the chamber, and being adapted to be put into oscillations by the pressure wave, the transducer having a reflective portion;
   - An interferometer having a first and a second arm and an output, with the first arm ending in the transducer, and the second arm including an optical path changer element and an actuator connected to the optical path changer element to change the optical path defined by the second arm of the interferometer;
   - A first polarizing beam splitter;
   - A second laser source for interferometer reading, adapted to emit a second laser beam impinging onto the first polarizing beam splitter, the first polarizing beam splitter being adapted to split the second laser beam in the first and the second arm of the interferometer, so that the split beam travelling in the first arm is back-reflected by the reflective portion of the transducer, and the split beam travelling in the second arm is back-reflected by the optical path changer element, so that the resulting back-reflected split beams interfere in the interferometer;
   - A second polarizing beam splitter adapted to split the interfering light at the output of the interferometer in two beams which are orthogonally polarized;
   - A first detector adapted to detect one of the two orthogonally polarized beam exiting the interferometer and to emit a corresponding first interference signal;
   - A second detector adapted to detect the other of the two orthogonally polarized beam exiting the interferometer and to emit a corresponding second interference signal;
   - An electronic circuit configured to obtain a difference signal, the difference signal being function of the difference between the interference signal emitted by the first detector and the interference signal emitted by the second detector;
   - A feedback loop adapted to command the movements of the actuator in order to change the optical path of the second arm, so that the difference signal is kept equal to a desired constant value during the gas concentration measurements.
2. The sensor according to claim 1, wherein the transducer is realized in one of Silicon, SiC, SiO_2, Si_3N_4, including their amorphous or crystalline forms or in non-stoichiometric forms, and polymers. The transducer can be coated by a metal, a metal oxide, or a dielectric multilayer.

3. The sensor according to claim 1 or 2, wherein the transducer comprises a main component having a reflective element with at least the reflective portion, and a damping and insulation structure located between the chamber and the main component, the main component being connected to the chamber only via the damping and insulation structure.
4. The sensor according to one or more of the preceding claims, wherein the desired constant value is equal to zero.
5. The sensor according to one or more of the preceding claims, wherein the dimension of the transducer ranges from 10 μm to 2 cm.
6. A method to detect a gas concentration by means of a photoacoustic phenomenon, the method comprising:
   - Providing a chamber where a gas is located, the concentration of which is to be measured;
   - Providing a transducer in the chamber, the transducer comprising a reflective portion;
   - Generating a pressure wave in the chamber by means of a modulated excitation laser beam directed into the chamber, according to the photo-acoustic phenomenon, the pressure wave putting the transducer in oscillation;
   - Impinging with a second laser beam onto the reflective portion of the transducer;
   - providing an interferometer, having a first arm terminating into the transducer and a second arm terminating into an optical path changer element adapted to vary the path length of the second arm;
   - Directing a second laser beam towards the interferometer, the second laser beam forming a first back-reflected beam when reflected by the transducer and a second back reflected beam when reflected by the optical path changer element;
   - Creating an interference between the first and the second back-reflected beams;
   - Splitting the interfering back-reflected beams in a first and a second interference beam;
   - Polarizing the first and/or the second interference beam so that their polarization axes are mutually perpendicular;
   - Detecting the first interference beam and the second interference beam generating a first and a second signal;
   - generating a difference signal function of the difference between the first signal and the second signal;
   - Defining a working point value of the difference signal;
   - Adapting the optical path length of the second arm by actuating the actuator so that the difference signal is kept equal to the working point value during the gas concentration measurement.

7. The method according to claim 6, comprising the step of putting the transducer into oscillation at a frequency equal to the resonance frequency of the transducer or to a higher-order resonance.
8. The method according to claim 6, comprising the step of putting the transducer into oscillation at a frequency out of any resonance frequencies of the transducer.
9. The method according to one or more of claims 6 – 8, comprising the step of obtaining the gas concentration from the step of detecting the first interference beam or from the step of detecting the second interference beam if the frequency of the movements of the optical path changer element is much slower than modulation frequency of the excitation laser.
10. The method according to one or more of claims 6 – 8, comprising the step of:
    - Sending a signal to the optical path changer element so that the difference signal is kept equal to the working point value;
    - obtaining the gas concentration from the signal sent to the optical path changer element if the frequency of the movements of the optical path changer element is of the same order of magnitude of the modulation frequency of the excitation laser.
11. The method according to one or more of claims 6 – 10, wherein the step of impinging with a modulated excitation laser beam comprises:
    - Operating an excitation laser at a given current and temperature,
    - Adding a fast modulation at the given frequency to the driving current and,
    - Adding a slow modulation, with a frequency much slower than the given frequency, to the current in order to scan the excitation laser optical frequency across the molecular transition.

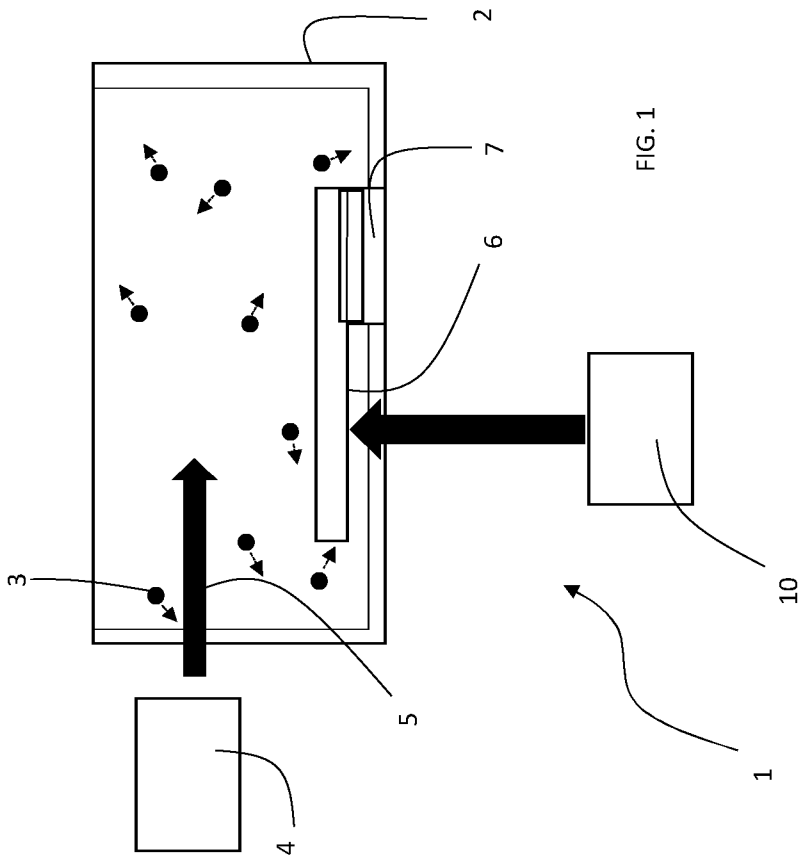

FIG. 1

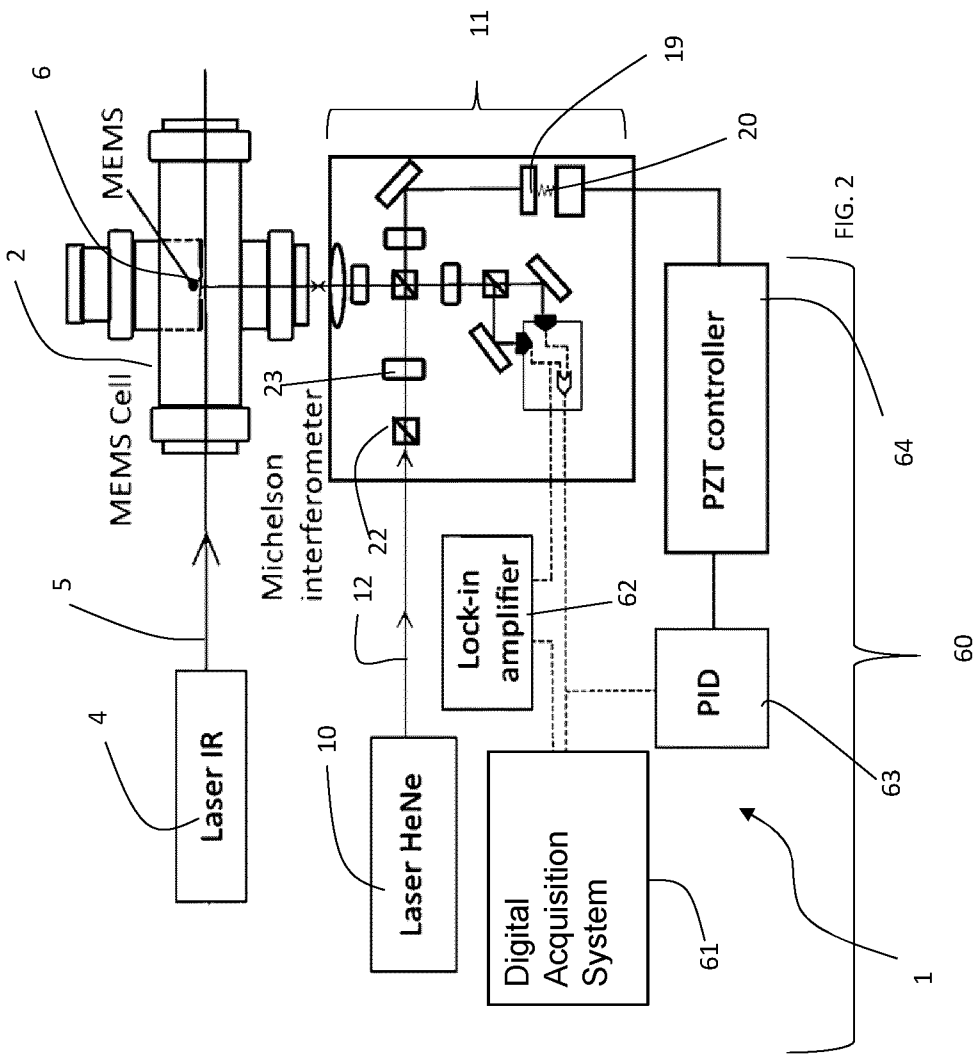
11
19
6
MEMS
20
2
MEMS Cell
23
Michelson interferometer
22
12
5
Laser IR
4
Laser HeNe
10
Lock-in amplifier
62
PZT controller
64
PID
63
60
Digital Acquisition System
61
1

FIG. 2

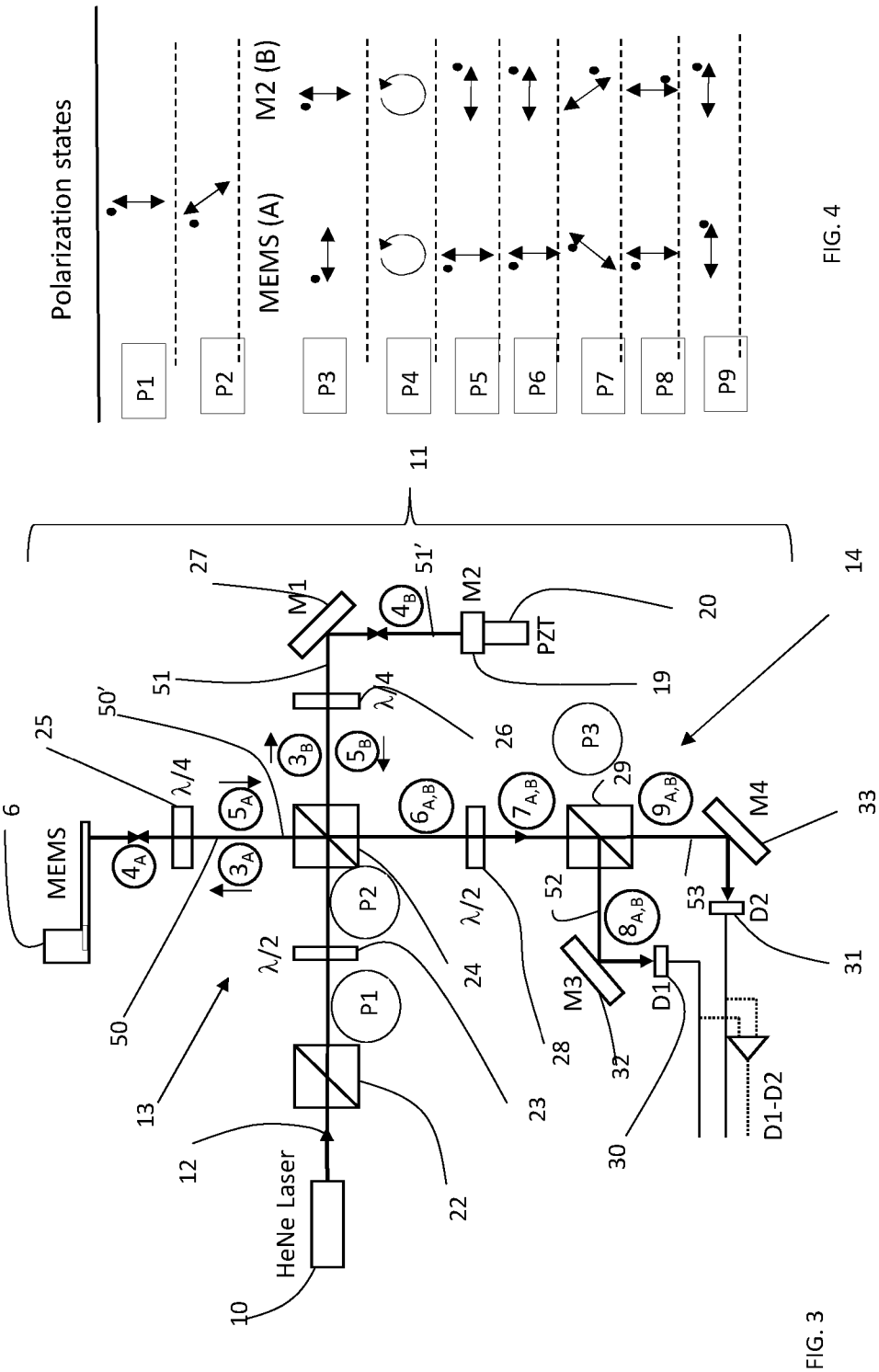
Polarization states
P1
P2
MEMS (A)
M2 (B)
P3
P4
P5
P6
P7
P8
P9
11
MEMS
HeNe Laser
M1
M2
M3
M4
PZT
D1
D2
D1-D2
P1
P2
P3
λ/2
λ/4
6
10
12
13
14
19
20
22
23
24
25
26
27
28
29
30
31
32
33
50
50'
51
51'
52
53

FIG. 4

FIG. 3

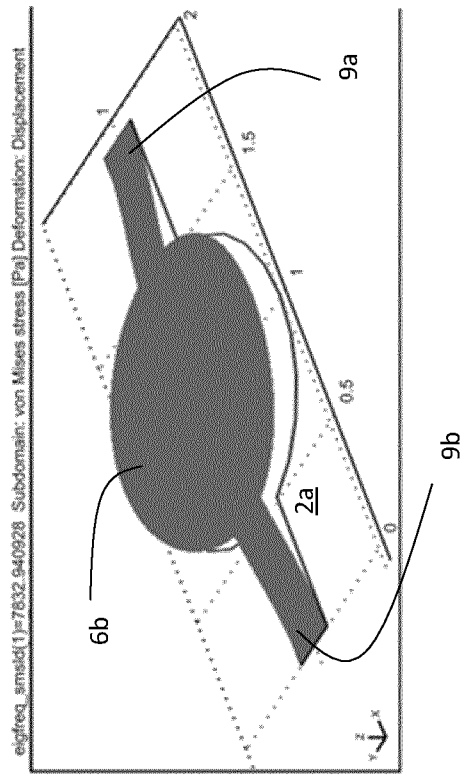

FIG. 7

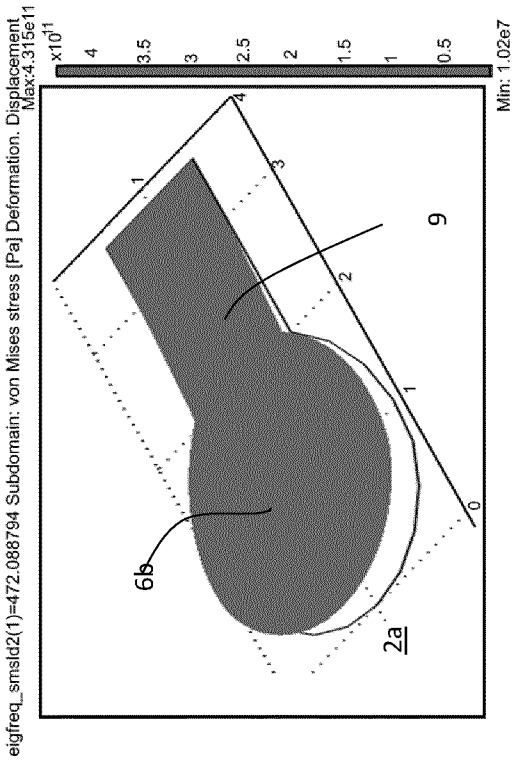

FIG. 8

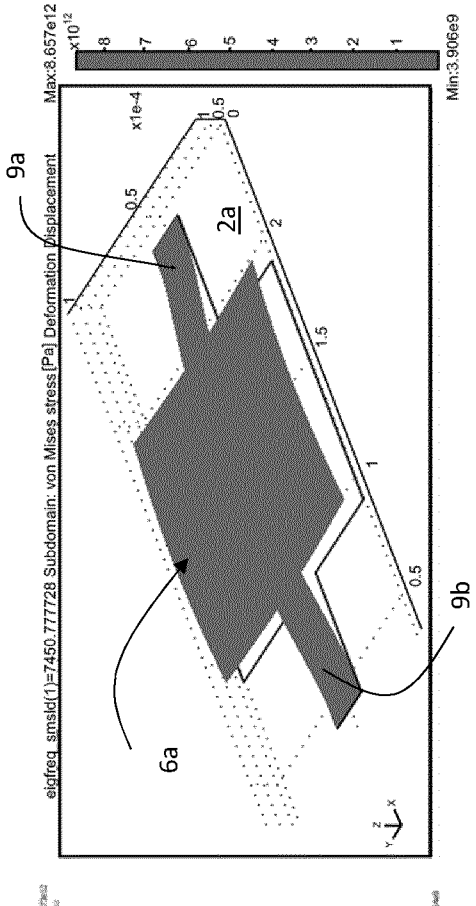

FIG. 5

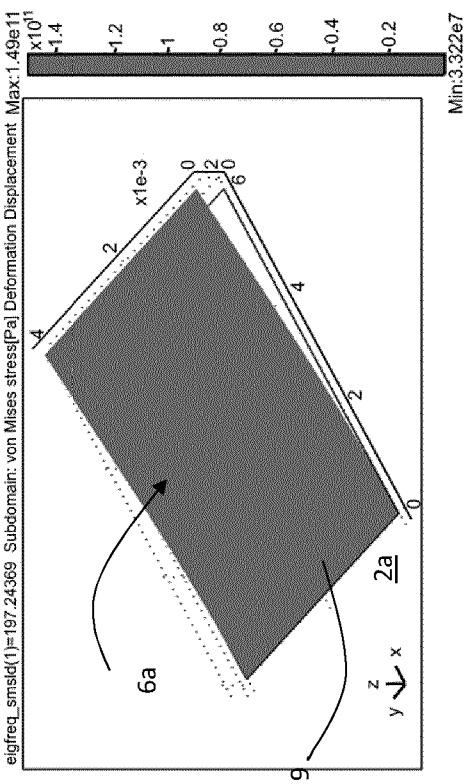

FIG. 6

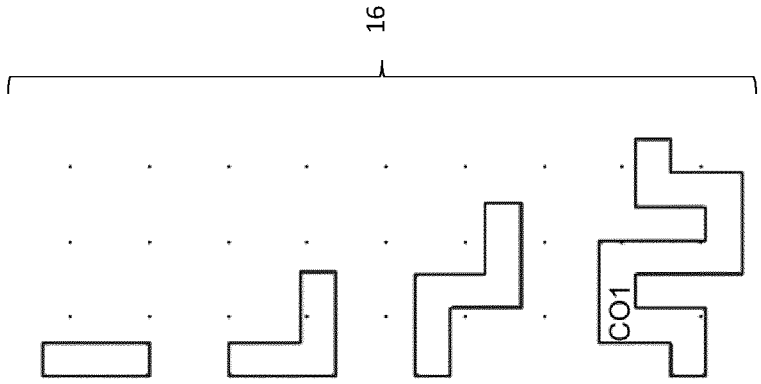

FIG. 11 FIG. 12 FIG. 13 FIG. 14

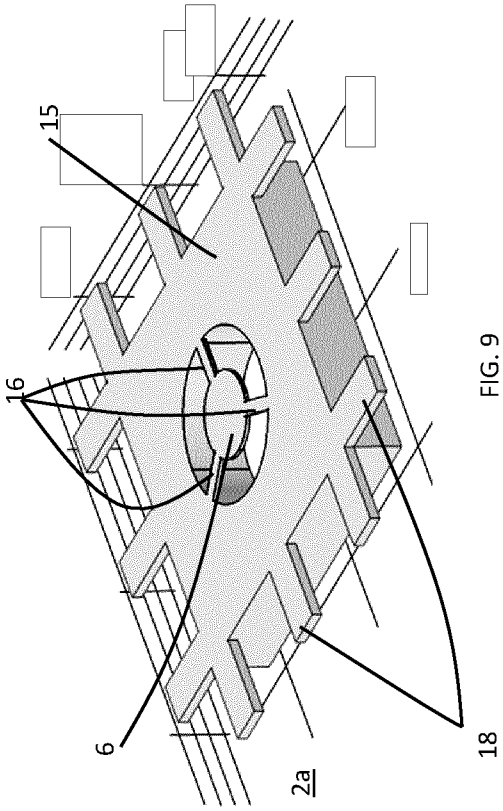

FIG. 9

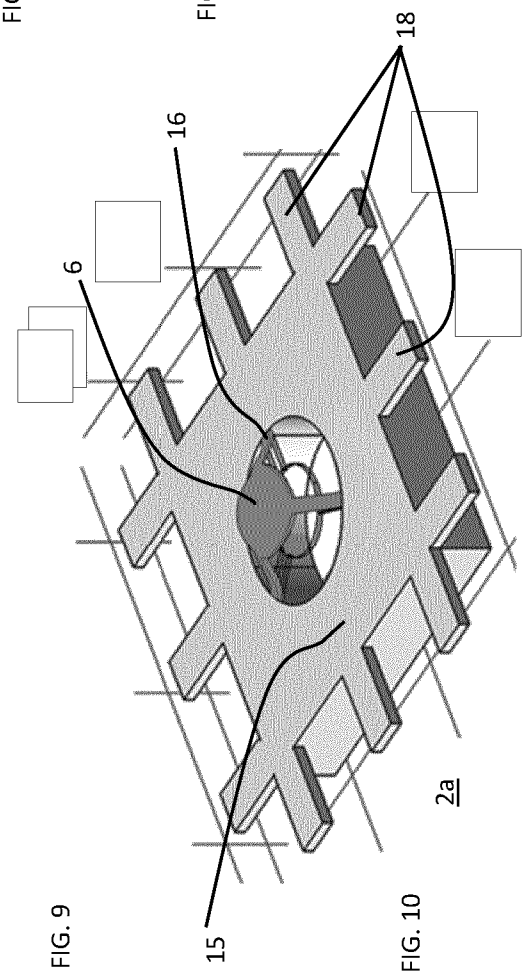

FIG. 10

FIG. 15

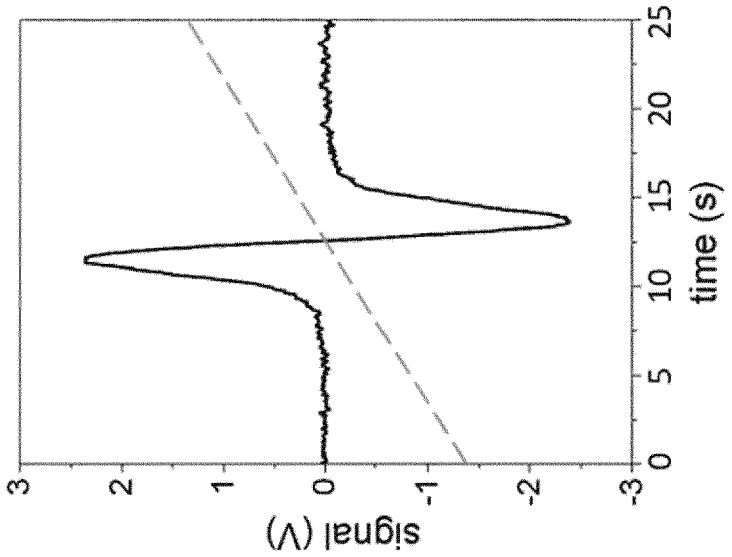

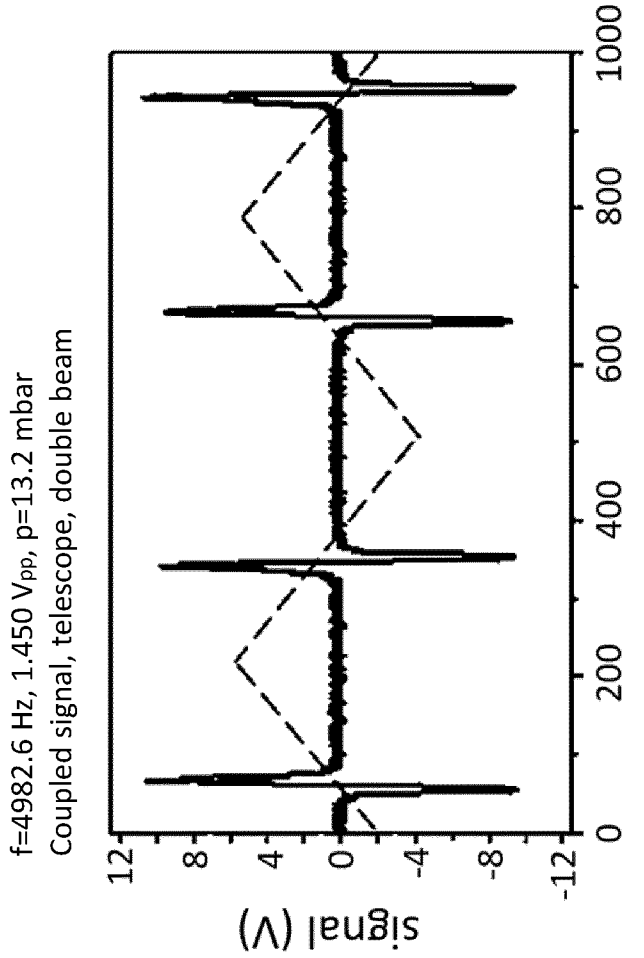
f=4982.6 Hz, 1.450 Vpp, p=13.2 mbar
Coupled signal, telescope, double beam
V ramp:600s, 1 Vpp,
Lock-in amp.: 10 mV, 30 ms
signal (V)
time (s)
12
8
4
0
-4
-8
-12
0
200
400
600
800
1000

FIG. 17

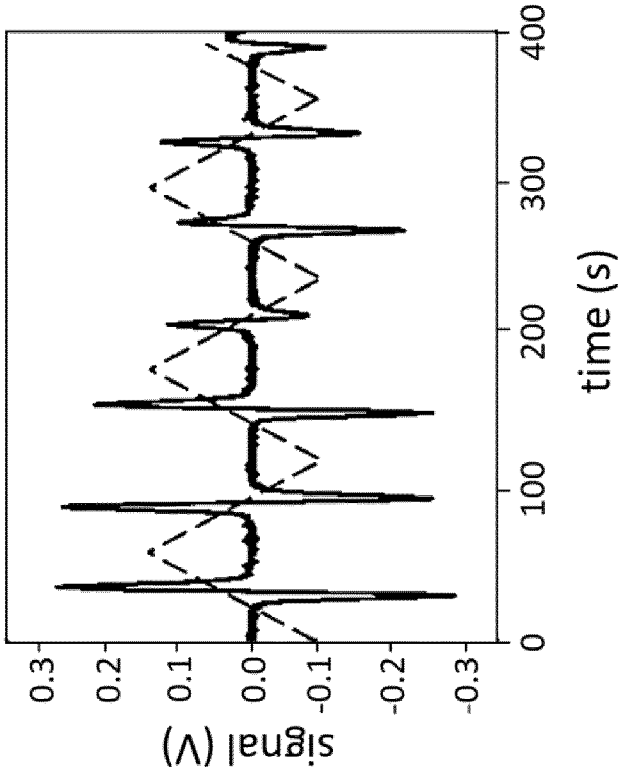
signal (V)
time (s)
0.3
0.2
0.1
0.0
-0.1
-0.2
-0.3
0
100
200
300
400

FIG. 16

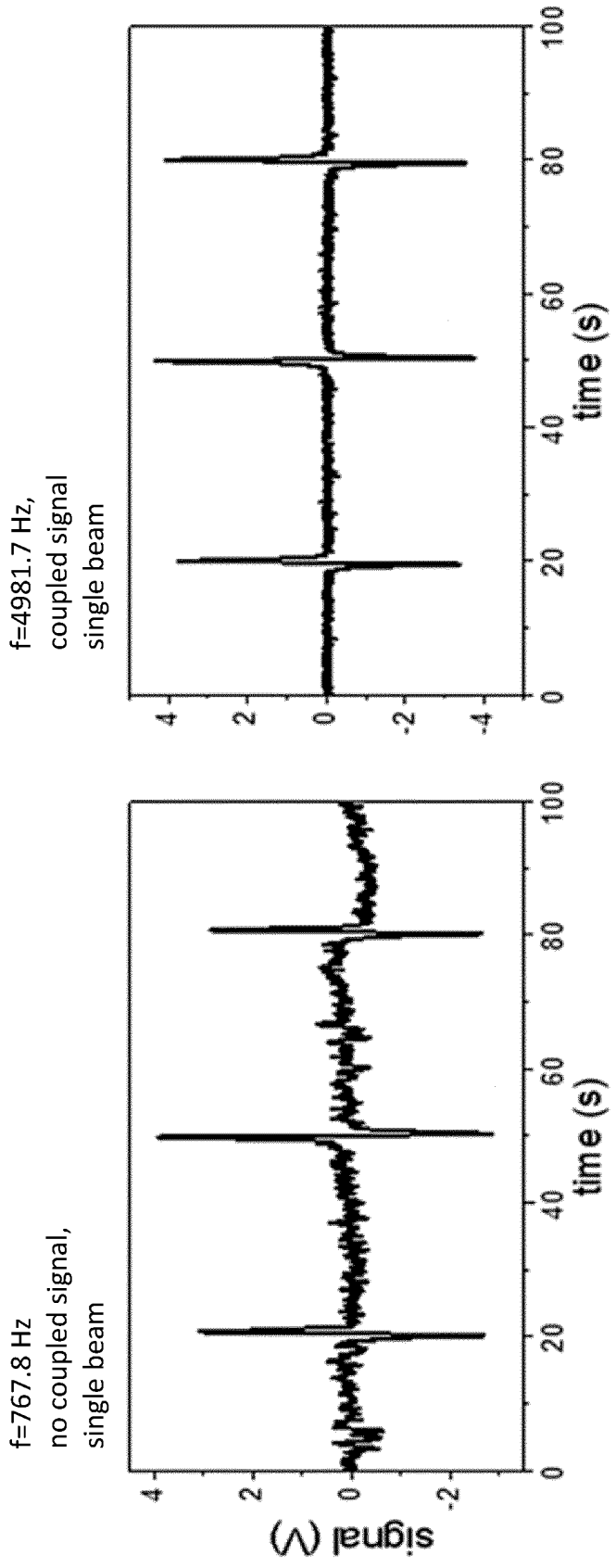
f=767.8 Hz
no coupled signal,
single beam
Power: 50 mW
Lock-in amp.: 0.3 mV, 30 ms
V ramp: 2 Vpp, 60 s
signal (V)
time (s)
f=4981.7 Hz,
coupled signal
single beam
Power: 50 mW
Lock-in amp.: 10 mV, 30 ms
V ramp: 2 Vpp, 60 s
time (s)

FIG. 18

FIG. 19

FIG. 20

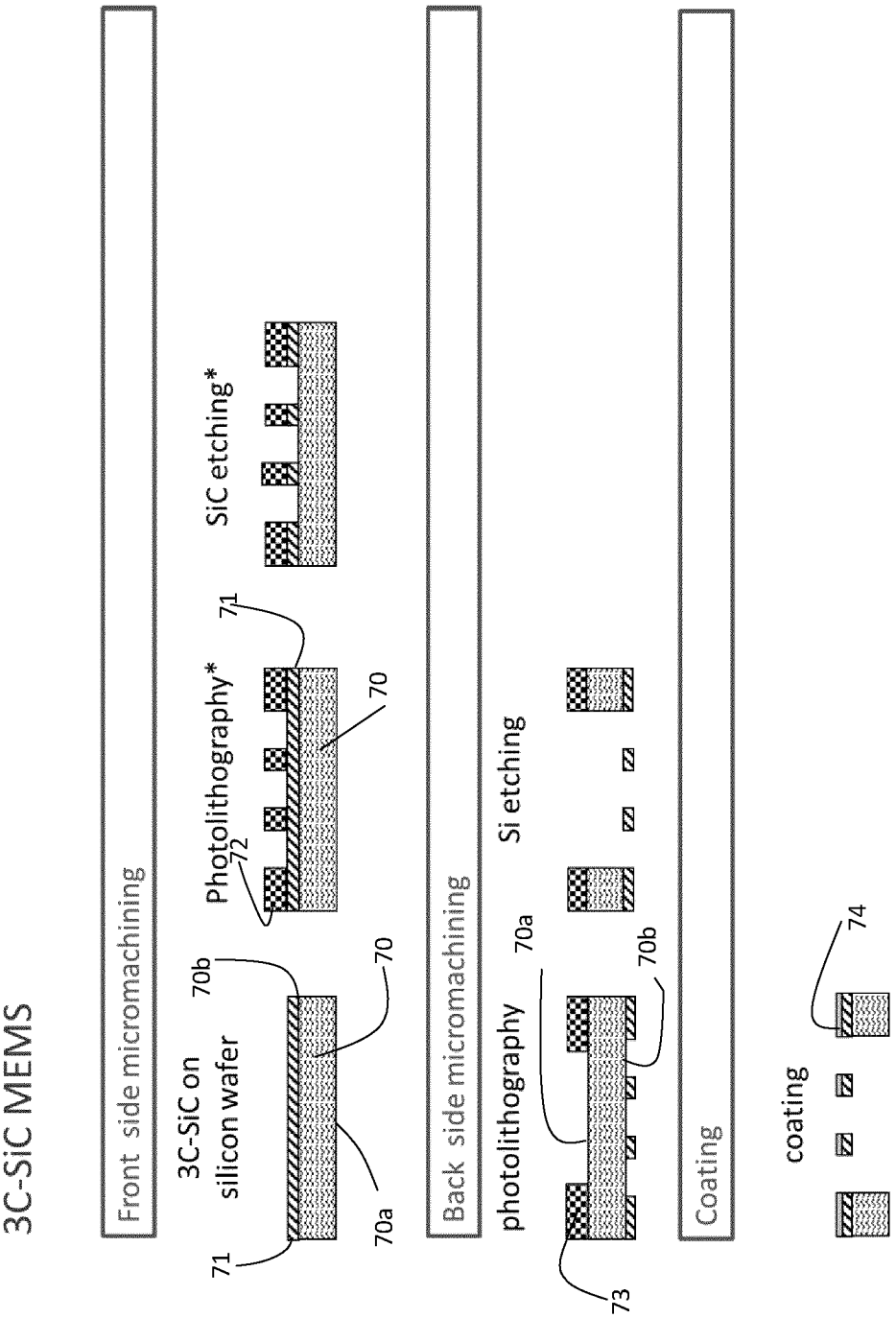
3C-SiC MEMS
Front side micromachining
3C-SiC on silicon wafer
70b
70
71
70a
Photolithography*
72
71
70
SiC etching*
Back side micromachining
photolithography
70a
Si etching
70b
73
Coating
coating
74

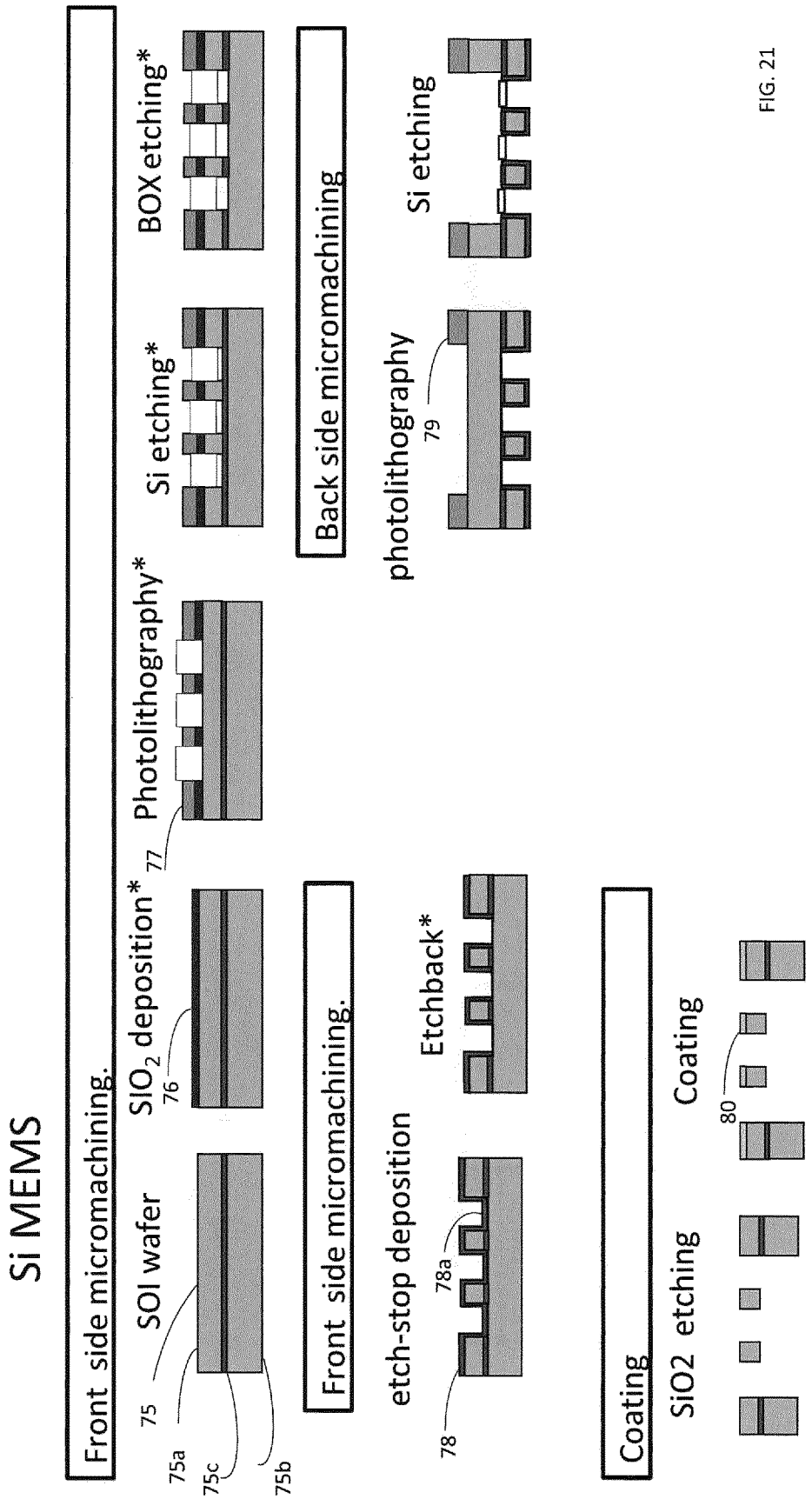
Si MEMS
Front side micromachining.
SOI wafer
75
75a
75c
75b
SiO2 deposition*
76
Photolithography*
77
Si etching*
BOX etching*
Front side micromachining.
Back side micromachining
etch-stop deposition
78
78a
Etchback*
photolithography
79
Si etching
Coating
SiO2 etching
Coating
80

FIG. 21

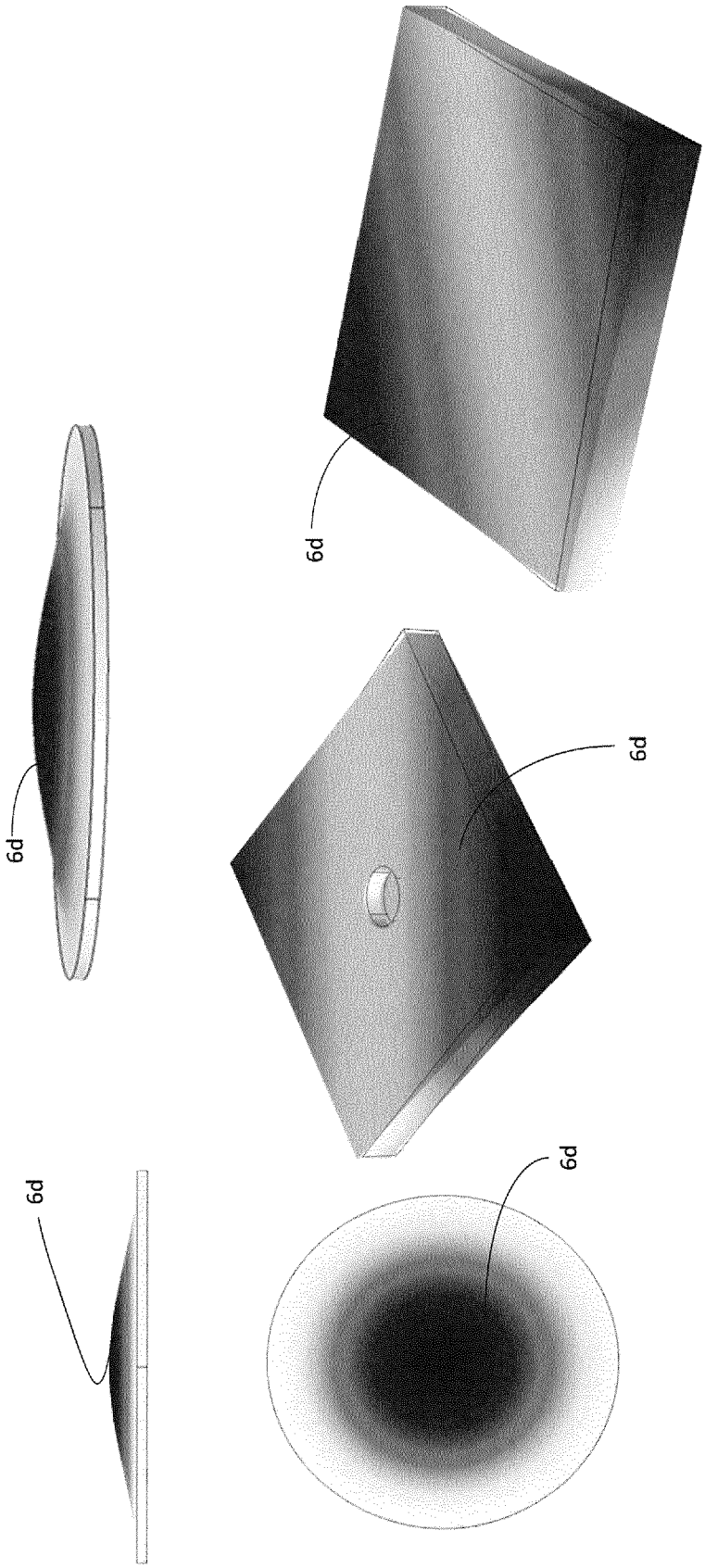

FIG. 22

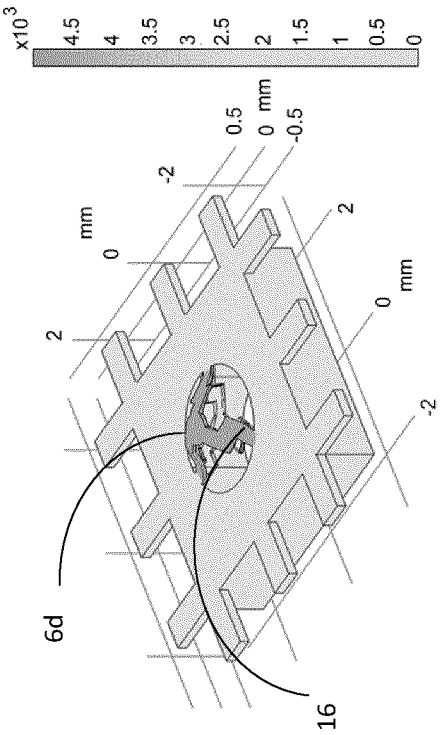
x10^3
4.5
4
3.5
3
2.5
2
1.5
1
0.5
0
mm
0.5
0
-0.5
-2
2
0
-2
6d
16

FIG. 23

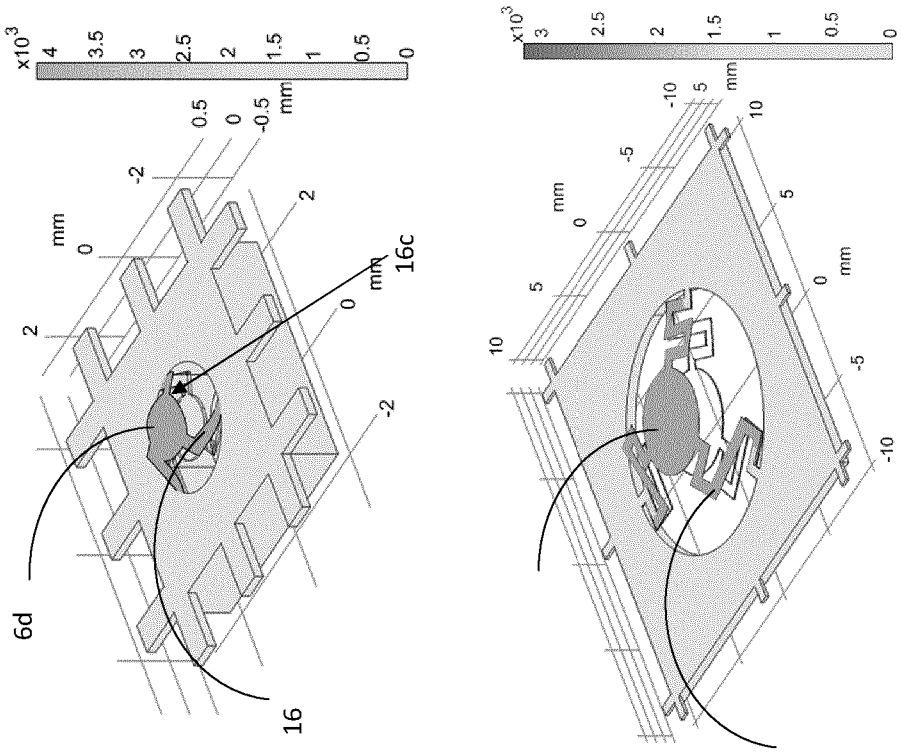
x10^3
4
3.5
3
2.5
2
1.5
1
0.5
0
mm
16c
6d
16
x10^3
3
2.5
2
1.5
1
0.5
0
mm
10
5
0
-5
-10

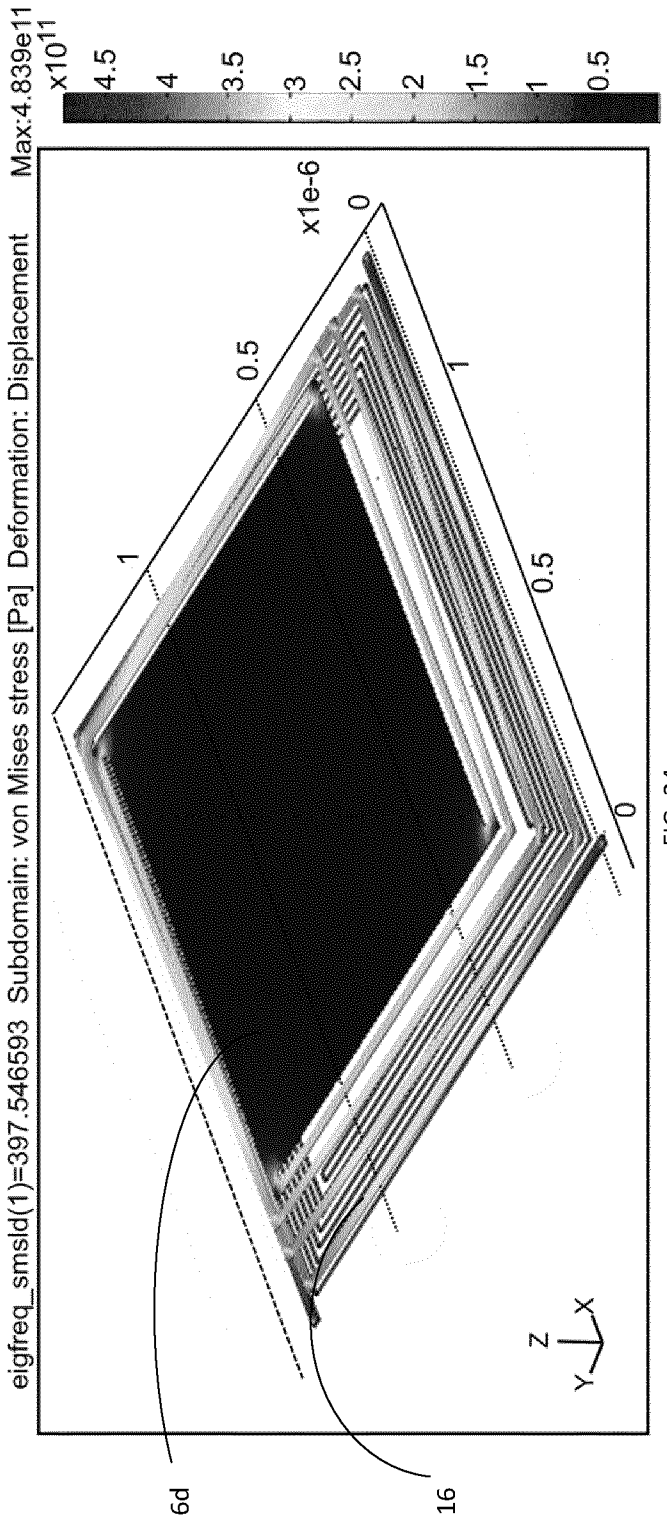
eigfreq_smsld(1)=397.546593 Subdomain: von Mises stress [Pa] Deformation: Displacement Max:4.839e11
x10^11
4.5
4
3.5
3
2.5
2
1.5
1
0.5
x1e-6
0
0.5
1
1
0.5
0
Z
Y
X
6d
16

FIG. 24

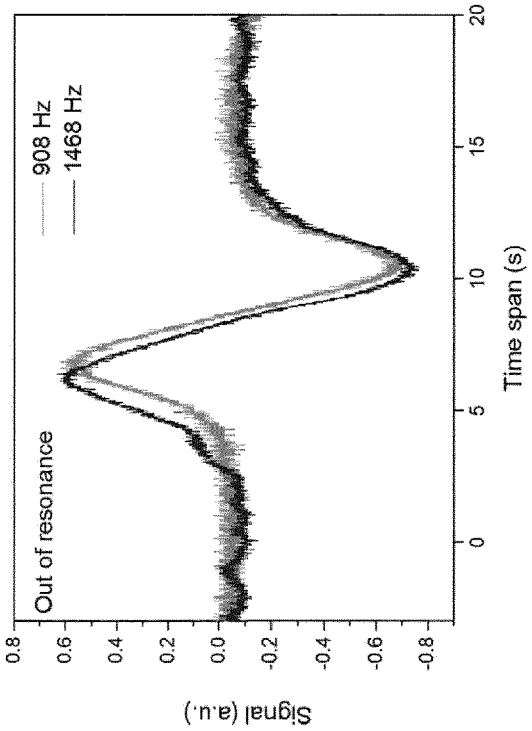

FIG. 25b

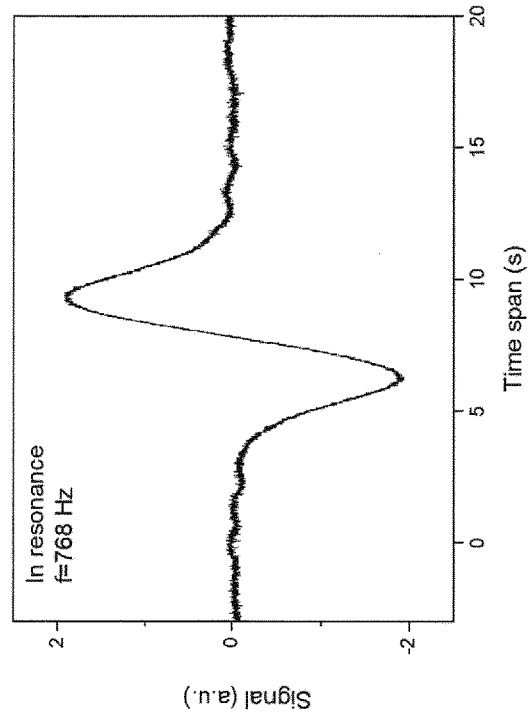

FIG. 25a

FIG. 26b

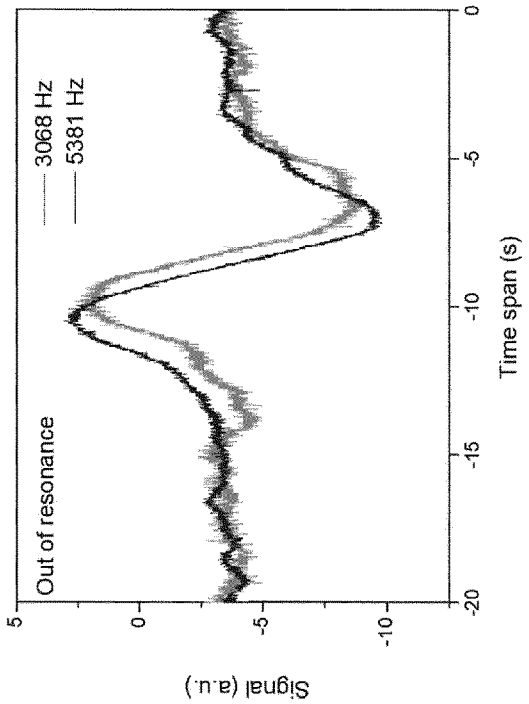

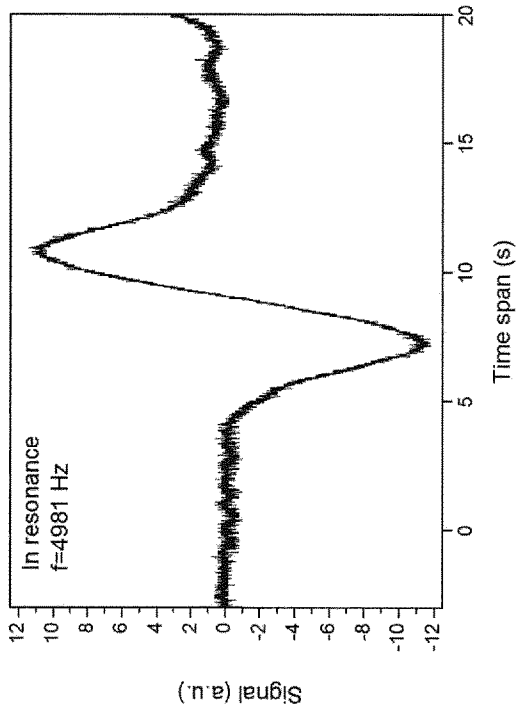

FIG. 26a

INTERNATIONAL SEARCH REPORT

International application No
PCT/EP2022/087976

A. CLASSIFICATION OF SUBJECT MATTER
INV. G01N21/17 G01N21/27 G01N29/24
ADD.

According to International Patent Classification (IPC) or to both national classification and IPC

B. FIELDS SEARCHED

Minimum documentation searched (classification system followed by classification symbols)
G01N G01B

Documentation searched other than minimum documentation to the extent that such documents are included in the fields searched

Electronic data base consulted during the international search (name of data base and, where practicable, search terms used)

EPO-Internal, WPI Data

C. DOCUMENTS CONSIDERED TO BE RELEVANT

Category*	Citation of document, with indication, where appropriate, of the relevant passages	Relevant to claim No.
A	CHU J H ET AL: "Michelson interferometric detection for optoacoustic spectroscopy", OPTICS COMMUNICATIONS, ELSEVIER, AMSTERDAM, NL, vol. 89, no. 2-4, 1 May 1992 (1992-05-01), pages 135-139, XP025490384, ISSN: 0030-4018, DOI: 10.1016/0030-4018(92)90146-I [retrieved on 1992-05-01] abstract; figures 1,3 page 138, left-hand column, paragraph 7 - right-hand column, paragraph 2 ----- -/--	1-11

[x] Further documents are listed in the continuation of Box C.

[x] See patent family annex.

* Special categories of cited documents :

"A" document defining the general state of the art which is not considered to be of particular relevance

"E" earlier application or patent but published on or after the international filing date

"L" document which may throw doubts on priority claim(s) or which is cited to establish the publication date of another citation or other special reason (as specified)

"O" document referring to an oral disclosure, use, exhibition or other means

"P" document published prior to the international filing date but later than the priority date claimed

"T" later document published after the international filing date or priority date and not in conflict with the application but cited to understand the principle or theory underlying the invention

"X" document of particular relevance;; the claimed invention cannot be considered novel or cannot be considered to involve an inventive step when the document is taken alone

"Y" document of particular relevance;; the claimed invention cannot be considered to involve an inventive step when the document is combined with one or more other such documents, such combination being obvious to a person skilled in the art

"&" document member of the same patent family

Date of the actual completion of the international search	Date of mailing of the international search report
3 February 2023	13/02/2023

Name and mailing address of the ISA/	Authorized officer
European Patent Office, P.B. 5818 Patentlaan 2 NL - 2280 HV Rijswijk Tel. (+31-70) 340-2040, Fax: (+31-70) 340-3016	Duijs, Eric

2

Form PCT/ISA/210 (second sheet) (April 2005)

C(Continuation). DOCUMENTS CONSIDERED TO BE RELEVANT

Category*	Citation of document, with indication, where appropriate, of the relevant passages	Relevant to claim No.
A	SICILIANI DE CUMIS MARIO ET AL: "A compact cantilever-based photoacoustic sensor for trace-gas detection", SPIE PROCEEDINGS; [PROCEEDINGS OF SPIE ISSN 0277-786X], SPIE, US, vol. 11288, 31 January 2020 (2020-01-31), pages 112882E-112882E, XP060130010, DOI: 10.1117/12.2545824 ISBN: 978-1-5106-3673-6 figures 1,6	1,6
A	GB 2 492 841 A (SECR DEFENCE [GB]) 16 January 2013 (2013-01-16) page 14, line 7 - page 25, line 22; figures 2,3	1,6
A	HERNANDEZ CARMEN M ET AL: "Photoacoustic characterization of the mechanical properties of thin films", APPLIED PHYSICS LETTERS, AMERICAN INSTITUTE OF PHYSICS, 2 HUNTINGTON QUADRANGLE, MELVILLE, NY 11747, vol. 80, no. 4, 28 January 2002 (2002-01-28), pages 691-693, XP012031420, ISSN: 0003-6951, DOI: 10.1063/1.1434303 figure 1	1,6
A	EP 0 339 625 A1 (CANADIAN PATENTS DEV [CA]) 2 November 1989 (1989-11-02) column 6, line 58 - column 8, line 50; figure 3	1,6

INTERNATIONAL SEARCH REPORT

Information on patent family members

International application No
PCT/EP2022/087976

Patent document cited in search report	Publication date	Patent family member(s)	Publication date
GB 2492841 A	16-01-2013	GB 2492841 A	16-01-2013
		WO 2013011253 A1	24-01-2013
EP 0339625 A1	02-11-1989	AT 85432 T	15-02-1993
		CA 1287388 C	06-08-1991
		DE 68904681 T2	19-05-1993
		EP 0339625 A1	02-11-1989
		JP 2859292 B2	17-02-1999
		JP H0216419 A	19-01-1990
		KR 890016361 A	28-11-1989
		US 4966459 A	30-10-1990